



UHASSELT



Maastricht University

KNOWLEDGE IN ACTION

Faculty of Sciences
School for Information Technology

Master of Statistics and Data Science

Master's thesis

A Stochastic Compartmental Model to Describe the Co-Circulation of Influenza and COVID-19 and Investigating the Potential Effects of Vaccination Strategies

Nadine Barth

Thesis presented in fulfillment of the requirements for the degree of Master of Statistics and Data Science, specialization Quantitative Epidemiology

SUPERVISOR :

Prof. dr. Andrea TORNERI

Transnational University Limburg is a unique collaboration of two universities in two countries: the University of Hasselt and Maastricht University.



UHASSELT

KNOWLEDGE IN ACTION

www.uhasselt.be

Universiteit Hasselt
Campus Hasselt:
Martelarenlaan 42 | 3500 Hasselt
Campus Diepenbeek:
Agoralaan Gebouw D | 3590 Diepenbeek

2023
2024



Maastricht University

Faculty of Sciences
School for Information Technology

Master of Statistics and Data Science

Master's thesis

A Stochastic Compartmental Model to Describe the Co-Circulation of Influenza and COVID-19 and Investigating the Potential Effects of Vaccination Strategies

Nadine Barth

Thesis presented in fulfillment of the requirements for the degree of Master of Statistics and Data Science,
specialization Quantitative Epidemiology

SUPERVISOR :

Prof. dr. Andrea TORNERI

Abstract

COVID-19 and influenza are two respiratory infectious diseases that cause a significant burden on the health care system. Their co-circulation is a realistic scenario for the foreseeable future and while their co-dynamics are not yet clear, a better understanding on possible interactions is important to be able to characterize their spread. Immunization plays a key role in the spread of any virus and in the specific case of COVID-19 and Influenza, cross-reactive immunity has been documented. Comprehending the role of different aspects of immunity in the spread of the diseases is crucial. Mathematical modeling provides a useful framework to identify the drivers of transmission, to investigate the impact of immune responses and to predict possible pressures on the health care system.

A compartmental model is developed that allows for the simulation of the transmission of COVID-19 and influenza simultaneously. Immunization and cross-reactive immunity by infection and by vaccination is incorporated. To take into account the heterogeneity in transmission, the model is formulated as a stochastic chain binomial model. It is fitted to incidence data from Belgium and the Netherlands using a likelihood free Monte Carlo Markov Chain approach. The next generation approach is applied to theoretically derive the basic reproduction numbers. Simulation based studies are performed for different scenarios in which the effect of (cross-)immunity as well as a less aggressive variant of COVID-19 are investigated.

This work highlights the importance of modeling the interaction between both diseases by showing that the number of infections (in total and at peak) and the probability of a major outbreak is decreased for influenza. It also shows that the magnitude of the decrease is dependent on the transmission rate of COVID-19. The simulations demonstrate that a heterologous immune response does have an impact on the spread of the disease with lower transmission rate when only naturally-induced. The importance of vaccination is illustrated as it is shown to effectively decrease disease burden on public health. The work suggests that cross-immunity reactions should be taken into account when designing effective vaccination strategies.

1 Introduction

COVID-19, a disease caused by the the severe acute respiratory syndrome Coronavirus 2 (SARS-CoV-2), has led to a global pandemic ([8]) with extraordinary health, social, and economic repercussions ([23], [17]). Although the end of the global pandemic has been declared May 5, 2023, ([25]) the virus keeps circulating and the possible emergence of new variants in the future in combination with the imperfect vaccine protection and waning immunity increase the likelihood that COVID-19 will remain a concern. Influenza at the same time remains a persistent seasonal threat, causing numerous infections and deaths annually. The co-circulation of two pathogens with similar symptoms presents a public health challenge due to difficulties in disease surveillance and potential testing and treatment delays. Understanding the spread and dynamics of the diseases is an important step in developing effective strategies to manage their impact. Mathematical models present a suitable framework to examine, analyze and predict the behavior of infectious diseases and a lot of effort has been put into developing such models for COVID-19 as well as influenza. The creation of co-circulation models is crucial since the simultaneous presence of both pathogens possibly impacts their transmission dynamics.

Vaccines play a vital role in reducing transmission, severity of disease and consequently overall health-care burden and are therefore a primary prevention measure to limit the spread of an infectious disease, in some cases even leading to the elimination of the pathogen. The inclusion of vaccination in mathematical models allows for the evaluation of its impact on the co-dynamics. Additionally, understanding this homologous immunity¹ is essential for predicting long-term trends and potential future outbreaks. Several studies suggest a positive heterologous immunity² effect between the two pathogens. ([35], [19], [11], [16]).

¹Homologous immunity refers to the protection against the same virus (e.g., immunity to COVID-19 after infection or vaccination against SARS-CoV-2)

²Heterologous immunity refers to the cross-protection between different viruses (e.g., partial immunity to influenza in individuals previously infected with or vaccinated against COVID-19, and vice versa)

Incorporating homologous as well as heterologous immunity in a model helps to create a more accurate representation of disease spread.

While co-circulation models have been developed that account for the protective effect of recovery from the same disease or vaccination targeting the same pathogen, they do not incorporate heterologous immunity effects. However, these effects could lead to very different transmission dynamics, especially when caused by vaccination. This thesis aims to explore the impact of homologous as well as heterologous immunity on the spread of COVID-19 and influenza and their combined load on the health care system accounting for the interaction between both pathogens. The results potentially form a basis for designing effective vaccination strategies for both diseases combined.

To simulate the co-circulation of COVID-19 and influenza in a closed population, a chain binomial compartmental model is developed that keeps track of the numbers of susceptible, infected, recovered and deceased individuals in function of calendar time and describes the flow between these states. To account for heterogeneity in transmission, the transfer from one compartment to another is dependent on a stochastic process. The model includes a pre-infectious state and accounts for symptomatic as well as asymptomatic infection. This model is fitted to incidence data from Belgium (for COVID-19) and the Netherlands (for influenza) using a likelihood-free Monte Carlo Markov Chain approach to inform the transmission parameters. The fitting procedure is described in Section ???. The basic reproduction number is derived theoretically using the next generation approach and is described in Section 2.3.

The model is used in a simulation based study. First, the impact of co-circulation compared to the circulation of both diseases separately is quantified, without taking into account any form of immunity. Then, the effect of homologous immunity through vaccination is simulated. The effect of heterologous immunity (by varying the protective effect on susceptibility) is investigated in a scenario where no vaccination is considered and in a scenario where the population is vaccinated. Finally, a less aggressive variant of COVID-19 is considered in combination with no vaccination to investigate the heterologous immunity effect.

By simulating different scenarios with regard to the different types of immunity, this thesis has the potential to guide policymakers in making informed decisions. Through this work, the aim is to contribute to a better understanding of the complex interplay between COVID-19 and influenza and to provide a flexible framework for future research.

This thesis is organized as follows. Section 2 provides a detailed description of the model, its compartments and parametrization. Also, details on the fitting procedure and the derivation of the reproduction number are provided in this section. The setup and scenarios of the simulation study as well as the results are presented in Section 3. Section 4.2 provides an interpretation of the results as well as limitations of the proposed approach, ideas for future research and ethical considerations. A conclusion is formulated in Section 5.

2 Methodology

2.1 Co-circulation Model

Mathematical models are widely used in epidemiology to model the spread and dynamics of infectious diseases. A very common type of equation-based model is the SIR compartmental model in which the population is divided into three compartments or states related to different stages of the disease: susceptible (S), infected (I), and recovered (R). The compartments represent the number of individuals corresponding to each stage at a specific point in time. A common adaptation of the SIR model is the SEIRD model which contains two additional compartments: a pre-infectious compartment exposed (E) in which an individual is infected but latent, and a dead (D) compartment for disease-related deaths. The movement between two compartments is defined by a mathematical expression depending on a specific rate.

The use of this type of model implies certain simplifying assumptions. First of all, the population is assumed to be constant which means that the total number of individuals remains constant over time. This insinuates that there are no births, deaths (other than those directly caused by the disease in question), or migration in or out of the population. The model is intended for relatively short-term simulations, which makes this assumption reasonable. Secondly, the population is assumed to be homogeneous. This implies that no differences between individuals are considered in terms of disease related parameters. Specifically, mixing within the population is assumed homogeneous which means that a (successful) contact between any two individuals in the population occurs at random with equal probability.

2.1.1 Epidemiological Dynamics

An adapted version of the SEIRD compartmental model is developed to investigate the co-circulation of COVID-19 and Influenza. In this model, individuals are fully susceptible to infection with both pathogens when in compartment S . At the beginning of the simulation, all individuals are assumed to be fully susceptible. After (successful) contact with an infectious individual, the susceptible individual moves to an exposed state E at transmission rate β . In this compartment, the individual is infected with the disease but is not able to transmit the disease to others. After a latent period γ^{-1} , the individual becomes infectious. The infection can be asymptomatic (I_a , with probability $\hat{\gamma}_a$) or symptomatic (I_s , with probability $1 - \hat{\gamma}_a$). Note that in reality, an individual can be infectious before showing clinical signs of infection (sub-clinical infectious, [13]). The choice of working with the latent period rather than the incubation period (which is considered the time between infection and showing symptoms) is made because of the importance to make the distinction between infectious and not infectious for the transmission dynamics. The distinction between pre-symptomatic and symptomatic is not less relevant. The infectious period has a duration δ^{-1} after which asymptomatic individuals recover and move to compartment R while symptomatic individuals either die with probability μ and move to compartment D or recover with probability $1 - \mu$ and move to compartment R . Individuals that recover from one of the diseases are now susceptible to the other disease and follow the same disease flow.

Figure 1 is a schematic representation of the model and shows the disease dynamics with all possible transmissions among the different compartments. A full list of compartments along with their description can be found in Table 1.

Symbol	Description
S	individuals fully susceptible to COVID-19 and influenza
V_1	susceptible individuals vaccinated against COVID-19 but not influenza
V_2	susceptible individuals vaccinated against influenza but not COVID-19
V_{12}	susceptible individuals vaccinated against COVID-19 and influenza
E_1	individuals that have been exposed to COVID-19 but are not yet infectious
E_2	individuals that have been exposed to influenza but are not yet infectious
E_1^+	individuals that recovered from influenza and have been exposed to COVID-19 but are not yet infectious
E_2^+	individuals that recovered from COVID-19 and have been exposed to influenza but are not yet infectious
I_{1a}	individuals that are infected with COVID-19 and can infect other susceptible individuals
I_{1s}	individuals that are infected with influenza and can infect other susceptible individuals
I_{1a}^+	individuals that recovered from influenza and are infected with COVID-19 and can infect other susceptible individuals
I_{2a}^+	individuals that recovered from COVID-19 and are infected with influenza and can infect other susceptible individuals

R_1	individuals that have recovered from COVID-19 and that have not yet been infected with (but are susceptible to) influenza
R_2	individuals that have recovered from influenza and that have not yet been infected with (but are susceptible to) COVID-19
R_{12}	individuals that have recovered from COVID-19 and influenza
D_1	individuals that died as a result of COVID-19 infection
D_2	individuals that died as a result of influenza infection
<hr/>	
β_1	rate at which an infectious individual transfers COVID-19 to a susceptible individual
β_2	rate at which an infectious individual transfers influenza to a susceptible individual
γ_1	rate at which an exposed individual becomes infectious with COVID-19 (= inverse of the length of the latent period)
γ_2	rate at which an exposed individual becomes infectious with influenza (= inverse of the length of the latent period)
$\hat{\gamma}_{1a}$	probability of asymptomatic COVID-19 infection
$\hat{\gamma}_{2a}$	probability of asymptomatic influenza infection
$\hat{\Gamma}_{1i}$	factor by which the probability of asymptomatic COVID-19 infection is changed when an individual has already been infected with influenza
$\hat{\Gamma}_{2i}$	factor by which the probability of asymptomatic influenza infection is changed when an individual has already been infected with COVID-19
δ_1	rate at which an individual recovers from COVID-19 (inverse of the length of the infectious period)
δ_2	rate at which an individual recovers from influenza (inverse of the length of the infectious period)
μ_1	probability of death due to COVID-19 infection
μ_2	probability of death due to influenza infection

Table 1: List of all compartments and transmission rates of the model in Figure 1 along with their explanation.

2.1.2 Immunity

Immunity is the body's ability to resist or defend against infection by pathogens such as viruses and bacteria. It can be acquired through previous infection (natural) or vaccination (vaccine-induced), which help the immune system recognize and combat specific pathogens more effectively in the future. Immunity is defined here to be either homologous, providing protection against the same pathogen, or heterologous, offering partial protection against different but related pathogens.

In the model, susceptible individuals undergo vaccination at a rate ω and transition to compartment V . Individuals can receive vaccination against either one (compartments V_1 for COVID-19 and V_2 for influenza) or both diseases (compartment V_{12}). Subsequently, individuals in compartment V follow the same disease flow as those in compartment S but with adapted transition parameters. It is important to note that vaccines offer only partial protection against the targeted disease.

Immunity is incorporated into the model to influence both, disease transmission and the probability of symptom development. Disease transmission is affected by the infectiousness of infectious individuals and the susceptibility of susceptible individuals. Immunity reduces infectiousness by a factor $\hat{\lambda}_I$ (for homologous immunity) or $\hat{\lambda}_i$ (for heterologous immunity) and reduces susceptibility by a factor $\hat{\Lambda}_I$ (for homologous immunity) or $\hat{\Lambda}_i$ (for heterologous immunity). Additionally, the probability of developing symptoms is decreased by a factor $\hat{\Gamma}_I$ (for homologous immunity) or $\hat{\Gamma}_i$ (for heterologous immunity).

The model excludes the possibility of simultaneous infection with both diseases. Literature reports

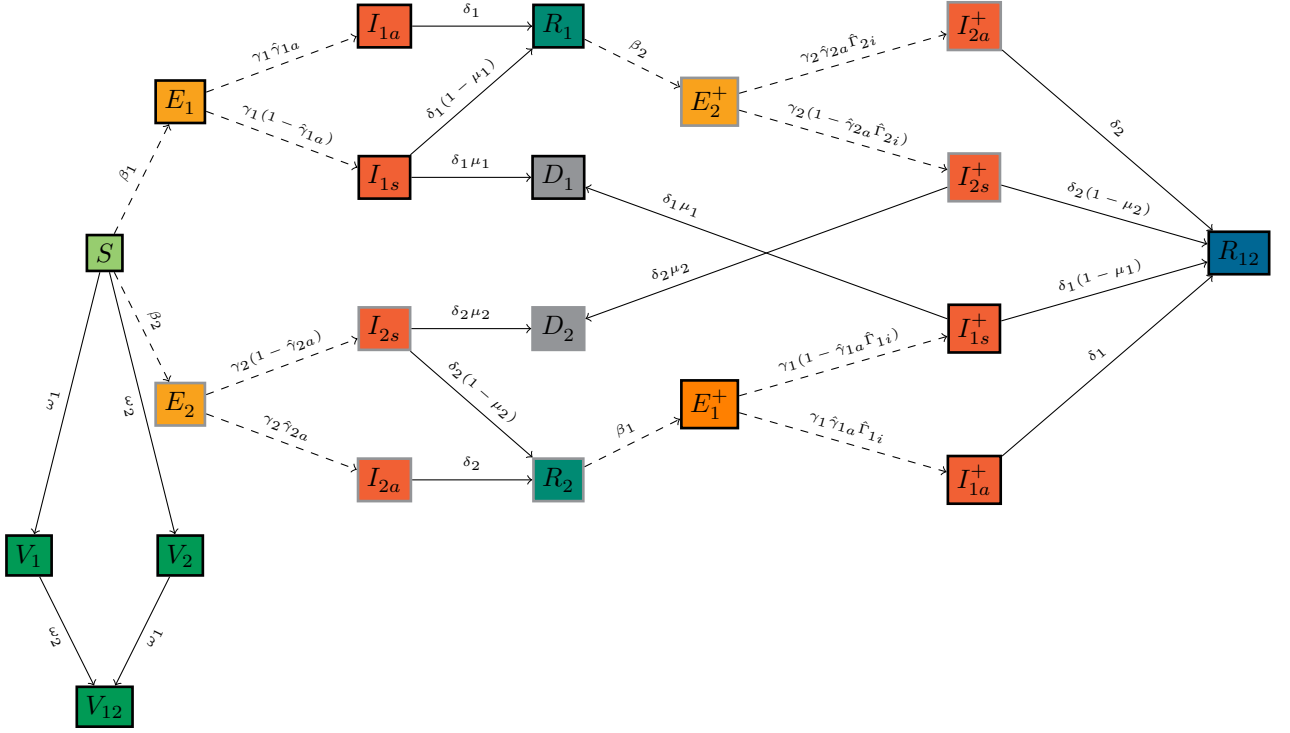


Figure 1: A schematic overview of the compartmental model. The index 1 refers to COVID-19 and 2 refers to influenza. Rectangles of the same color represent the same type of class. Individuals in green classes are (partly) susceptible to both diseases. An orange color indicates that individuals are infected but cannot yet transfer the disease, this only happens in the red compartments. Individuals in blue-green compartments recovered from one disease and are susceptible to the other disease and in the blue compartment, they recovered from both diseases. Individuals in the gray compartment are dead. The color of the border indicates the disease associated with the compartment: black for COVID-19 and gray for influenza. A "+" symbol denotes individuals who have previously been infected with the other pathogen and have acquired heterologous immunity. Dashed lines indicate flows influenced by immunity.

that the incidence of co-infection with COVID-19 and influenza is low ([27], [18]) making this a reasonable assumption. The effects of immunity are assumed to be constant. This implies that re-infection with the same pathogen is not possible.

2.1.3 Model Formulation

As biological systems are inherently stochastic, the incorporation of randomness and noise into the model is necessary to address uncertainties associated with parameter estimation and unmodeled factors. In a stochastic compartmental model, transitions between compartments are probabilistic, capturing the inherent randomness in disease transmission and population dynamics. This modeling approach accommodates individual-level variability.

The co-circulation model proposed is a chain binomial model, more specifically the Reed-Frost model and is a stochastic alternative to the deterministic SEIRD model formulation using ordinary differential equations (the system of ODE's can be found in Table ?? in the Appendix). This model assumes that infection spreads in discrete units of time governed by the binomial probability distribution. Let $I(t)$ be the number of infectious individuals and N the total population size, then $I(t)/N$ denotes the proportion of infectious individuals in the population and assuming homologous mixing, the probability of a contact being with an infectious individual. The transmission rate represents the number of new infections caused by a single infectious individual per unit of time and is denoted by β , t is a certain point in time and Δ

the length between two time points at which the model states are evaluated. The probability of disease transmission during a successful contact between a susceptible and an infectious individual within time interval $]t + \Delta]$ is denoted by p . Assuming that all individuals are equally susceptible and infectious and that the number of new infections depends on the number of infectious individuals in the population, p is dependent on time and can be expressed as: $p(t) = 1 - \exp(-\Delta\beta I(t)/N)$. The infectious individuals are sub-divided into compartments I_a for asymptomatic infection and I_s for symptomatic infection with respective transmission rates β_a and β_s . Additionally, a differentiation is made between infected individuals that have already been infected with the other disease (denoted by a plus indicating that heterologous immunity has been acquired) with heterologous effect on infectiousness being $\hat{\lambda}_i$. Then, the expression of the probability of disease transmission becomes:

$$p(t) = 1 - \exp\left(-\Delta\left\{\beta_a\left[\frac{I_a(t)}{N} + \hat{\lambda}_i\frac{I_a^+(t)}{N}\right] + \beta_s\left[\frac{I_s(t)}{N} + \hat{\lambda}_i\frac{I_s^+(t)}{N}\right]\right\}\right) \quad (1)$$

Let the number of susceptible individuals at time point t be denoted by $S(t)$, then the number of new infections (denoted by E^*) at time point $t + \Delta$ is expected to be $S(t) \cdot p(t)$ and follows a binomial distribution (Equation 2).

$$E^*(t + \Delta) \sim \text{Bin}(S(t), p(t)) \quad (2)$$

The expression 2 represents the flow from the compartment $S(t)$ to compartment $E(t)$ between time point t and time point $t + \Delta$ or the in-flow of compartment $E(t)$. The number of individuals leaving compartment E or the number of individuals entering compartment $I(t)$ (ignoring for the time being the distinction between symptomatic and asymptomatic infections) within the same time interval is denoted by

$$I^*(t + \Delta) \sim \text{Bin}(E(t), 1 - \exp(-\Delta\gamma)) \quad (3)$$

The number of individuals in compartment E at time point $t + \Delta$ is computed as follows:

$$E(t + \Delta) = E(t) + E^*(t + \Delta) - I^*(t + \Delta) \quad (4)$$

The transition between other compartments is derived similarly. The full specification of the model for both diseases (Figure 1) is shown in Tables 2 and 3.

$E_1^*(t + \Delta) \sim \text{Bin}(S(t), 1 - \exp\{-\Delta/N[\beta_{1a}(I_{1a}(t) + \hat{\lambda}_{1i}I_{1a}^+(t)) + \beta_{1s}(I_{1s}(t) + \hat{\lambda}_{1i}I_{1s}^+(t))]\})$
$I_{1a}^*(t + \Delta) \sim \text{Bin}(E_1(t), 1 - \exp[-\Delta\gamma_1\hat{\gamma}_{1a}])$
$I_{1s}^*(t + \Delta) \sim \text{Bin}(E_1(t), 1 - \exp[-\Delta\gamma_1(1 - \hat{\gamma}_{1a})])$
$R_{1a}^{*s}(t + \Delta) \sim \text{Bin}(I_{1a}(t), 1 - \exp[-\Delta\delta_1])$
$R_{1s}^{*s}(t + \Delta) \sim \text{Bin}(I_{1s}(t), 1 - \exp[-\Delta\delta_1(1 - \mu_1)])$
$D_1^+(t + \Delta) \sim \text{Bin}(I_{1s}(t), 1 - \exp[-\Delta\delta_s\mu_1])$ $D_1^{+*}(t + \Delta) \sim \text{Bin}(I_{1s}^+(t), 1 - \exp[-\Delta\delta_1\hat{\delta}_{1i}\mu_1])$
$E_1^{+*}(t + \Delta) \sim \text{Bin}(R_2(t), 1 - \exp[-\Delta/N \cdot \hat{\lambda}_{1i}[\beta_{1a}(I_{1a}(t) + \hat{\lambda}_{1i}I_{1a}^+(t)) + \beta_{1s}(I_{1s}(t) + \hat{\lambda}_{1i}I_{1s}^+(t))]])$
$I_{1a}^{+*}(t + \Delta) \sim \text{Bin}(E_1^+(t), 1 - \exp[-\Delta\gamma_1\hat{\gamma}_{1a}\hat{\Gamma}_{1i}])$
$I_{1s}^{+*}(t + \Delta) \sim \text{Bin}(E_1^+(t), 1 - \exp[-\Delta\gamma_1(1 - \hat{\gamma}_{1a}\hat{\Gamma}_{1i})])$
$E_2^*(t + \Delta) \sim \text{Bin}(S(t), 1 - \exp\{-\Delta/N[\beta_{2a}(I_{2a}(t) + \hat{\lambda}_{2i}I_{2a}^+(t)) + \beta_{2s}(I_{2s}(t) + \hat{\lambda}_{2i}I_{2s}^+(t))]\})$
$I_{2a}^*(t + \Delta) \sim \text{Bin}(E_2(t), 1 - \exp[-\Delta\gamma_2\hat{\gamma}_{2a}])$
$I_{2s}^*(t + \Delta) \sim \text{Bin}(E_2(t), 1 - \exp[-\Delta\gamma_2(1 - \hat{\gamma}_{2a})])$
$R_{2a}^{*s}(t + \Delta) \sim \text{Bin}(I_{2a}(t), 1 - \exp[-\Delta\delta_2])$
$R_{2s}^{*s}(t + \Delta) \sim \text{Bin}(I_{2s}(t), 1 - \exp[-\Delta\delta_2(1 - \mu_2)])$
$D_2^*(t + \Delta) \sim \text{Bin}(I_{2s}(t), 1 - \exp[-\Delta\delta_2\mu_2])$
$D_2^{+*}(t + \Delta) \sim \text{Bin}(I_{2s}^+(t), 1 - \exp[-\Delta\delta_2\hat{\delta}_{2i}\mu_2])$

$$\begin{aligned}
E_2^{+*}(t+\Delta) &\sim \text{Bin}(R_1(t), 1 - \exp[-\Delta/N \cdot \hat{\Lambda}_{2i}[\beta_{2a}(I_{2a}(t) + \hat{\lambda}_{2i}I_{2a}^+(t)) + \beta_{2s}(I_{2s}(t) + \hat{\lambda}_{2i}I_{2s}^+(t))]]) \\
I_{2a}^{+*}(t+\Delta) &\sim \text{Bin}(E_2^+(t), 1 - \exp[-\Delta\gamma_2\hat{\gamma}_{2a}\hat{\Gamma}_{2i}]) \\
I_{2s}^{+*}(t+\Delta) &\sim \text{Bin}(E_2^+(t), 1 - \exp[-\Delta\gamma_2(1 - \hat{\gamma}_{2a}\hat{\Gamma}_{2i})]) \\
\hline
R_{12;1s+}^*(t+\Delta) &\sim \text{Bin}(I_{1s}^+(t), 1 - \exp[-\Delta\delta_1\hat{\delta}_{1i}(1 - \mu_1)]) \\
R_{12;2s+}^*(t+\Delta) &\sim \text{Bin}(I_{2s}^+(t), 1 - \exp[-\Delta\delta_2\hat{\delta}_{2i}(1 - \mu_2)]) \\
R_{12;1a+}^*(t+\Delta) &\sim \text{Bin}(I_{1a}^+(t), 1 - \exp[-\Delta\delta_1\hat{\delta}_{1i}]) \\
R_{12;2a+}^*(t+\Delta) &\sim \text{Bin}(I_{2a}^+(t), 1 - \exp[-\Delta\delta_2\hat{\delta}_{2i}]) \\
\hline
\hline
\end{aligned}$$

Table 2: Distributions describing the flow between the different compartments in the chain-binomial model.

$$\begin{aligned}
S(t+\Delta) &= S(t) - E_1^*(t+\Delta) - E_2^*(t+\Delta) & E_2(t+\Delta) &= E_2(t) + E_2^*(t+\Delta) - I_{2a}^*(t+\Delta) - I_{2s}^*(t+\Delta) \\
E_1(t+\Delta) &= E_1(t) + E_1^*(t+\Delta) - I_{1a}^*(t+\Delta) - I_{1s}^*(t+\Delta) & I_{2a}(t+\Delta) &= I_{2a}(t) + I_{2a}^*(t+\Delta) - R_{2a}^*(t+\Delta) \\
I_{1a}(t+\Delta) &= I_{1a}(t) + I_{1a}^*(t+\Delta) - R_{1a}^*(t+\Delta) & I_{2s}(t+\Delta) &= I_{2s}(t) + I_{2s}^*(t+\Delta) - R_{2s}^*(t+\Delta) - D_2^*(t+\Delta) \\
I_{1s}(t+\Delta) &= I_{1s}(t) + I_{1s}^*(t+\Delta) - R_{1s}^*(t+\Delta) - D_1^*(t+\Delta) & R_2(t+\Delta) &= R_2(t) + R_2^*(t+\Delta) - E_1^{+*}(t+\Delta) \\
R_1(t+\Delta) &= R_1(t) + R_1^*(t+\Delta) - E_2^{+*}(t+\Delta) & E_2^+(t+\Delta) &= E_2^+(t) + E_2^{+*}(t+\Delta) - I_{2a}^{+*}(t+\Delta) - I_{2s}^{+*}(t+\Delta) \\
E_1^+(t+\Delta) &= E_1^+(t) + E_1^{+*}(t+\Delta) - I_{1a}^{+*}(t+\Delta) - I_{1s}^{+*}(t+\Delta) & I_{1a}^+(t+\Delta) &= I_{1a}^+(t) + I_{1a}^{+*}(t+\Delta) - R_{12;1a+}^*(t+\Delta) \\
I_{1a}^+(t+\Delta) &= I_{1a}^+(t) + I_{1a}^{+*}(t+\Delta) - R_{12;1a+}^*(t+\Delta) & I_{1s}^+(t+\Delta) &= I_{1s}^+(t) + I_{1s}^{+*}(t+\Delta) - R_{12;1s+}^*(t+\Delta) \\
I_{1s}^+(t+\Delta) &= I_{1s}^+(t) + I_{1s}^{+*}(t+\Delta) - R_{12;1s+}^*(t+\Delta) & I_{2s}^+(t+\Delta) &= I_{2s}^+(t) + I_{2s}^{+*}(t+\Delta) - R_{12;2s+}^*(t+\Delta) \\
R_{12}(t+\Delta) &= R_{12}(t) + R_{12;2a+}^*(t+\Delta) + R_{12;2s+}^*(t+\Delta) + R_{12;1s+}^*(t+\Delta) + R_{12;1a+}^*(t+\Delta) \\
D_1(t+\Delta) &= D_1(t) + D_1(t+\Delta) + D_1^+(t+\Delta) & D_2(t+\Delta) &= D_2(t) + D_2(t+\Delta) + D_2^+(t+\Delta) \\
\hline
\hline
\end{aligned}$$

Table 3: Set of equations determining the total number of individuals in each compartment at time step $t + \Delta$.

2.2 Fitting the Model

Accurate estimation of model parameters is essential for the model to reflect real-world dynamics. Therefore, the proposed model is fitted to incidence data from COVID-19 and influenza to ensure that estimated parameters are grounded in observed reality. Fitted models allow for the exploration of various scenarios, helping to predict the potential outcomes of different public health measures such as vaccination strategies. A Monte Carlo Markov Chain approach is particularly well-suited for fitting infectious disease models to data because it provides a robust and flexible framework for handling complex models and allows to estimate a large number of parameters simultaneously. However, MCMC estimation comes at a high computational cost and achieving convergence can be challenging. Additionally, well-suited data from different sources has to be available. Because handling these aspects would go beyond the scope of this project, transmission rates have been estimated during the model fitting procedure for both diseases separately and all other parameters values are selected from estimates reported in literature. The chosen values with respective references are listed in Table B1 in the Appendix. Although the model allows for immunity to affect the infectiousness and susceptibility of an individual as well as the probability to develop symptoms, only the effect on susceptibility is considered in order to simplify the model and be able to find suitable estimates in the literature.

For the fitting procedure, the co-circulation model is adapted such that it corresponds to the an SEIRD model with one disease only (see Figure 2). All model parameters apart from β are assigned values from Table B1. The mathematical expressions defining the model are shown in Table B2 in the Appendix. Due to the stochastic nature of the model, 100 simulations are run for each disease to generate data. The number of weekly symptomatic infections is computed and compared to publicly available incidence data. For COVID-19, a subset (weeks 9 to 12 of 2020) of the data from Sciensano with daily new confirmed cases in Belgium is used ([29]). For influenza, the data comes from Infectieradar ([28]), an online platform

where participants can self-report symptoms. A subset of data for the Netherlands ³ has been selected to correspond to the increasing part of a single wave (weeks 34 to 40 of 2022). The weekly incidence is computed to eliminate the effect of reporting differences depending on the day of the week.

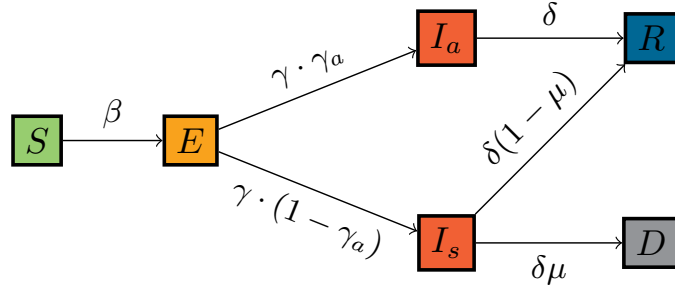


Figure 2: Susceptible (S) individuals get infected with transmission rate β and enter an exposed (E) state. They become infectious with rate γ and either develop symptoms (I_s) with probability $1 - \gamma_a$ or remain asymptomatic (I_a) with probability γ_a . Individuals leave the infectious state with rate δ ; asymptomatic individuals recover (R) and symptomatic individuals either die (D) with probability μ or recover with probability $1 - \mu$.

An MCMC approach with a Metropolis-Hastings algorithm is used to estimate the value of the transmission rates of COVID-19 and influenza. A sequence of samples is generated and each new sample is accepted or rejected resulting in a sample from a (truncated) normal distribution whose mean is considered as an estimate of the parameter to be estimated. Classical MCMC methods require the computation of a likelihood function. The computation of the likelihood function (Equation 5) is however problematic in this case because there no information about the number of exposed individuals is available in the data. Therefore, an adaptation of a likelihood-free MCMC approach is used that does not require the computation of a likelihood function but uses the mean squared error (MSE) as evaluation criterion instead. A graphical representation of the algorithm used is shown in Figure 3.

$$\sum_{t=1}^T \left[\ln \binom{E}{c} + c \cdot \ln(p) + (E - c) \cdot \ln(1 - p) \right], \text{ with } p = 1 - \exp(-\Delta\gamma(1 - \gamma_a)) \quad (5)$$

A starting value β_0 is chosen within an interval $[0.5; 2]$ based on an educated guess. Their value however does not impact the final estimate as shown in the results. 100 simulations of the SEIR model in Figure 2 with equations from Table B2 are performed with this value of β and the mean squared error (MSE) is computed for each simulation according to the formula in 2.2 with $I_s^*(t)$ the new symptomatic cases at time point t from the simulated data and $C(t)$ the incidence at time point t from the available data set and T the total number of weeks considered.

$$MSE = \frac{1}{T} \sqrt{\sum_{t=1}^T \left(C(t) - I_s^*(t) \right)^2} \quad (6)$$

The MSE of the different simulations is expected to be very different and therefore, the mean of the 100 MSE's is used as an evaluation criterion. The lower the MSE, the better the approximation of the simulated data to the real incidence data. In the next steps, a proposal value β^* is drawn from a normal distribution with mean the previous value of β (in the first iteration, this is β_0) and standard deviation σ . The evaluation criterion $mean(MSE^*)$ is computed as explained. The acceptance or rejection of the proposal value β^* is based on this evaluation criterion: when $mean(MSE^*)$ is lower than $mean(MSE)$, it

³Belgium not available

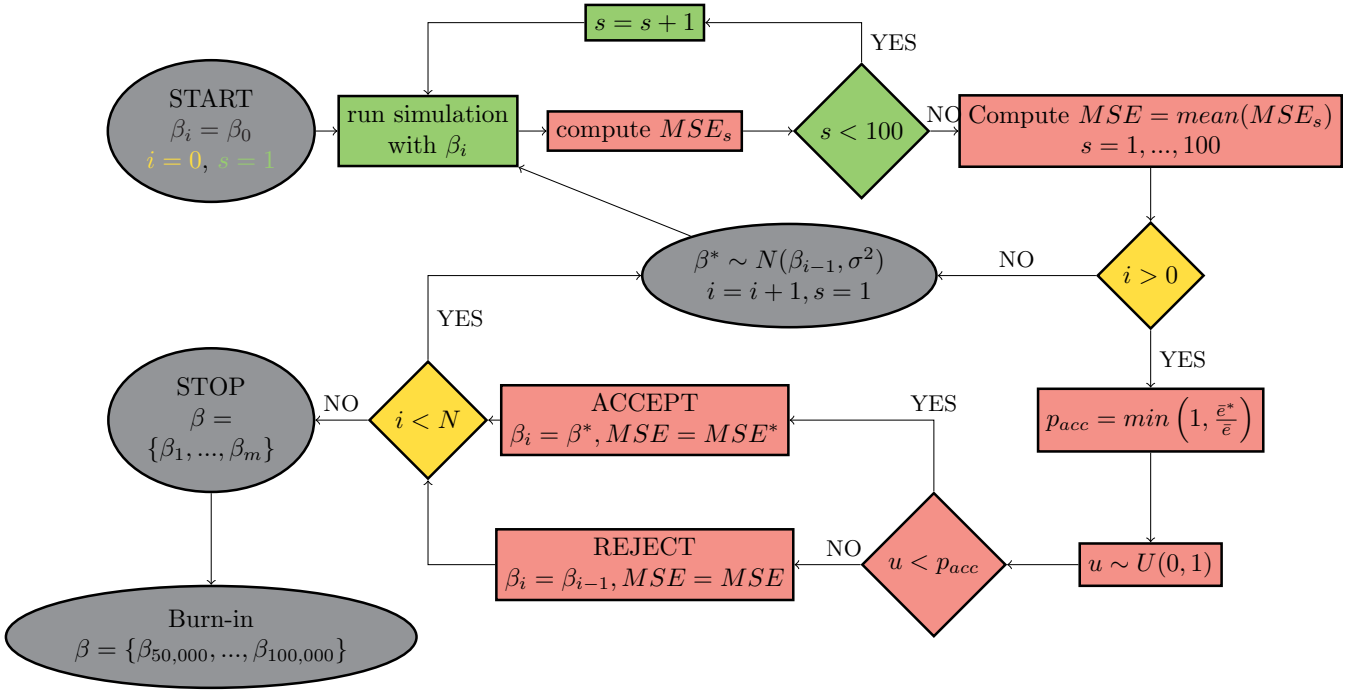


Figure 3: Flow chart of the MCMC algorithm. Gray nodes are related to the values of the parameter β , green nodes show the steps related to the simulation of the stochastic SEIR model, rose nodes are related to the evaluation criterion and the acceptance or rejection of the proposed value of β and yellow nodes are related to the number of iterations. A simulation of the stochastic SEIR model is s and an iteration of the MCMC algorithm is i .

means that the sample arising from simulations with β^* are considered to approximate the real incidence better than the sample arising from simulations with β . In that case, the proposal value β^* is accepted. However, also when this is not the case, the proposal value is still accepted with probability the ratio of the two MSE's. Therefore, a value u is drawn randomly in the interval $[0; 1]$ is from a uniform distribution and compared to the ratio. When the value u is smaller than the probability of acceptance p_{acc} , then the proposal value β^* is accepted, otherwise, it is rejected (Equation 7).

$$p_{acc} = \min \left(1, \frac{\bar{MSE}^*}{\bar{MSE}} \right) \quad (7)$$

The last step in an iteration i is the update of the parameters: $\beta_i = \beta^*$ if the proposal value has been accepted and in that case, $MSE = MSE^*$. In case that the proposal value has been rejected, β and MSE remain unchanged ($\beta_i = \beta_{i-}$ and $MSE = MSE^*$). In total, 100,000 iterations of this algorithm are performed. To make sure that initial fluctuations are not represented in the final sample of the parameter, a burn-in of 50,000 iterations is applied and to make sure that the initial value of the parameter β_0 does not influence the final sample, five different chains of the algorithm are executed with diverging starting values. The final estimate of the transmission rate is obtained by computing the mean of the final samples for all chains. The convergence of the chains is assessed graphically through trace-plots and (smoothed) histograms of the final sample. Also the acceptance probability is assessed.

The tuning of the MCMC parameters has been done through a trial-and-error approach. The standard deviation of the proposal distribution has been chosen as to be sufficiently small to have not too many rejections and sufficiently large to have an acceptable diffusion.

2.2.1 COVID-19

The subset of the data used to fit the model represents the beginning of the pandemic in Belgium. A total population of 11.7 Million individuals (corresponding approximately to the population size of Belgium) and 350 infectious individuals (200 exposed, 104 symptomatic and 46 asymptomatic, corresponding to the ratio of symptomatic/asymptomatic cases used for the model) for the simulations.⁴ It is assumed that there are no recovered individuals and that no individuals have died from infection. The standard deviation for the normal distribution of the proposal value has been tuned to be 0.40.

Figure 4 provides as a graphical tool for assessing the convergence of the different chains. Figure 4a shows the trace plots of the final samples of β . Although at times the values of β seem to explore higher values, it converges back to similar values. This is probably due to the random and stochastic nature of the method used. Figure 4b shows histograms of the final sample of β . The somewhat awkward shape can be explained by the use of a truncated proposal distribution (see Section 4.2 for further discussion).

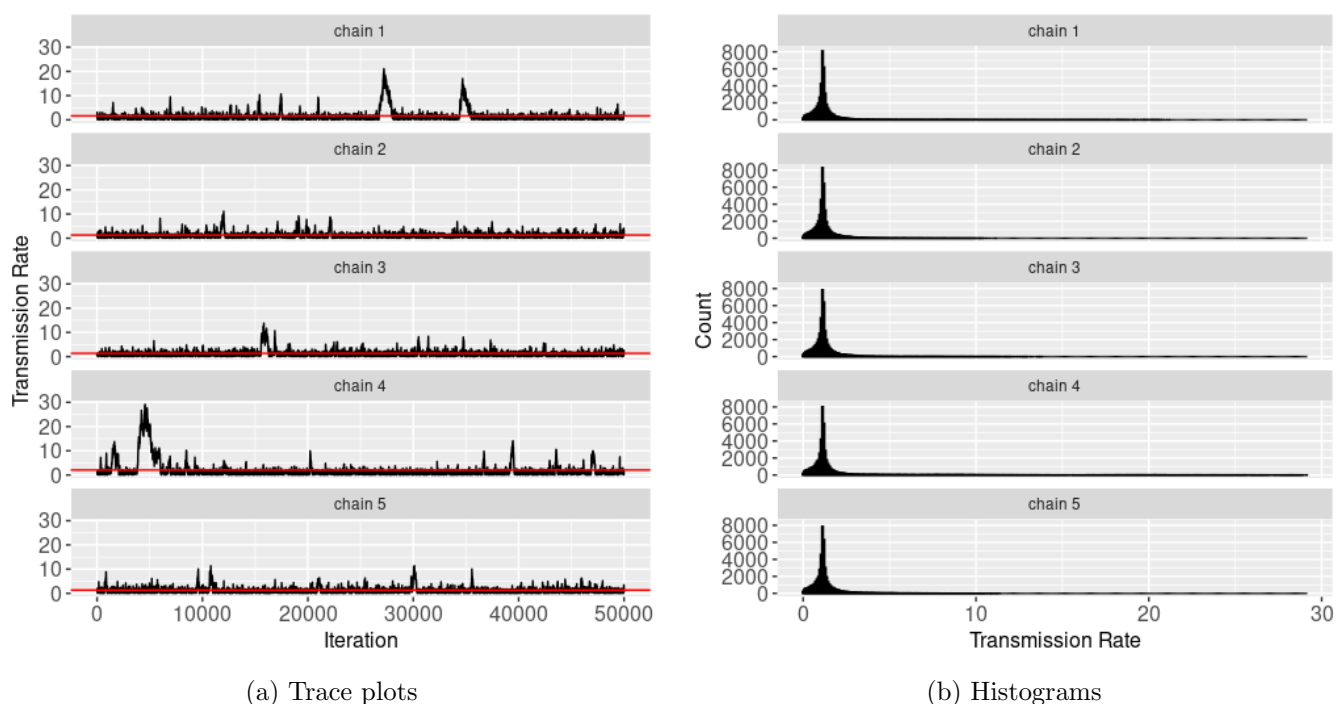


Figure 4: Graphs for the assessment of convergence of the MCMC chains and the quality of the final sample for COVID-19.

Table 4 shows the initial values (β_0) for the chains with the respective estimated value of β and acceptance rate. The estimated transmission rate β_1 for COVID-19 is the mean of the values of the chains shown in Table 4, namely 1.14. This corresponds to a value of R_0 of 10.05 which is high compared to estimated values in the literature ([34]). This estimate is based on the part of the epidemic where an effect of interventions was not visible and hence, the model does not capture these effects which results in a high estimate of the basic reproduction number. Figure 5 shows the incidence of the real data and the simulated curves from the model with the estimated value of β .

⁴Different numbers of initial infections have been explored and the number chosen corresponds to the one that produces data that best approximates the real data.

chain	β_0	β	acceptance rate
1	0.5	1.147040	0.66106
2	0.8	1.139709	0.64938
3	1.0	1.143503	0.65117
4	1.5	1.147411	0.65759
5	2.0	1.140717	0.65119
final estimate		1.133323	0.654078

Table 4: Results of the different chains of the MCMC estimation of β for COVID-19 along with the final estimate.

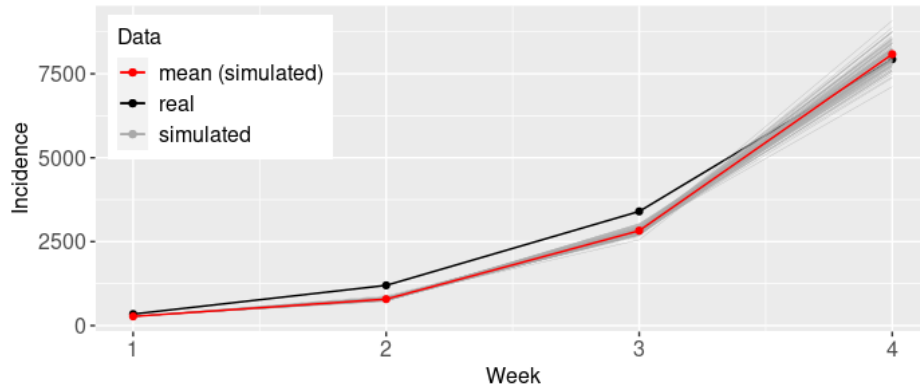


Figure 5: Incidence (symptomatic infections) of COVID-19 based on estimated transmission rate compared to the incidence according to the data.

2.2.2 Influenza

The subset of the data is chosen such that the beginning (increasing part) of a wave is represented. A total population of 17 million individuals is used (approximately corresponding to the population size of the Netherlands) with 1,100 infectious cases (500 exposed, 301 symptomatic and 199 asymptomatic⁵). It is assumed that there are no recovered individuals and that no individuals have died from infection. The parameters are fixed to be equal to those used in the co-circulation model. The standard deviation for the normal distribution of the proposal value is 0.18.

Figure 6 shows the trace plots for the different chains with a (smoothed) histogram of the final sample. The trace plots show that the chains seem to have reached convergence. Table 5 shows the initial values of for the chains with the respective estimated value of β and acceptance rate. The estimated rate of transmission for influenza is 0.3. This corresponds to a value of R_0 of 1.21, which is in line with estimates from scientific literature ([4]). Figure 7 shows a graph of the real data and the simulated curves from the model with estimated value of β .

⁵Different numbers of initial infections have been explored and the number chosen corresponds to the one that produces data that best approximates the real data.

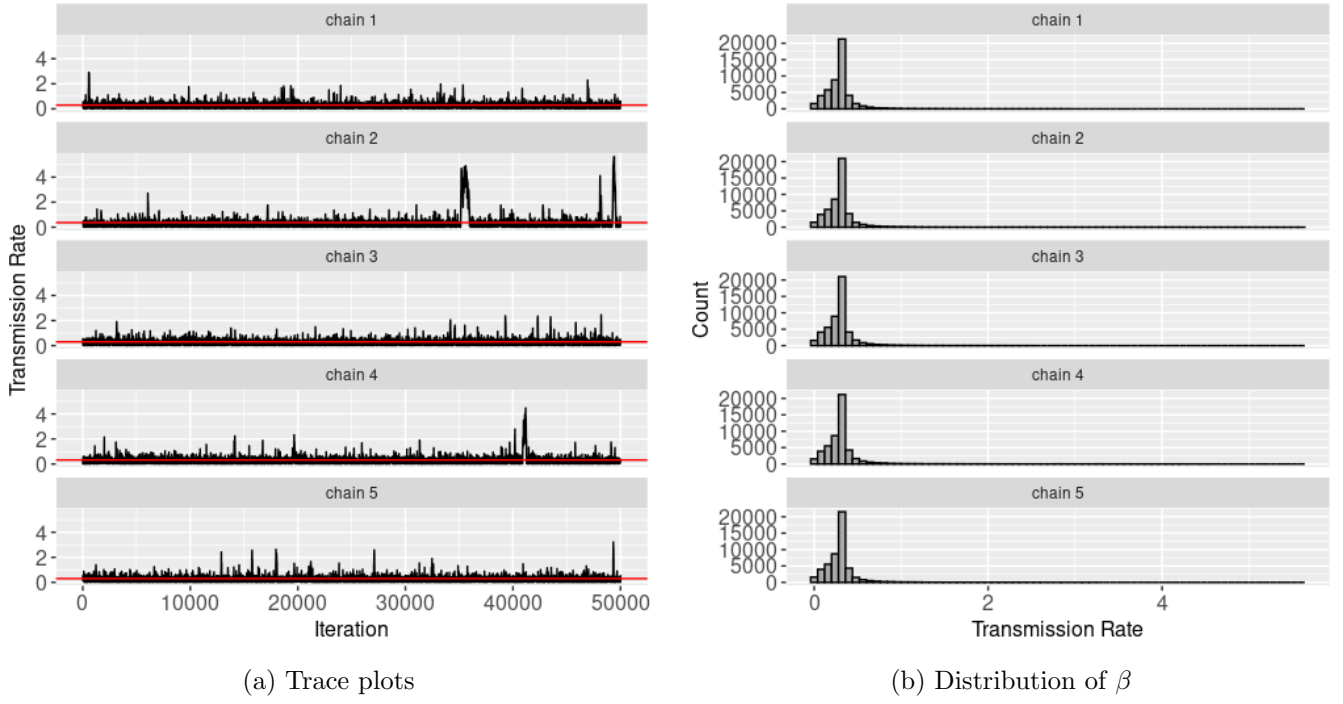


Figure 6: Graphs for the assessment of convergence of the MCMC chains and the quality if the final sample for influenza.

chain	β_0	β	acceptance rate
1	0.5	0.29957	0.58132
2	0.8	0.30129	0.58460
3	1.0	0.30018	0.58247
4	1.5	0.30042	0.58702
5	2.0	0.29950	0.57873
final estimate		0.300	0.5828

Table 5: Results of the different chains of the MCMC estimation of β for COVID-19 along with the final estimate.

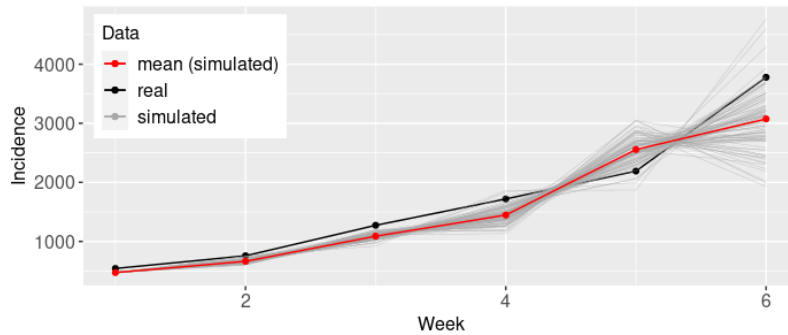


Figure 7: Incidence (symptomatic infections) of influenza based on estimated transmission rate compared to the incidence according to the data.

2.3 Theoretical Derivation of the Basic Reproduction Number

Given the high estimate of the transmission rate of COVID-19 obtained during the fitting procedure, the basic reproduction number R_0 is theoretically derived to be able to set the transmission rate for the use in the simulation study. The basic reproduction number is one of the most important parameters to describe the spread of an infectious disease and indicates how contagious a disease is. More specifically, it indicates the average number of secondary infections caused by a single infectious individual in a fully susceptible population. This means that for an R_0 larger than 1, an outbreak is possible. The larger R_0 , the faster the disease spreads. An R_0 smaller than 1 does not result in an outbreak and eventually gets extinct. To compute the reproduction number for compartmental models, a method called next generation approach has been developed ([10]).

The system of ODE's (Table B3 in the Appendix) is divided into disease classes (E , I_a and I_s) and non-disease classes (S , R and D). The next generation matrix \mathbf{G} is a matrix that contains elements g_{ij} that represent the expected number of cases in disease-class i caused by a single infected individual in disease-class j . To build this matrix, the computation of two vectors is needed: the vector \mathbf{f} contains the different ways that new infections can occur and vector \mathbf{v} contains the different ways that infections can be transferred from one class to another.

$$\mathbf{f} = \begin{pmatrix} \frac{S}{N}(I_a\beta_a + I_s\beta_s) \\ 0 \\ 0 \end{pmatrix} \text{ and } \mathbf{v} = \begin{pmatrix} -\gamma E \\ \gamma\gamma_a E - \delta I_a \\ \gamma(1 - \gamma_a)E - \delta I_s \end{pmatrix} \quad (8)$$

The next generation matrix \mathbf{G} is the product of two components: $\mathbf{F} = \frac{\partial f_i(x_0)}{\partial x_j}$ and \mathbf{V}^{-1} with $\mathbf{V} = \frac{\partial v_i(x_0)}{\partial x_j}$ and x_0 corresponding to the disease-free equilibrium state (at which $E = I_a = I_s = R = D = 0$, hence $S = N$ and $S/N = 1$).

$$\mathbf{G} = \mathbf{F}\mathbf{V}^{-1} = \begin{pmatrix} 0 & \beta_a & \beta_s \\ 0 & 0 & 0 \\ 0 & 0 & 0 \end{pmatrix} \begin{pmatrix} \frac{-1}{\gamma} & 0 & 0 \\ -\frac{\gamma_a}{\delta} & \frac{-1}{\delta} & 0 \\ \frac{-(1-\gamma_a)}{\delta} & 0 & \frac{-1}{\delta} \end{pmatrix} = \begin{pmatrix} \frac{\beta_a\gamma_a}{\delta} + \frac{\beta_s\gamma_s}{\delta} & \frac{-\beta_a}{\delta} & \frac{-\beta_s}{\delta} \\ 0 & 0 & 0 \\ 0 & 0 & 0 \end{pmatrix} \quad (9)$$

R_0 is the leading Eigenvalue of \mathbf{G} .

$$R_0 = \frac{\beta_a\gamma_a + \beta_s(1 - \gamma_a)}{\delta} \quad (10)$$

Details of the computations can be found in the Appendix.

3 Simulation Study

The co-circulation model is used to perform a simulation study for different scenarios. First, the scenarios are described in Section 3.1. Next, the general settings of the simulations are listed in Section 3.2. Section 3.3 contains a list of summary measures used to describe the results. Finally, the results of the study are shown in Section 3.4.

3.1 Scenarios

The goal of the first scenario is to explore the dynamics of COVID-19 and Influenza without the effects of immunity. First, the spread of the diseases is simulated when they are circulating separately (independence). This is done by introducing one disease at day 0 and setting the introduction time of the other disease to be higher than the number of days in a simulation. Next, the simultaneous circulation of both diseases is simulated by introducing both pathogens at day 0. The population is assumed to be

fully susceptible and is not vaccinated ($\omega_1 = \omega_2 = 0$). Heterologous immunity is not considered in this scenario by setting the parameters $\hat{\lambda}_{1i} = \hat{\lambda}_{2i} = \hat{\Lambda}_{1i} = \hat{\Lambda}_{2i} = 1$. Without heterologous immunity, the only interaction between both diseases is through the assumption that co-infection is not possible. Therefore, this scenario mainly shows the impact of that assumption. The scenario with co-circulation is considered to be the baseline scenario.

Vaccination is an important intervention when it comes to controlling an epidemic. When (a portion of) the population is vaccinated, the dynamics of the diseases are expected to change. Scenario 2 studies these changes. An individual can either be not vaccinated at all, vaccinated against COVID-19 but not influenza, against influenza but not COVID-19 or against both diseases. The vaccine efficacy is assumed to be 86.3% for COVID-19 ([14]) and 34.9% for influenza ([26]) in line with results from the literature (see Section 2.2). The vaccination rate is chosen such that a certain coverage is attained after 1 month. To simulate a realistic scenario, two different values are selected, corresponding to 85% (corresponding to the vaccination rate of the general population in Belgium, [3]) of the population being vaccinated against COVID-19 and 22.6% (corresponding to the vaccination rate of the general population in the Netherlands, [15]) of the population being vaccinated against Influenza after one month. This results in a high vaccination rate for COVID-19 and a low vaccination rate for influenza. Heterologous immunity is not considered in this scenario by setting the parameters $\hat{\lambda}_{1i} = \hat{\lambda}_{2i} = \hat{\Lambda}_{1i} = \hat{\Lambda}_{2i} = 1$.

The basic reproduction number of the current COVID-19 strain is lower than that of the original strain (that is considered in this thesis). Therefore, scenario 3 explores the co-dynamics of both diseases when they have the same basic reproduction number. This results in a transmission rate of $\beta_1 = 0.137$. The population is assumed to be fully susceptible and is not vaccinated ($\omega_1 = \omega_2 = 0$). Heterologous immunity is not considered in this scenario by setting the parameters $\hat{\lambda}_{1i} = \hat{\lambda}_{2i} = \hat{\Lambda}_{1i} = \hat{\Lambda}_{2i} = 1$. Since a large number of simulations turn out to show still active infections after 500 days, the simulations are performed for 1000 days.

In the co-circulation model, the effect of heterologous immunity becomes important as it is expected to impact the disease dynamics. Heterologous immunity is assumed to reduce an individual's susceptibility by $(1 - \lambda) \cdot 100\%$. Scenario's 4, 5 and 6 explore the effect of heterologous immunity. The magnitude of the heterologous effect is varied in each scenario while keeping all other parameters constant. The vaccine with the lowest protective effect against infection considered in this thesis is that of influenza ($\sim 36\%$) and Assuming that any homologous effect is more powerful than a heterologous effect, four values for the latter one are chosen to vary between 0 and 30% (corresponding to parameter values of $\lambda = \{1, 0.9, 0.8, 0.7\}$). The heterologous effects are assumed to be equal for both diseases. In scenario 4, the effect of heterologous immunity is explored without taking into account vaccination ($\omega_1 = \omega_2 = 0$). Scenario 5 is similar to scenario 4, but the less aggressive strain of COVID-19 is considered ($\beta_1 = 0.137$). Since for a considerable amount of simulations, there are still new infections after 500 days, therefore, the duration of a simulation is prolonged to 1000 days. Vaccination has the potential to greatly impact the course of an epidemic. With vaccination, the heterologous immune effect is expected to play a bigger role since more individuals have acquired immunity than in the case where it could only be acquired naturally. Scenario 6 aims at investigating the effect of heterologous immunity in a vaccinated population (as described in scenario 2). The original COVID-19 strain is considered ($\beta_1 = 0.375$).

3.2 Simulation Settings

The simulation study is performed with a stochastic model. This implies that each simulation is subject to this stochasticity and yields different results. A large number of simulations is performed and summary statistics of the quantities of interest are computed. The number of simulations should be sufficiently large to present clear and stable results. To determine the number of simulations needed to achieve a stable outcome, the mean attack rate, peak prevalence and peak moment is shown for an increasing number

of simulations (Figure 8). It appears that all three quantities are relatively stable at 1000 simulations. Therefore, it seems reasonable to run 1000 simulations for each scenario.

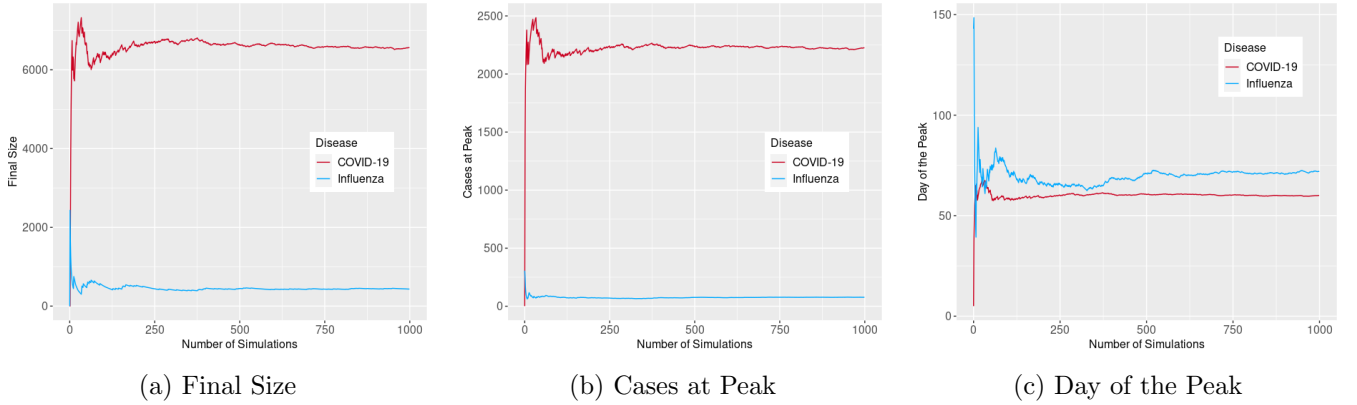


Figure 8: Mean quantities for an increasing number of simulations.

A simulation runs in time steps of one day. The duration of one simulation should not be shorter than the duration of any outbreaks since the quantities of interest can be misleading in that case (think of attack rate that cannot be computed correctly as long as the virus is still active and causing new infections). Therefore, 1000 simulations with 500 days each have been examined. The day of the last new infection is recorded for COVID-19 and Influenza. Figure 9 shows the distribution of the days of the last infections. The latest day of the last infection for any of the diseases in all simulations is day 488. Therefore, it seems reasonable simulate an epidemic for 500 days.

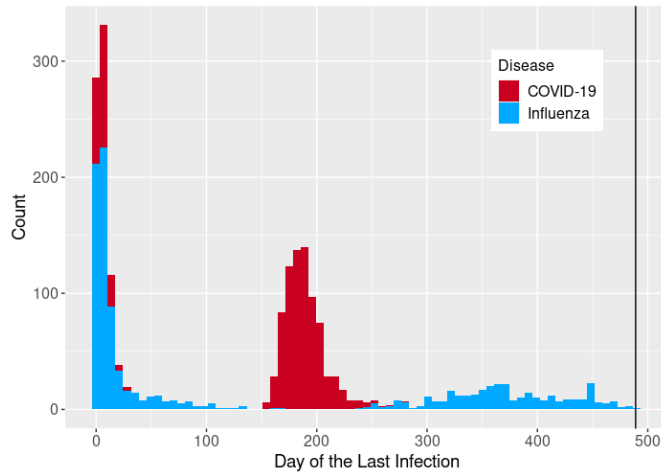


Figure 9: Histogram of the days of the last infection for all simulations. The vertical line indicates the maximum.

A single index case is introduced in a population of size 10,000 at day 0 for each of the diseases. The parameter values for each simulation correspond to the values in Table B1 unless stated otherwise. For the transmission rate of COVID-19, value of that is more in line with scientific literature has been chosen rather than the estimate from the fitting procedure, namely $\beta = 0.375$ which corresponds to $R_0 = 3.3$.

3.3 Representation of Results

To evaluate an epidemic, different metrics are at our disposal. This simulation study focuses the following quantities computed for each simulated epidemic:

- **Attack Rate:** The attack rate or final size is defined as the proportion of the population that got infected throughout the entire running time. Both symptomatic as well as asymptomatic infections are considered. The attack rate is reported for COVID-19 and influenza separately. This metric helps to understand the scale of an outbreak and the extent of the population that is affected. It informs the authorities about the scale of interventions needed, such as the distribution of vaccines, medications, or other healthcare resources. It also provides valuable insights into the transmissibility of a disease. The attack rate is also used to evaluate the effectiveness of vaccination programs.
- **Extinction Probability:** The extinction probability indicates how likely an infectious disease is to die out in a population without causing a (major) outbreak. In a deterministic model, the basic reproduction number R_0 is a well known threshold to determine whether a pathogen will cause an outbreak or whether it will get extinct. In a stochastic model, the probability of extinction is closely related to the basic reproduction number and can be approximated by $R_0^{-I_0}$ (with I_0 the initial number of index cases) for models with one infectious group ([2]) which is not the case for the co-circulation model proposed. Therefore, an approach based on the distribution of attack rates is applied. The distribution of attack rates is typically bimodal and allows for a clear cutoff between "very small" (outbreaks) and "larger" (no outbreaks) values. This cutoff is determined graphically (through a histogram). Practically, the extinction probability is the proportion of simulations that result in very small attack rates. When no cutoff can be determined, the extinction probability is not computed. The extinction probability is computed for COVID-19 and influenza separately. Examining the extinction probability can help in assessing the effectiveness of public health interventions.
- **Cases (Prevalence) at Peak:** The cases at peak is the largest number of simultaneously infected (symptomatic as well as asymptomatic) individuals (prevalence). It is analysed for both diseases separately as well as both diseases combined (daily sum of the prevalences). The prevalence at peak helps to understand how quickly a disease spreads and is a key metric that informs a wide range of strategic decisions aimed at minimizing the impact of an outbreak. It is crucial to determine the potential burden on the health care system (hospital capacity, ICU beds, medical staff availability, ...) and to plan allocation of resources. It is also an important metric that drives policy makers to implement interventions.
- **Day of the Peak:** The day of the peak indicates when the maximum number of cases will occur and is expressed in days since the start of the simulation. It is analyzed for each disease separately as well as for both diseases combined. The timing of the peak is important for the preparedness of the healthcare system and for the timing of public health interventions. By understanding when the peak is likely to occur, interventions can be timed to flatten the curve and reduce the peak prevalence, thereby mitigating the spread of the disease.
- **Duration of an Outbreak:** The duration of an outbreak is defined as the number of days between the first infection and the last recovery. It is important to note that only non-extinct simulations are considered. For scenarios in which the probability of extinction cannot be computed, this quantity is ignored. The duration of an outbreak gives an idea about the intensity of an epidemic. Very long outbreaks with a relatively low attack rate are often less problematic than very short outbreaks with a large final size. However, the duration of an outbreak can have an important psychological impact on the population.

Apart from the duration of an outbreak, all quantities are computed for the totality of simulations, not only for those that are considered to be outbreaks. Quantities are represented relative to the entire population size and is therefore expressed in percent (or as a value in the interval $[0; 1]$). Since the model

is of stochastic nature, each simulation yields different results and therefore, the full distribution of the different metrics is shown as well as the mean and the 95% quantile range.

3.4 Results

3.4.1 Scenario 1: Co-circulation versus Independence

The results of the baseline scenario (co-circulation) are reported first and then compared to the scenario without interaction.

The extinction probability is more than three times lower for COVID-19 (20.8%) than for influenza (66.7%). COVID-19 affects a larger proportion of the population on average (75.7%) than influenza (14.4%). This is no surprise given the higher basic reproduction number for COVID-19. Even though major influenza outbreaks on average affect less people in total, they are much longer (375 days, 95% quantile interval [261;488]) than major COVID-19 outbreaks (190 days 95% quantile interval [164;230]). The peak for both diseases combined occurs on average at day 74 with a prevalence of 22.6% at peak. The mean prevalence at peak is 22.3% for COVID-19 (on day 60) and 0.8% for influenza (on day 72).

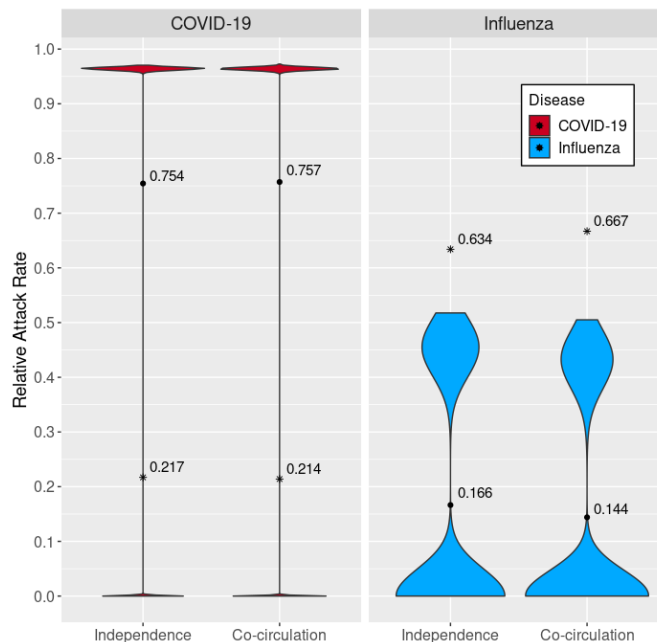


Figure 10: (Scenario 1) Distribution of relative attack rates of COVID-19 and influenza for the scenarios with independence and with co-circulation. The black dots represent the mean attack rates. The asterisk represents the probability of extinction.

Figure 10 shows that the interaction between both diseases through the impossibility of co-infection causes less major outbreaks for influenza (probability of extinction increases with 3.3%) and the mean attack rate decreases with 2.2% compared to independence. The duration of major influenza outbreaks is increased on average by 47 days on average with co-circulation (see Figure 12). Figure 11 shows that the moment of the influenza peak is delayed by 9 days on average for influenza when both diseases interact while the prevalence at peak remains unaffected. Co-circulation appears to have no impact on the dynamics of COVID-19. Qualitatively similar observations are made when considering outbreaks only (see Figures C1, C2 and C3 in the Appendix). Tables C1 and C2 in the Appendix provide 95% quantile ranges as well as all summary statistics for major outbreaks only.

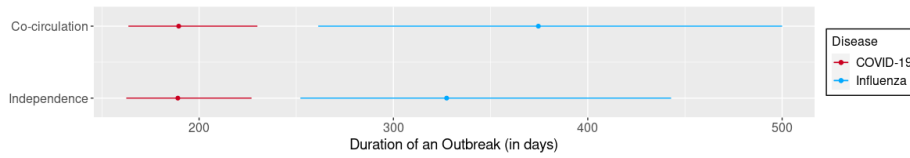


Figure 12: (Scenario 1) Mean duration of influenza and COVID-19 major outbreaks with 95% quantile ranges for the scenarios with independence and with co-circulation.

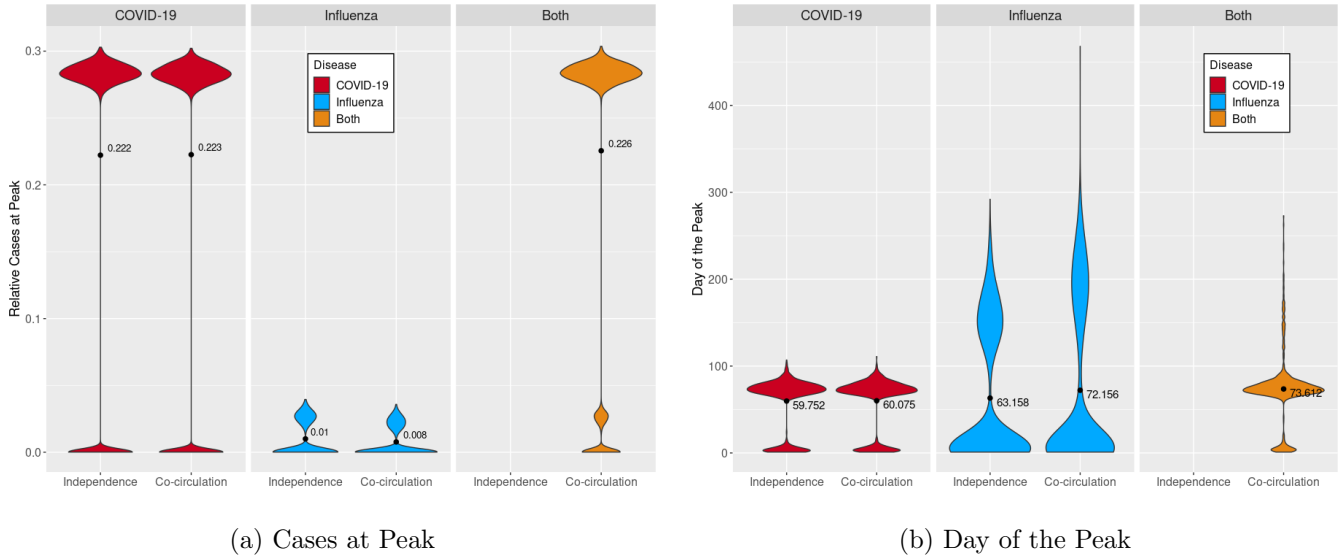


Figure 11: (Scenario 1) Distributions related to the peak for COVID-19 and influenza for the scenarios with independence and with co-circulation. The black dots represent the means of the distributions.

3.4.2 Scenario 2: Effect of Vaccination

The scenario with vaccination is compared to the baseline scenario.

Vaccination effectively decreases the attack rates of both diseases to very low levels (0.4% for COVID-19 and 2.4% for influenza), as shows Figure 13. The extinction probability can no longer be computed according to the definition given in Section 3.3 since the distributions is no longer bimodal. It appears that all simulations get extinct or at least no large outbreaks occur. The maximum attack rate for COVID-19 is 2.7% in the case of vaccination. For influenza, the maximum attack rate is higher (23.2%) but no clear cut-off value can be determined for major outbreaks versus extinction.

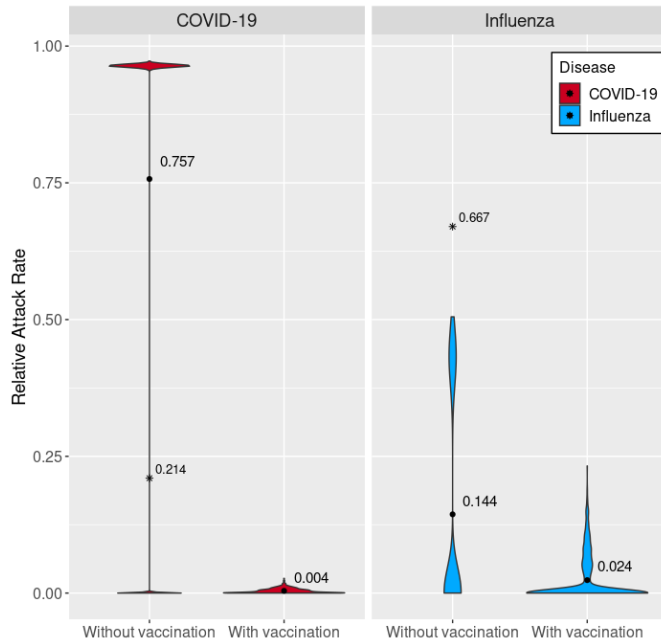
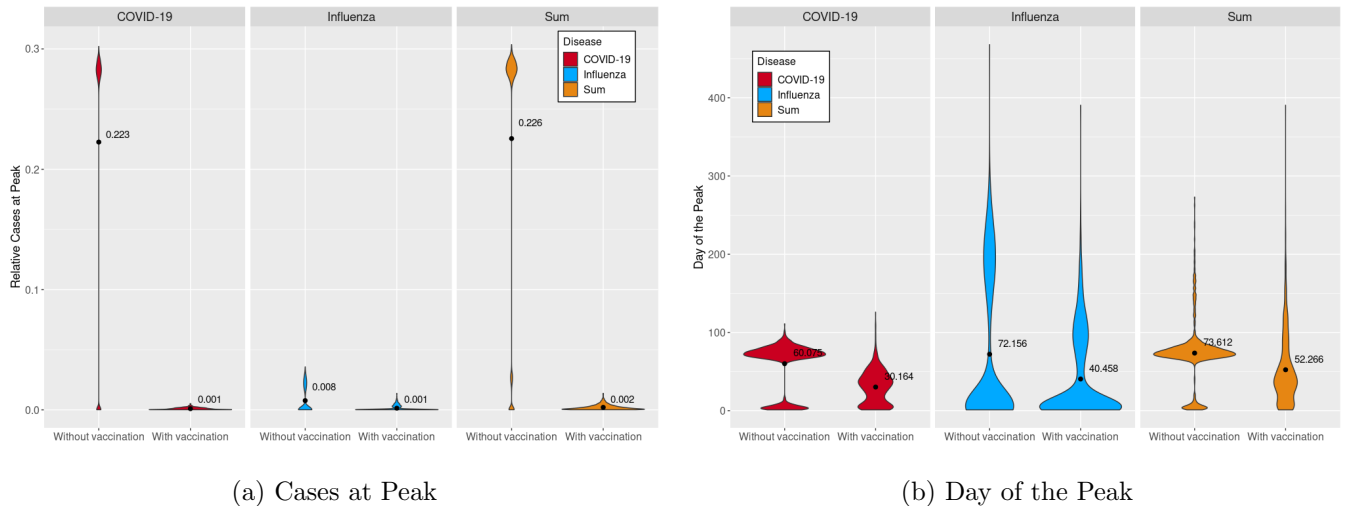


Figure 13: (Scenario 2) Distribution of relative attack rates of COVID-19 and influenza for the scenarios with and without vaccination. The black dots represent the mean attack rates. The asterisk represents the probability of extinction.

Figure 14 shows that also the mean prevalences at peak are decreased by vaccination. Both diseases combined on average only affect at most 0.2% of the population while this is 0.1% for COVID-19 and influenza. The moment of the peak occurs 21 days earlier for both diseases combined (day 52) and about a month earlier for COVID-19 (day 50) as well as influenza (day 40). Tables C3 and C4 in the Appendix provide 95% quantile ranges.



(a) Cases at Peak

(b) Day of the Peak

Figure 14: (Scenario 3A) Distributions related to the peak for COVID-19 and influenza for the scenarios with and without vaccination. The black dots represent the means of the distribution.

3.4.3 Scenario 3: Less Aggressive COVID-19

The scenario with a less aggressive strain of COVID-19 is compared to the baseline scenario. When a less aggressive variant of COVID-19 is considered, less people are affected by COVID-19 (as can be expected). The mean attack rate is drastically decreased to 12.7% (see Figure 15) and the mean prevalence at peak is

decreased to 0.7% (see Figure 16a) with a peak that occurs on average 51 days later. The mean duration of a major outbreak increases significantly for COVID-19 to 659 days. 95% of all major COVID-19 outbreaks are longer than 486 days. For Influenza, an opposite trend is observed: the mean attack rate is slightly increased to 15.8% and the mean prevalence at peak is increased to 0.9% for a peak that occurs on average 13 days earlier. The mean duration of a major outbreak decreases slightly to 328 days which means that COVID-19 outbreaks are on average much longer than for influenza, also shown in Figure 17. When considering major outbreaks only, the observations are quantitatively similar (see Figures C4, C5 and C6 in the Appendix). Also for the extinction probabilities, the trend is opposite for the two diseases: it increases to 67.2% for COVID-19 but decreases slightly to 64.9% for Influenza.

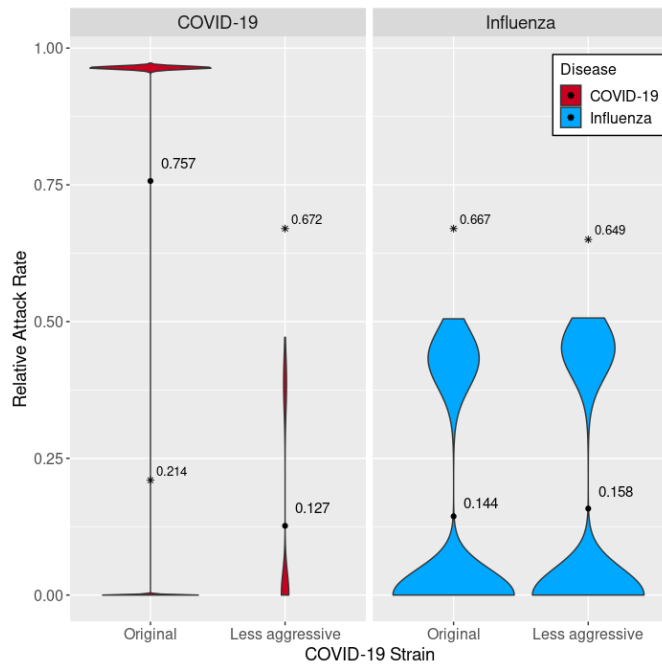


Figure 15: (Scenario 3) Distribution of relative attack rates of COVID-19 and influenza for the scenarios with the original and a less aggressive COVID-19 strain. The black dots represent the mean attack rates. The asterisk represents the probability of extinction.

Figure 16 shows that the moment of the peak occurs on average nearly 2 months (59 days) later for both diseases combined. On average, only 1.5% of the population is affected by either COVID-19 or influenza at the peak. Tables C5 and C6 in the Appendix provide 95% quantile ranges.

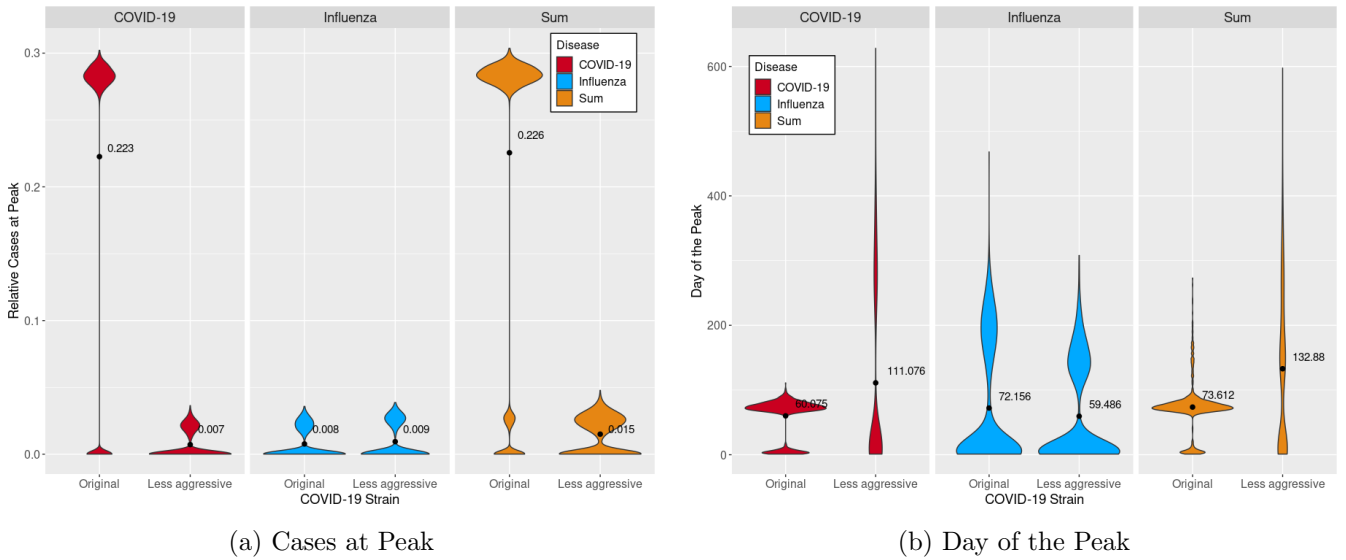


Figure 16: (Scenario 3) Distributions related to the peak for COVID-19 and influenza for the scenarios with the original and a less aggressive COVID-19 strain. The black dots represent the means of the distributions.

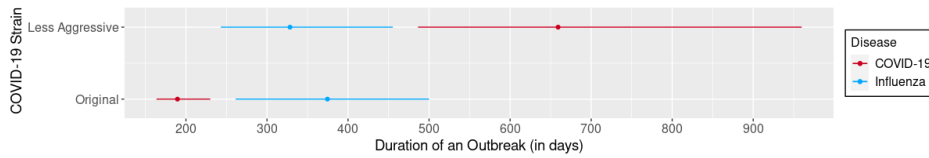


Figure 17: (Scenario 3) Mean duration of influenza and COVID-19 major outbreaks with 95% quantile ranges for the scenarios with independence and with co-circulation.

3.5 Scenario 4: Co-Circulation Accounting for Heterologous Immunity

The baseline scenario corresponds to the scenario without immunity (0%) and is compared to the scenarios with protective effects of 10, 20 and 30%. Individuals who have recovered from COVID-19 are less susceptible to infection with influenza and vice versa. A decreasing attack rate is observed in Figure 19 for influenza with increasing heterologous effect (14.4, 11.6, 5.5 and 2.5 % for heterologous effect of {0, 10, 20, 30}, respectively). However, this effect is not visible when only outbreaks are taken into account (see Figure C7 in the Appendix). The extinction probabilities and the mean duration of major outbreaks (Figure 18) do not appear to be affected by heterologous immunity. However, the upper bound of the 95% quantile range of major outbreak duration decreases with increasing heterologous effect.

Figure 20 shows that as heterologous immunity increases, the peak occurs earlier on average (with small irregularities) and the prevalence at peak is lower for influenza. The prevalence at peak as well as the day of the peak are not affected by heterologous immunity.

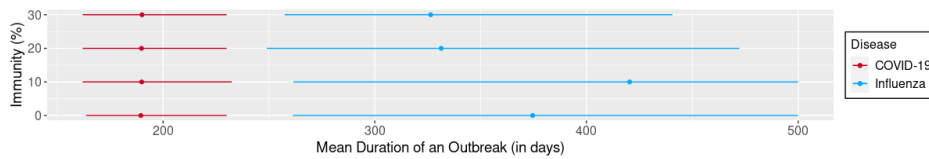


Figure 18: (Scenario 4) Mean duration of influenza and COVID-19 outbreaks with 95% percentile range for 4 different levels of heterologous immunity effect (0, 10, 20 and 30%).

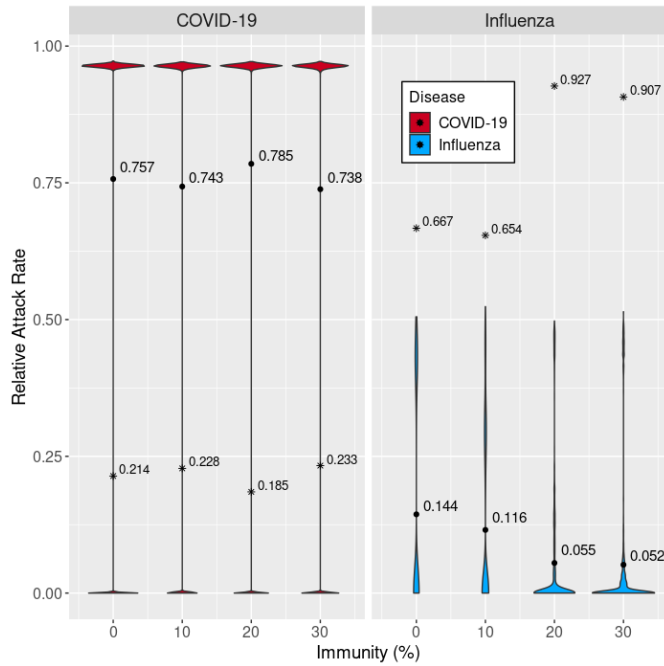


Figure 19: (Scenario 4) Distribution of relative attack rates of COVID-19 and influenza for the scenarios with no (0%), low (10%), moderate (20%) and high (30%) heterologous effect on the susceptibility to infection. The black dots represent the mean attack rates. The asterisk represents the probability of extinction.

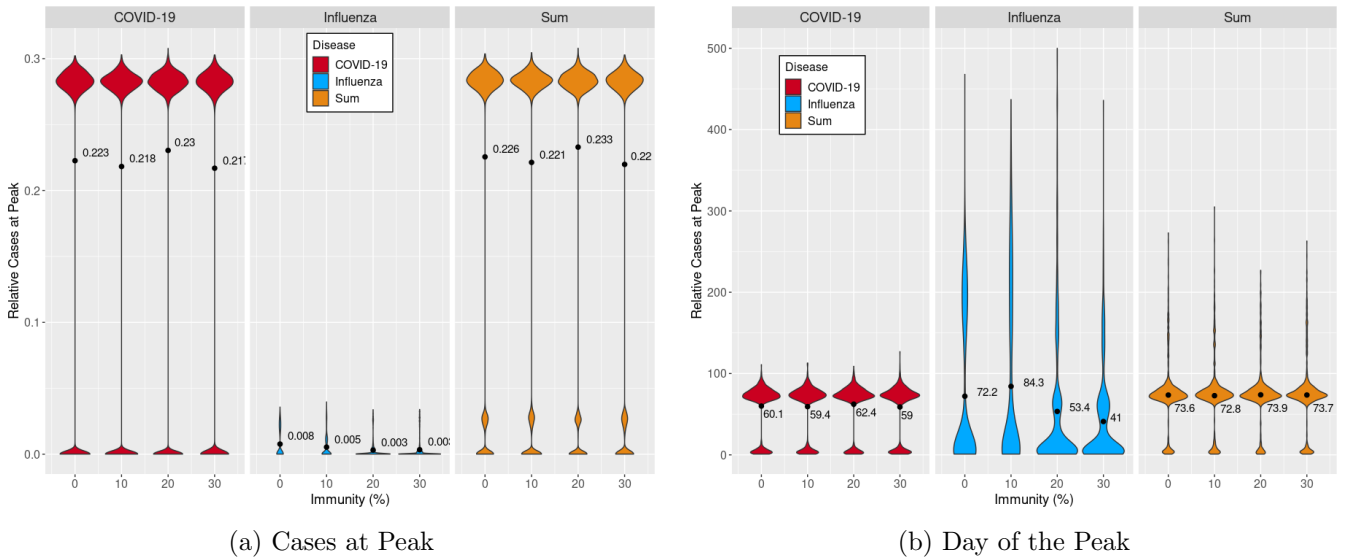


Figure 20: (Scenario 4) Distributions related to the peak for COVID-19 and influenza for the scenarios with no (0%), low (10%), moderate (20%) and high (30%) heterologous effect on the susceptibility to infection. The black dots represent the means of the distributions.

3.6 Scenario 5: Co-Circulation Accounting for Heterologous Immunity with a less Aggressive Variant of COVID-19

The heterologous effect causes the number of COVID-19 infections to decrease both, overall and at peak. The mean attack rates are 11.7% for low, 9.9% for moderate and 9.8% for high heterologous immunity compared to 12.7% for no immunity. The prevalences at peak are 0.6% for low and 0.5% for moderate and high heterologous immunity compared to 0.7% for no immunity. These trends are also observed when

only major outbreaks are taken into account (see Figures C10 and C11 in the Appendix). Figure 23 shows that major COVID-19 outbreaks become slightly longer on average with increasing heterologous effect (668 days for low, 679 days for moderate and 683 days for high heterologous immunity compared to 659 days for no immunity). An effect on the dynamics of influenza or both diseases combined is not observed. The moment of the peak does not appear to be affected either.

Although the trend is not monotonic, the extinction probability shows an increasing trend for COVID-19 and a decreasing trend for influenza with increasing heterologous immunity (see Figure 21).

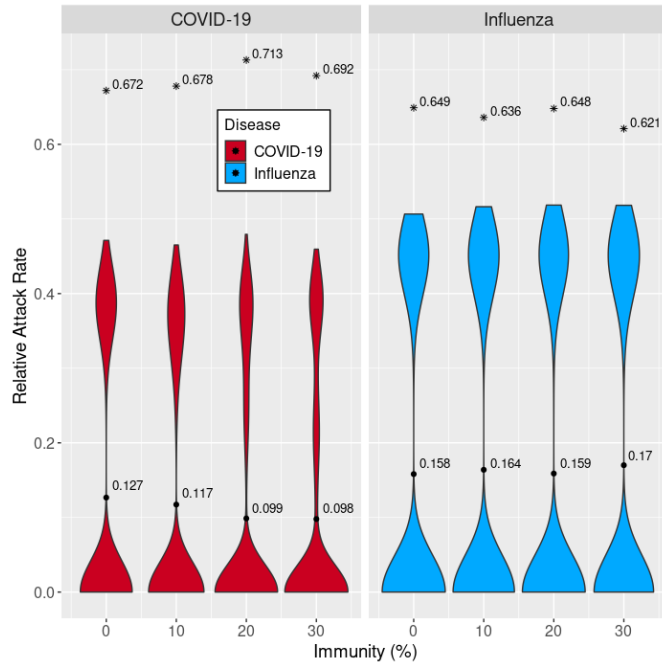
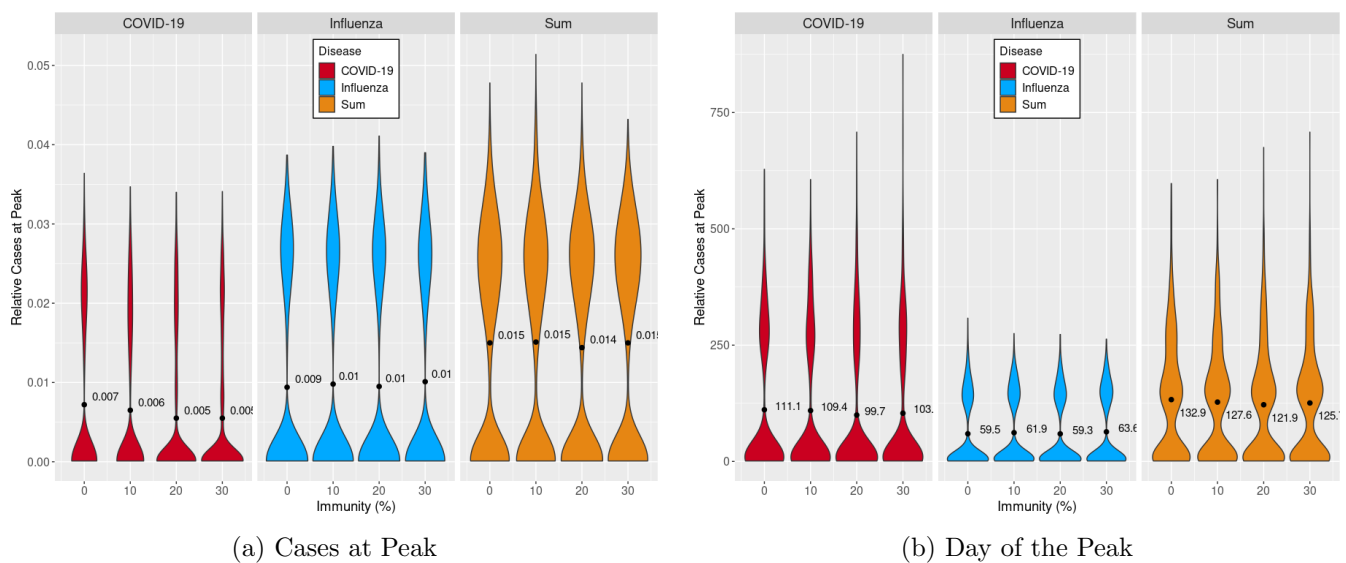


Figure 21: (Scenario 5) Distribution of relative attack rates of COVID-19 (less aggressive variant) and influenza for the scenarios with no (0%), low (10%), moderate (20%) and high (30%) heterologous effect on the susceptibility to infection. The black dots represent the mean attack rates. The asterisk represents the probability of extinction



(a) Cases at Peak

(b) Day of the Peak

Figure 22: (Scenario 2B) Distributions related to the peak for COVID-19 (less aggressive variant) and influenza for the scenarios with no (0%), low (10%), moderate (20%) and high (30%) heterologous effect on the susceptibility to infection. The black dots represent the means of the distributions

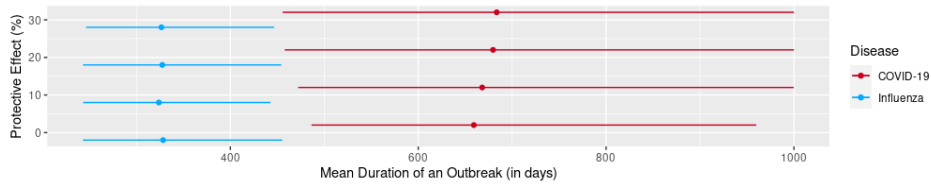


Figure 23: (Scenario 5) Mean duration of influenza and COVID-19 outbreaks with 95% percentile range for 4 different levels of heterologous immunity (for the scenarios with no (0%), low (10%), moderate (20%) and high (30%) heterologous effect on the susceptibility to infection).

3.7 Scenario 6: Heterologous Immunity Effect with Vaccination

Figure 24 shows a clear decline in influenza infections both, overall and at peak. The mean attack rates are 1.6% for low, 0.9% for moderate and 0.5% for high heterologous immunity compared to 2.4% for no immunity and the prevalences at peak are 0.11% for low, 0.07% for moderate and 0.05% for high heterologous immunity compared to 0.14% for no immunity. The influenza peak occurs several days earlier with increasing heterologous effect (day 39 for low, day 31 for moderate and day 23 for high heterologous immunity compared to day 41 for no immunity). The trends regarding the peak of the epidemic (prevalence as well as moment) are also observed for both diseases combined. No effects are observed for COVID-19, but an effect of unobservable magnitude cannot be ruled out.

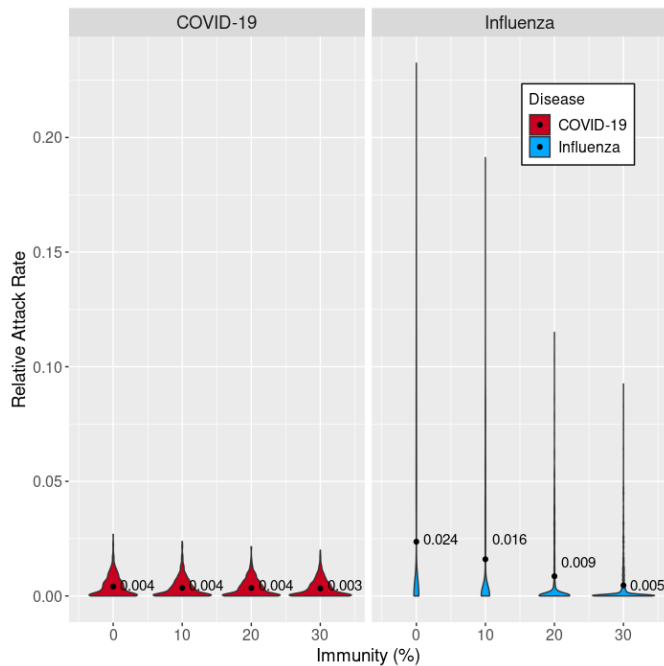


Figure 24: (Scenario 6) Distribution of relative attack rates of COVID-19 and influenza for the scenarios with no (0%), low (10%), moderate (20%) and high (30%) heterologous effect on the susceptibility to infection in combination with vaccination and considering the original COVID-19 strain. The black dots represent the mean attack rates.

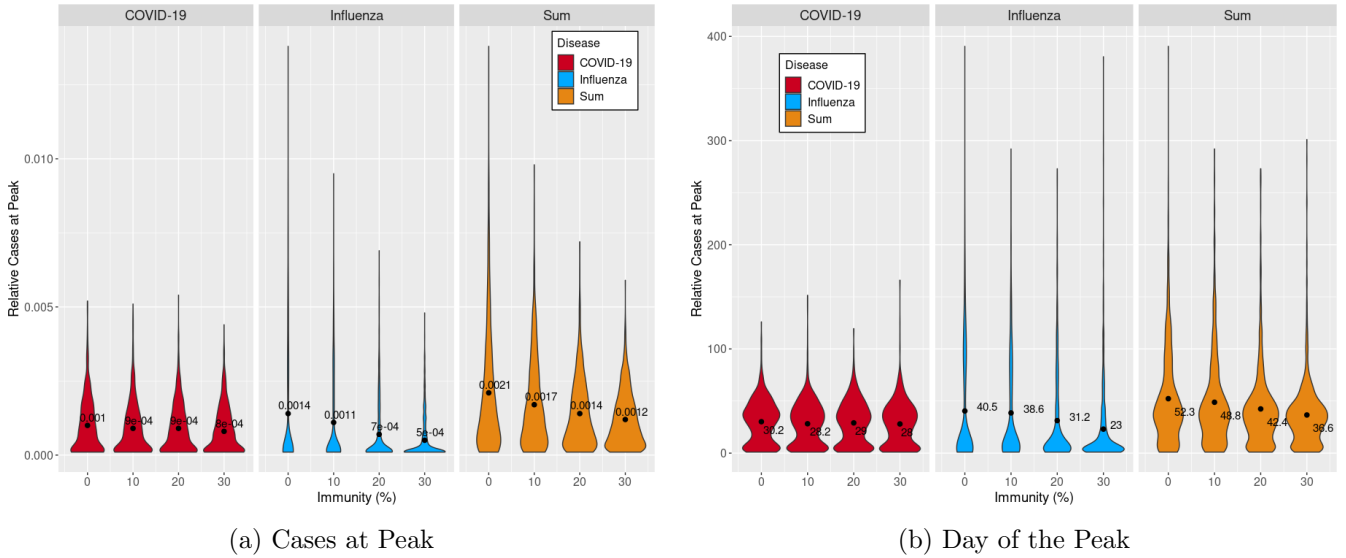


Figure 25: (Scenario 6) Distributions for both diseases combined and for the two diseases separately, for the scenarios with no (0%), low (10%), moderate (20%) and high (30%) heterologous effect on the susceptibility to infection in combination with vaccination and considering the original COVID-19 strain. The black dots represent the mean attack rates.

4 Discussion

4.1 Interpretation of Results

Scenario 1 shows the effect impact of co-circulation on the dynamics of both diseases. If co-infection is ruled out, the exposed and infected individuals are not susceptible to the other disease during the latent and infectious periods, meaning that the number of susceptibles is lower. The high transmission rate of COVID-19 results in a significant number of people becoming infected with the disease, and the relatively long latent and infectious periods means that a large number of people can temporarily not be infected with influenza. The combination of a low number of simultaneous influenza infections and the reduced number of susceptible people means that the extinction probability increases. The same reasoning explains the decline in mean attack rate. This decrease is not driven by the increase in extinction probability as it can be observed even when only major outbreaks are taken into account. In principle, the same applies to COVID-19, however, no effect is visible. This is likely due to the lower number of influenza infections compared to COVID-19 infections and associated smaller decline in those susceptible. In addition, the latent and infectious periods for influenza are much shorter, meaning that the number of individuals (temporarily) not susceptible to COVID-19 is relatively small which explains that no impact on COVID-19 is observed.

Scenario 2 shows that vaccination is indeed a very effective way to reduce the number of infections (both, overall and at peak) to the point where major outbreaks no longer occur. The vaccine efficacy and vaccination rate are higher for COVID-19 than for influenza, which explains the stronger impact on the dynamics of COVID-19.

Scenario 3 shows that a less aggressive COVID-19 strain causes fewer COVID-19 infections. Since there is an interaction between the two diseases, a change in COVID-19 also leads to changes in the spread and dynamics of influenza. Counter intuitively, more people are affected by influenza when COVID-19 is less aggressive, both overall and at peak. Since no form of immunity is taken into account in this scenario, this increase is likely due to the assumption that co-infection is not possible. If fewer people are affected by COVID-19, fewer people are temporarily excluded from influenza infection. In this scenario, the two

diseases have the same basic reproduction and their extinction probabilities are similar. The increase in extinction probability is expected for COVID-19 because this quantity is closely related to the basic reproduction number. An influenza outbreak is slightly shorter compared to the baseline scenario but has a higher peak, while a COVID-19 outbreak lasts much longer but is also much "flatter" compared to the baseline scenario. Because COVID-19 circulates in the population for a long time, the assumption that immunity lasts forever and that re-infection is not possible becomes unrealistic. If re-infection is considered, it can be expected that COVID-19 will not die out, will circulate constantly and thus become a much greater persistent threat.

The effect of a heterologous immune reaction was also investigated. This effect becomes important once an individual has acquired homologous immunity either through infection or vaccination. If vaccination is not considered (scenarios 4 and 5), heterologous immunity only becomes relevant once individuals have recovered. For the original COVID-19 strain (scenario 4), effects are only observed for influenza. Since the number of COVID-19 recoveries is relatively large compared to the number of influenza recoveries (and therefore the number of individuals with reduced susceptibility to COVID-19), which limits the impact of the protective effect, the heterologous effect is expected to be larger for influenza. The peak of both diseases together is largely driven by COVID-19, which explains why no effect is observed for both diseases together, although an effect is observed for influenza. However, when a less aggressive COVID-19 strain is considered (scenario 5), effects of heterologous immunity are observed for COVID-19 but not no longer for influenza. In this scenario, the number of individuals affected by COVID-19 is, on average, significantly smaller than with the original strain and is, on average, even lower than the number of individuals affected by influenza, causing the heterologous effect to become visible for COVID-19. When a portion of the population is vaccinated against a disease, that portion is less susceptible to the disease in question due to the homologous immune response and the vaccinated population is also slightly less susceptible to the other disease. As more individuals are vaccinated against COVID-19, the effect of this type of immunity is expected to be more visible for influenza. Also, the heterologous immunity effect is stronger relative to the homologous effect for influenza than it is for COVID-19. For COVID-19, the homologous immunity effect is very strong, reducing the attack rates to very low levels. The heterologous effect is expected to lower it even more, but the possible effect is of course less strong.

4.2 Limitations and Future Research

This thesis uses a mathematical modeling approach to study the co-dynamics of COVID-19 and influenza and investigate the effects of homologous and heterologous immunity on these dynamics. A model is always a simplification of reality that requires a number of assumptions. While these assumptions simplify the model and the mathematics involved, they have important implications.

The model assumes a constant population. In reality, populations undergo constant change due to births, deaths and migration. Ignoring these factors can lead to oversimplification that may not capture the full dynamics of disease spread. It also introduces limitations in terms of realism and long-term accuracy. However, by keeping the population constant, the model focuses exclusively on the transmission dynamics of the diseases (in this case, COVID-19 and influenza), making it easier to isolate the effects of interest. Given the relatively short time frame of a simulation, only minimal changes in the population are expected with negligible impact on the results, making this assumption acceptable.

The population is assumed to be homologous, meaning that each individual in the population is considered equal in terms of disease parameters. In fact, age affects the susceptibility to COVID-19 and the probability of developing symptoms ([9]). Due to differences in contact patterns, different transmission rates are assumed among different age groups ([21]). In the future, the model should be adapted to account for different age groups. Another possible extension is the inclusion of risk factors.

The model assumes that if an individual is infected with one disease, they cannot be infected with the

other disease. Although it is possible to become infected with both diseases simultaneously, the prevalence of co-infection with COVID-19 and influenza reported in the literature is low ([31], [20]), so this assumption is not expected to have a significant effect on the results.

Although this model includes immunity, it is in many ways a simplification of reality. First of all, no distinction is made between natural and vaccine-induced immunity and both are assumed to be constant. This also implies that an individual cannot be re-infected with the same disease. Studies show that for both diseases, the immunity wanes after a certain period of time, making re-infection possible. For influenza, the prevalence of re-infection was low and the time between two consecutive infections was relatively high in most cases, suggesting that the assumption made is acceptable given the duration of a simulation ([33], [27]). However, for COVID-19, the literature suggests that re-infection is possible in a shorter period of time ([5], [22]) and neglecting this could lead to a lower number of COVID-19 infections, which in turn has an impact on influenza infections depending on the situation, as shown by the results of this thesis. When considering re-infections, care should be taken to describe different disease courses in such cases, if the data indicate this. No distinction is made between infection-induced and vaccine-induced heterologous immunity. Furthermore, it is assumed that the heterologous effects are the same for both diseases and that immunity only affects the susceptibility of an individual. Once data on these mechanisms is available, the assumptions in the model can be relaxed without further adjustments.

In the model, vaccination of the susceptible population occurs at rate ω . The number of individuals vaccinated at a certain time is a stochastic process that depends on the number of susceptible individuals. On average, this means: the more susceptible individuals, the more vaccinations. That is not how it works in a real population. In general, the number of people who can be vaccinated in a given period (e.g. per day) can be expected to be relatively constant or perhaps increases over time (as capacity increases). The rate is also expected to decline towards the end, as most individuals who want to get vaccinated have already done so. In addition, the rate is calibrated so that the vaccination coverage in Belgium is reached after about a month. Thereafter, the fully susceptible population continues to be vaccinated at the same rate and eventually the entire susceptible population is vaccinated. The model assumes full the effect of the vaccine after a single dose and immediately after vaccination. In fact, not every individual in a population is equally likely to get vaccinated. This is not taken into account in this model and should be considered as an aspect of a more heterogeneous population. In the future, adjustments to the vaccination parameters should be made so that the population is only vaccinated up to a certain coverage and that the vaccination is not dependent on the number of susceptible individuals.

Estimation of the transmission rate was carried out using an adapted likelihood-free MCMC method, since the computation of the likelihood is problematic in this case. In the future, suitable methods for approximate Bayesian computation (ABC) should be explored. The Metropolis-Hastings algorithm used has the advantage of being easily implemented but its performance is sensitive to the choice of the proposal distribution. The tuning of the standard deviation of the proposal distribution was performed through a trial-and-error approach, there is no guarantee that it is close to optimal. Other methods should be explored such as gradient-based approaches or Hamiltonian Monte Carlo methods, which avoid the random walk that negatively affects the efficiency of the algorithm. Furthermore, the proposal distribution is truncated (restricted to strictly positive values). Currently, this is not taken into account when computing the acceptance probability. Methods that avoid the use of a truncated proposal distribution should be explored (such as parameter transformation). Alternatively, the use of a truncated proposal distribution should be properly accounted for.

Selecting a set of model parameters from the literature is not trivial. Both diseases are constantly evolving and so are their characteristics. Furthermore, a wide range of methods and data have been used to determine parameter values, consequently leading to a wide range of possible values. It is a big challenge to choose the values that best suit this particular model. The impact of parameter choices on the results should be examined in a sensitivity analysis in the future.

Analysis of the results is based on all infections, symptomatic and asymptomatic. However, not all infections pose a problem for public health. While asymptomatic cases play an important role in the spread of a disease, they do not directly affect the healthcare system. Symptomatic individuals however can place a burden on general practitioners and pharmaceutical supplies, but also on economy, for example through absenteeism from work. Some symptomatic individuals may require intensive medical care through hospitalization. This is not directly included in the model and should be accounted for in a possible extension, including different effects of immunity on the likelihood of being hospitalized. The same holds for disease-related deaths. They are incorporated in the model but the probability of death is not yet influenced by any form of immunity.

All co-circulation scenarios in this work introduce both pathogens simultaneously. The impact of different introduction times should be studied as influenza is considered a seasonal threat while COVID-19 can be considered a persistent threat. In addition to a different approach to modeling vaccination, other policies related to vaccination should also be considered. A flexible running time can be considered in which a simulation automatically stops as soon as there are no more infectious individuals present. This avoids unnecessary long running times and stopping simulations while epidemics are still ongoing.

4.3 Ethical Considerations

The work presented involves simulation studies in which no human individuals were directly affected. The data used is publicly available and not personally identifiable, ensuring privacy and confidentiality. Some ethical considerations related to mathematical modeling of infectious diseases are discussed.

Ultimately, the model is intended to serve as guidance and support for decision makers. It is crucial to ensure that the model is accurate and transparent, as misleading results can lead to inappropriate policy decisions, potentially harming public health. Therefore the structure of the model as well as assumptions, limitations, and uncertainties associated with the results are clearly communicated.

Decisions should not solely be based on the results of this model, but other aspects such as real-world feasibility and societal impact should also be included in the decision making process. In particular, the impact of interventions on different population groups should be considered. Although no specific interventions are proposed based on the results of the simulation study, potential interventions focus on immunization of individuals and, more specifically, vaccination. Interventions should always aim to maximize benefits and minimize harm to the population, protecting public health while aiming to respect individual autonomy. While vaccines generally support the principles of beneficence and non-maleficence, vaccine hesitancy and equitable access to vaccines are important factors to keep in mind.

A model should be as realistic as possible to ensure its applicability and relevance. The model parameters were selected in accordance with scientific literature and real world data were used to fit the model. The simulated scenarios realistic.

The stakeholders of the presented co-circulation model include researchers in infectious disease modeling and public health officials, as well as healthcare providers, vaccine manufacturers and the general public.

5 Conclusion

Since COVID-19 and influenza are expected to co-exist for the foreseeable future, understanding the spread and co-dynamics of both diseases is critical. A key component in the interaction between COVID-19 and influenza is the presence of a heterologous immune response. Here, a stochastic compartmental model is proposed that allows modeling the co-circulation of both diseases and offers the possibility of incorporating vaccine-induced homologous immunity and vaccine-induced as well as infection-induced heterologous immunity in a very flexible way. Once better information on transmission parameters or vaccination be-

comes available, the model can be easily adapted and also extended to include compartments such as patient isolation, hospitalization or severity of infection if needed. The proposed model allows for conducting a wide variety of simulation studies that help contribute to understanding the complex dynamics of COVID-19 and influenza and shed light on the role of heterologous immunity. It also allows testing different vaccination strategies to help policymakers make informed decisions. Further research on this type of immunity is needed to provide high-quality estimates for model parameters.

This work shows that when preparing for future epidemics, it is not sufficient to model the spread and dynamics of both diseases separately to estimate their combined impact. It is important to account for their interaction to make more accurate predictions. It is shown that the interaction between COVID-19 and influenza results in the the total number of influenza infections, as well as the peak prevalence and the probability of major outbreaks, being lower than if both diseases were assumed to circulate independently. However, taking this interaction into account, influenza outbreaks last longer on average. This is important information for organizing health care, as a longer but smaller epidemic requires different preparation. The simulation study also shows that these impacts depend on the transmission potential of COVID-19, demonstrating the importance of keeping model parameters as current as possible at all times. It also shows that the transmission rate of COVID-19 has a major impact on the duration of an outbreak, which in turn impacts how healthcare services operate.

Although little is known about the extent of a heterologous immune effect between COVID-19 and influenza, this study shows that it impacts the number of infections of the disease at a lower transmission rate. It also shows that when the population is vaccinated (assuming a significantly higher vaccination rate and higher protection for COVID-19), the heterologous effect leads to a decrease in influenza infections and the total number of infections (for both diseases combined). The results motivate further research on how the effects of heterologous immunity can be exploited to develop optimal vaccination strategies, and the proposed model provides a solid framework for this.

Acknowledgements

I thank my supervisor Prof. Andrea Torneri for the time and energy he invested in supervising this thesis project, for constructive discussions and feedback and for allowing me to take the initiative in making decisions about this research and last but not least for believing in me. I thank Prof. Dr. Niel Hens for giving me the opportunity to communicate my research interests and to initiate the first contact with my supervisor. Last but not least, I thank my husband and children for emotional support and understanding during the time of this thesis and throughout my studies.

References

- [1] S Abrams et al. “Modelling the early phase of the Belgian COVID-19 epidemic using a stochastic compartmental model and studying its implied future trajectories”. In: *Epidemics* 35 (2021). DOI: 10.1016/j.epidem.2021.100449.
- [2] L Allen and G Lahodny. “Extinction thresholds in deterministic and stochastic epidemic models”. In: *Journal of Biological Dynamics* 6 (2 2012), pp. 590–611. DOI: 10.1080/17513758.2012.665502.
- [3] F Berete et al. “Vaccinatie Gezondheidsenquête 2018 (Sciensano)”. In: (2019). URL: https://www.sciensano.be/sites/default/files/va_nl_2018.pdf.
- [4] M Biggerstaff et al. “Estimates of the reproduction number for seasonal, pandemic, and zoonotic influenza: a systematic review of the literature”. In: *2014* 14 (480 2014). DOI: <https://doi.org/10.1186/1471-2334-14-480>.
- [5] Stein Caroline et al. “Past SARS-CoV-2 infection protection against re-infection: a systematic review and meta-analysis”. In: *The Lancet* 104 (10379 2023). DOI: [https://doi.org/10.1016/S0140-6736\(22\)02465-5](https://doi.org/10.1016/S0140-6736(22)02465-5).
- [6] Fabrice Carrat et al. “Time Lines of Infection and Disease in Human Influenza: A Review of Volunteer Challenge Studies”. In: *American Journal of Epidemiology* 167.7 (2008), pp. 775–785. DOI: 10.1093/aje/kwm375.
- [7] A. Cori et al. “Estimating influenza latency and infectious period durations using viral excretion data”. In: *Epidemics* 4.3 (2012), pp. 132–138. ISSN: 1755-4365. DOI: <https://doi.org/10.1016/j.epidem.2012.06.001>. URL: <https://www.sciencedirect.com/science/article/pii/S175543651200031X>.
- [8] D Cucinotta and M Vanelli. “WHO Declares COVID-19 a Pandemic”. In: *Acta Biomed* 19 (2020), pp. 157–160. DOI: 10.23750/abm.v91i1.9397.
- [9] Nicholas G. Davies et al. “Age-dependent effects in the transmission and control of COVID-19 epidemics”. In: *Nature Medicine* 26 (2020), pp. 1205–1211. DOI: 10.1038/s41591-020-0962-9.
- [10] O Diekmann, J A P Heesterbeek, and J A J Metz. “On the definition and the computation of the basic reproduction ratio R_0 in models for infectious diseases in heterogeneous populations”. In: *Journal of Mathematical Biology* 28 (4 1990), pp. 365–382. DOI: 10.1007/BF00178324.
- [11] Günther Fink et al. “Inactivated trivalent influenza vaccination is associated with lower mortality among patients with COVID-19 in Brazil”. In: *BMJ evidence-based medicine* (2020). DOI: 10.1136/bmjebm-2020-111549.
- [12] Molenberghs Geert et al. “COVID-19 mortality, excess mortality, deaths per million and infection fatality ratio, Belgium, 9 March 2020 to 28 June 2020”. In: *Euro Surveill.* 27.7 (2022). URL: <https://doi.org/10.2807/1560-7917.ES.2022.27.7.2002060>.
- [13] Xi He et al. “Temporal dynamics in viral shedding and transmissibility of COVID-19”. In: *Nature Medicine* 26.5 (2020), pp. 672–675. DOI: 10.1038/s41591-020-0869-5. URL: <https://doi.org/10.1038/s41591-020-0869-5>.
- [14] Paul T. Heath et al. “Safety and Efficacy of NVX-CoV2373 Covid-19 Vaccine”. In: *New England Journal of Medicine* 385.13 (2021), pp. 1172–1183. DOI: 10.1056/NEJMoa2107659. eprint: <https://www.nejm.org/doi/pdf/10.1056/NEJMoa2107659>. URL: <https://www.nejm.org/doi/full/10.1056/NEJMoa2107659>.
- [15] M Heins et al. “Monitor Vaccinatiegraad Nationaal Programma Grieppreventie (NPG) 2022”. In: *Utrecht: Nivel* (2023).

- [16] Seyed M. Hosseini-Moghaddam et al. “Association of Influenza Vaccination With SARS-CoV-2 Infection and Associated Hospitalization and Mortality Among Patients Aged 66 Years or Older”. In: *JAMA Network Open* 5.9 (2022), e2233730–e2233730. DOI: 10.1001/jamanetworkopen.2022.33730. URL: <https://doi.org/10.1001/jamanetworkopen.2022.33730>.
- [17] T Kneip, A Börsch-Supan, and K Andersen-Ranberg. “Social, health and economic impact of the COVID-19 pandemic from a European perspective”. In: *International Journal of Ageing* 14 (2022), pp. 789–792. DOI: 10.1007/s10433-022-00744-9.
- [18] Ruiyun Li et al. “Substantial undocumented infection facilitates the rapid dissemination of novel coronavirus (SARS-CoV-2)”. In: *Science* 368.6490 (2020), pp. 489–493. DOI: 10.1126/science.abb3221.
- [19] Daniela Marin-Hernandez, Robert E Schwartz, and Douglas F Nixon. “Epidemiological evidence for association between higher influenza vaccine uptake in the elderly and lower COVID-19 deaths in Italy”. In: *Journal of medical virology* 93.1 (2021). DOI: 10.1002/jmv.26120. URL: <https://pubmed.ncbi.nlm.nih.gov/32497290/>.
- [20] Dadashi Masoud et al. “COVID-19 and Influenza Co-infection: A Systematic Review and Meta-Analysis”. In: *Frontiers in Medicine* 8.681469 (2021). DOI: 10.3389/fmed.2021.681469.
- [21] Joël Mossong et al. “Social Contacts and Mixing Patterns Relevant to the Spread of Infectious Diseases”. In: *PLOS Medicine* 5 (3 2008). DOI: 10.1371/journal.pmed.0050074.
- [22] Nhu Ngoc Nguyen et al. “SARS-CoV-2 Reinfection and Severity of the Disease: A Systematic Review and Meta-Analysis”. In: *Viruses* 15 (4 2023). DOI: 10.3390/v15040967.
- [23] M Nicola et al. “The socio-economic implications of the coronavirus pandemic (COVID-19): A review”. In: *International Journal of Surgery* 78 (2020), pp. 185–193. DOI: 10.1016/j.ijssu.2020.04.018.
- [24] H Nishiura et al. “Estimation of the asymptomatic ratio of novel coronavirus infections (COVID-19)”. In: *International journal of infectious diseases* 94 (2020), pp. 154–155. DOI: 10.1016/j.ijid.2020.03.020.
- [25] World Health Organization. “Statement on the Fifteenth Meeting of the International Health Regulations (2005) Emergency Committee Regarding the Coronavirus Disease (COVID-19) Pandemic”. In: (2023). URL: [https://www.who.int/news/item/05-05-2023-statement-on-the-fifteenth-meeting-of-the-international-health-regulations-\(2005\)-emergency-committee-regarding-the-coronavirus-disease-\(covid-19\)-pandemic?adgroupsurvey=%7Badgroupsurvey%7D%26gclid=EAIaIQobChMI40jtsdbe_gIVjQRyCh07igt4EAAAYASACEgJ9pfD_BwE%26fbclid=IwAR2M8EAYiSrAodX582nHkP2AigpSX8pYIsLsPwqYh4SG26RGokGe7E](https://www.who.int/news/item/05-05-2023-statement-on-the-fifteenth-meeting-of-the-international-health-regulations-(2005)-emergency-committee-regarding-the-coronavirus-disease-(covid-19)-pandemic?adgroupsurvey=%7Badgroupsurvey%7D%26gclid=EAIaIQobChMI40jtsdbe_gIVjQRyCh07igt4EAAAYASACEgJ9pfD_BwE%26fbclid=IwAR2M8EAYiSrAodX582nHkP2AigpSX8pYIsLsPwqYh4SG26RGokGe7E).
- [26] A. Prezzi, X. Saelens, and D. Vandijck. “Epidemiology of influenza over a ten-year period in Belgium: overview of the historical and current evidence”. In: *Virology Journal* 20.1 (2023). DOI: 10.1186/s12985-023-02238-1.
- [27] O Price, FA Birrell, and EJ Mifsud. “Epidemiology of repeat influenza infection in Queensland, Australia”. In: *Epidemiol Infect* 150 (2022). DOI: 10.1017/S0950268822001157.
- [28] Welzijn en Sport Rijksinstituut voor Volksgezondheid en Milieu Ministerie van Volksgezondheid. “Infectieradar”. Version 22-02-2024. In: (2024). URL: <https://www.infectieradar.nl/results>.
- [29] Sciensano. “Confirmed cases by date, age, sex and province”. Version 23-01-2024. In: (2024). DOI: <https://epistat.sciensano.be/covid/>.

- [30] Lone Simonsen et al. “Using Clinical Research Networks to Assess Severity of an Emerging Influenza Pandemic”. In: *Clinical Infectious Diseases* 67.3 (May 2018), pp. 341–349. ISSN: 1058-4838. DOI: 10.1093/cid/ciy088. eprint: <https://academic.oup.com/cid/article-pdf/67/3/341/25156461/ciy088.pdf>. URL: <https://doi.org/10.1093/cid/ciy088>.
- [31] SD Tarzjani et al. “Clinical challenge of co-infection of SARS-CoV-2 with influenza during the influenza circulation season: suggestions for prevention”. In: *Germes* 13.2 (2023). DOI: 10.18683/germs.2023.1384.
- [32] K. Van Kerckhove et al. “The impact of illness on social networks: implications for transmission and control of influenza”. In: *American journal of epidemiology* 178.11 (2013), pp. 1655–1662. DOI: 10.1093/aje/kwt196.
- [33] Jing Wang et al. “Epidemiology of influenza virus reinfection in Guangxi, China: a retrospective analysis of a nine-year influenza surveillance data: Characteristics of influenza virus reinfection”. In: *International Journal of Infectious Diseases* 120 (2022), pp. 135–141. ISSN: 1201-9712. DOI: <https://doi.org/10.1016/j.ijid.2022.04.045>. URL: <https://www.sciencedirect.com/science/article/pii/S120197122200248X>.
- [34] Cheng-Jun Yu et al. “Assessment of basic reproductive number for COVID-19 at global level: A meta-analysis”. In: *Medicine* 100 (18 2021). DOI: 10.1097/MD.00000000000025837.
- [35] Claudio Zanettini et al. “Influenza Vaccination and COVID-19 Mortality in the USA: An Ecological Study”. In: *Vaccines* 9.5 (2021). ISSN: 2076-393X. DOI: 10.3390/vaccines9050427. URL: <https://www.mdpi.com/2076-393X/9/5/427>.

Appendix A - Detailed Model

Deterministic SEIRD Model

The system of ODE's corresponding to a deterministic version of the presented model are shown in the table.

$\frac{d}{dt} S(t) = -S(t)[\beta_{1a}(I_{1a}(t) + \hat{\lambda}_{1i}I_{1a}^+(t)) + \beta_{1s}(I_{1s}(t) + \hat{\lambda}_{1i}I_{1s}^+(t)) + \beta_{2a}(I_{2a}(t) + \hat{\lambda}_{2i}I_{2a}^+(t)) + \beta_{2s}(I_{2s}(t) + \hat{\lambda}_{2i}I_{2s}^+(t))]$
$\frac{d}{dt} E_1(t) = S(t)[\beta_{1a}(I_{1a}(t) + \hat{\lambda}_{1i}I_{1a}^+(t)) + \beta_{1s}(I_{1s}(t) + \hat{\lambda}_{1i}I_{1s}^+(t))] - E_1(t)\gamma_1$
$\frac{d}{dt} I_{1a}(t) = E_1(t)\gamma_1\hat{\gamma}_{1a} - I_{1a}(t)\delta_1$
$\frac{d}{dt} I_{1s}(t) = E_1(t)\gamma_1(1 - \hat{\gamma}_{1a}) - I_{1s}(t)\delta_1$
$\frac{d}{dt} R_1(t) = I_{1a}(t)\delta_1 + I_{1s}(t)\delta_1(1 - \mu_1) - R_1(t)[\beta_{2a}(I_{2a}(t) + \hat{\lambda}_{2i}I_{2a}^+(t)) + \beta_{2s}(I_{2s}(t) + \hat{\lambda}_{2i}I_{2s}^+(t))]$
$\frac{d}{dt} D_1(t) = [I_{1s}(t) + I_{1s}^+(t)]\delta_1\mu_1$
$\frac{d}{dt} E_1^+(t) = R_2(t)[\beta_{1a}(I_{1a}(t) + \hat{\lambda}_{1i}I_{1a}^+(t)) + \beta_{1s}(I_{1s}(t) + \hat{\lambda}_{1i}I_{1s}^+(t))] - E_1^+(t)\gamma_1$
$\frac{d}{dt} I_{1a}^+(t) = E_1^+(t)\gamma_1\hat{\gamma}_{1a}\hat{\Gamma}_{1i} - I_{1a}^+(t)\delta_1$
$\frac{d}{dt} I_{1s}^+(t) = E_1^+(t)\gamma_1(1 - \hat{\gamma}_{1a}\hat{\Gamma}_{1i}) - I_{1s}^+(t)\delta_1$
$\frac{d}{dt} E_2(t) = S(t)[\beta_{2a}(I_{2a}(t) + \hat{\lambda}_{2i}I_{2a}^+(t)) + \beta_{2s}(I_{2s}(t) + \hat{\lambda}_{2i}I_{2s}^+(t))] - E_2(t)\gamma_2$
$\frac{d}{dt} I_{2a}(t) = E_2(t)\gamma_2\hat{\gamma}_{2a} - I_{2a}(t)\delta_2$
$\frac{d}{dt} I_{2s}(t) = E_2(t)\gamma_2(1 - \hat{\gamma}_{2a}) - I_{2s}(t)\delta_2$
$\frac{d}{dt} R_2(t) = I_{2a}(t)\delta_2 + I_{2s}(t)\delta_2(1 - \mu_2) - R_2(t)[\beta_{1a}(I_{1a}(t) + \hat{\lambda}_{1i}I_{1a}^+(t)) + \beta_{1s}(I_{1s}(t) + \hat{\lambda}_{1i}I_{1s}^+(t))]$
$\frac{d}{dt} D_2(t) = [I_{2s}(t) + I_{2s}^+(t)]\delta_2\mu_2$
$\frac{d}{dt} E_2^+(t) = R_1(t)\beta_{2a}(I_{2a}(t) + \hat{\lambda}_{2i}I_{2a}^+(t)) + \beta_{2s}(I_{2s}(t) + \hat{\lambda}_{2i}I_{2s}^+(t)) - E_2^+(t)\gamma_2$
$\frac{d}{dt} I_{2a}^+(t) = E_2^+(t)\gamma_2\hat{\gamma}_{2a}\hat{\Gamma}_{2i} - I_{2a}^+(t)\delta_2\hat{\delta}_{2i}$
$\frac{d}{dt} I_{2s}^+(t) = E_2^+(t)\gamma_2(1 - \hat{\gamma}_{2a}\hat{\Gamma}_{2i}) - I_{2s}^+(t)\delta_2\hat{\delta}_{2i}$
$\frac{d}{dt} R_{12}(t) = I_{2a}^+(t)\delta_a\hat{\delta}_{2i} + I_{2s}^+(t)\delta_s\hat{\delta}_{2i}(1 - \mu_2) + I_{1s}^+(t)\delta_1(1 - \mu_1) + I_{1a}^+(t)\delta_1\hat{\delta}_{1i}$

Table A1: Set of ODE's describing the deterministic version of the simplified Model shown in Figure 1

Detailed Model Schemes and Equations

The first model shows the flow of fully susceptible individuals.

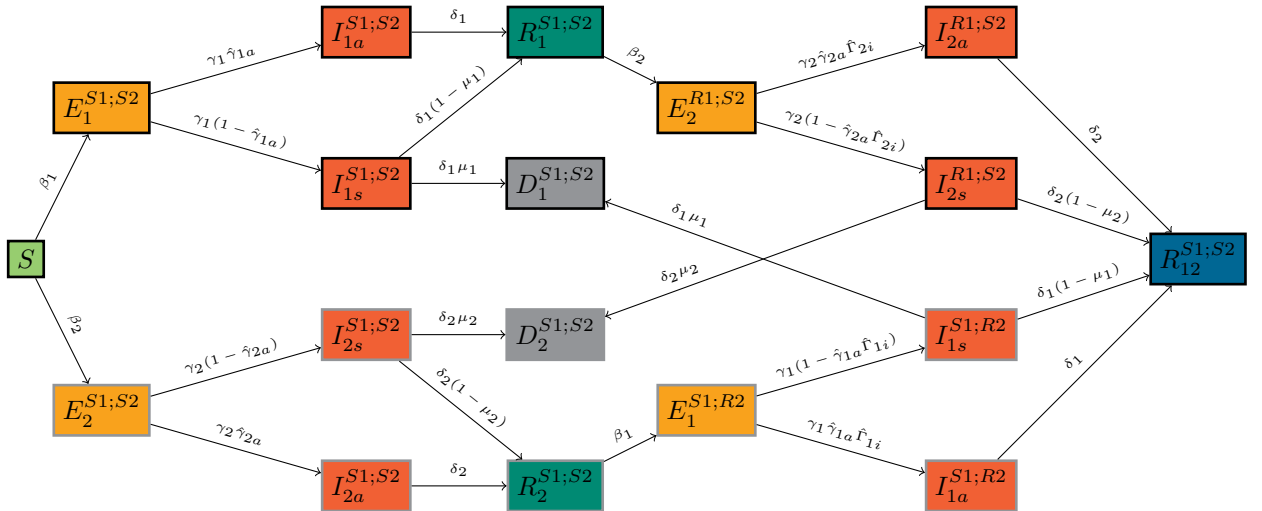


Figure A1: Model 1: disease course for fully susceptible individuals

$$E_1^{*S1S2}(t+\Delta) \sim \text{Bin}\left(S(t), 1 - \exp\left[\frac{-\Delta}{N} \cdot p_1\right]\right)$$

$$\begin{aligned}
& E_1^{*S1R2}(t+\Delta) \sim \text{Bin}\left(R_2^{S1S2}(t), 1 - \exp\left[-\frac{\Delta}{N} \cdot \hat{\Lambda}_{1i} \cdot p_1\right]\right) \\
& p_1 = \beta_{1a} \cdot \left[I_{1a}^{S1S2}(t) + \hat{\lambda}_{1i} \cdot (I_{1a}^{S1R2}(t) + I_{1a}^{S1V2}(t) + I_{1a}^{S1VR2}(t)) + \hat{\lambda}_{1I} \cdot (I_{1a}^{V1S2}(t) + I_{1a}^{V1R2}(t) + I_{1a}^{V1V2}(t) + I_{1a}^{V1VR2}(t)) \right] \\
& \quad + \beta_{1s} \cdot \left[I_{1s}^{S1S2}(t) + \hat{\lambda}_{1i} \cdot (I_{1s}^{S1R2}(t) + I_{1s}^{S1V2}(t) + I_{1s}^{S1VR2}(t)) + \hat{\lambda}_{1I} \cdot (I_{1s}^{V1S2}(t) + I_{1s}^{V1R2}(t) + I_{1s}^{V1V2}(t) + I_{1s}^{V1VR2}(t)) \right] \\
& I_{1a}^{*S1S2}(t+\Delta) \sim \text{Bin}\left(E_1^{S1S2}(t), 1 - \exp[-\Delta \cdot \gamma_1 \cdot \hat{\gamma}_{1a}]\right) \\
& I_{1s}^{*S1S2}(t+\Delta) \sim \text{Bin}\left(E_1^{S1S2}(t), 1 - \exp[-\Delta \cdot \gamma_1 \cdot (1 - \hat{\gamma}_{1a})]\right) \\
& I_{1a}^{*S1R2}(t+\Delta) \sim \text{Bin}\left(E_1^{S1R2}(t), 1 - \exp[-\Delta \cdot \gamma_1 \cdot \hat{\gamma}_{1a} \cdot \hat{\Gamma}_{1i}]\right) \\
& I_{1s}^{*S1R2}(t+\Delta) \sim \text{Bin}\left(E_1^{S1R2}(t), 1 - \exp[-\Delta \cdot \gamma_1 \cdot (1 - \hat{\gamma}_{1a} \cdot \hat{\Gamma}_{1i})]\right) \\
& R_{1a}^{*S1S2}(t+\Delta) \sim \text{Bin}\left(I_{1a}^{S1S2}(t), 1 - \exp[-\Delta \cdot \delta_1]\right) \\
& R_{1s}^{*S1S2}(t+\Delta) \sim \text{Bin}\left(I_{1s}^{S1S2}(t), 1 - \exp[-\Delta \cdot \delta_1 \cdot (1 - \mu_1)]\right) \\
& D_{1s}^{S1S2}(t+\Delta) \sim \text{Bin}\left(I_{1s}^{S1S2}, 1 - \exp[-\Delta \cdot \delta_1 \cdot \mu_1]\right) \\
& D_{1s}^{S1R2}(t+\Delta) \sim \text{Bin}\left(I_{1s}^{S1R2}, 1 - \exp[-\Delta \cdot \delta_1 \cdot \mu_1]\right) \\
& E_2^{*S1S2}(t+\Delta) \sim \text{Bin}\left(S(t), 1 - \exp\left[-\frac{\Delta}{N} \cdot p_2\right]\right) \\
& E_2^{*R1S2}(t+\Delta) \sim \text{Bin}\left(R_1^{S1S2}(t), 1 - \exp\left[-\frac{\Delta}{N} \cdot \hat{\Lambda}_{2i} \cdot p_2\right]\right) \\
& p_2 = \beta_{2a} \cdot \left[I_{2a}^{S1S2}(t) + \hat{\lambda}_{2i} \cdot (I_{2a}^{R1S2}(t) + I_{2a}^{V1S2}(t) + I_{2a}^{VR1S2}(t)) + \hat{\lambda}_{2I} \cdot (I_{2a}^{S1V2}(t) + I_{2a}^{R1V2}(t) + I_{2a}^{V1V2}(t) + I_{2a}^{VR1V2}(t)) \right] \\
& \quad + \beta_{2s} \cdot \left[I_{2s}^{S1S2}(t) + \hat{\lambda}_{2i} \cdot (I_{2s}^{R1S2}(t) + I_{2s}^{V1S2}(t) + I_{2s}^{VR1S2}(t)) + \hat{\lambda}_{2I} \cdot (I_{2s}^{S1V2}(t) + I_{2s}^{R1V2}(t) + I_{2s}^{V1V2}(t) + I_{2s}^{VR1V2}(t)) \right] \\
& I_{2a}^{*S1S2}(t+\Delta) \sim \text{Bin}\left(E_2^{S1S2}(t), 1 - \exp[-\Delta \cdot \gamma_2 \cdot \hat{\gamma}_{2a}]\right) \\
& I_{2s}^{*S1S2}(t+\Delta) \sim \text{Bin}\left(E_2^{S1S2}(t), 1 - \exp[-\Delta \cdot \gamma_2 \cdot (1 - \hat{\gamma}_{2a})]\right) \\
& I_{2a}^{*R1S2}(t+\Delta) \sim \text{Bin}\left(E_2^{R1S2}(t), 1 - \exp[-\Delta \cdot \gamma_2 \cdot \hat{\gamma}_{2a} \cdot \hat{\Gamma}_{2i}]\right) \\
& I_{2s}^{*R1S2}(t+\Delta) \sim \text{Bin}\left(E_2^{R1S2}(t), 1 - \exp[-\Delta \cdot \gamma_2 \cdot (1 - \hat{\gamma}_{2a} \cdot \hat{\Gamma}_{2i})]\right) \\
& R_{2a}^{*S1S2}(t+\Delta) \sim \text{Bin}\left(I_{2a}^{S1S2}(t), 1 - \exp[-\Delta \cdot \delta_2]\right) \\
& R_{2s}^{*S1S2}(t+\Delta) \sim \text{Bin}\left(I_{2s}^{S1S2}(t), 1 - \exp[-\Delta \cdot \delta_2 \cdot (1 - \mu_2)]\right) \\
& D_{2s}^{S1S2}(t+\Delta) \sim \text{Bin}\left(I_{2s}^{S1S2}, 1 - \exp[-\Delta \cdot \delta_2 \cdot \mu_2]\right) \\
& D_{2s}^{R1S2}(t+\Delta) \sim \text{Bin}\left(I_{2s}^{R1S2}, 1 - \exp[-\Delta \cdot \delta_2 \cdot \mu_2]\right) \\
& R_{1a2}^{S1S2}(t+\Delta) \sim \text{Bin}\left(I_{1a}^{S1R2}, 1 - \exp[-\Delta \cdot \delta_1]\right) \\
& R_{1a2}^{V1S2}(t+\Delta) \sim \text{Bin}\left(I_{1a}^{S1R2}, 1 - \exp[-\Delta \cdot \delta_1]\right) \\
& R_{1a2}^{S1V2}(t+\Delta) \sim \text{Bin}\left(I_{1a}^{S1VR2}, 1 - \exp[-\Delta \cdot \delta_1]\right) \\
& R_{1a2}^{V1V2}(t+\Delta) \sim \text{Bin}\left(I_{1a}^{V1VR2}, 1 - \exp[-\Delta \cdot \delta_1]\right) \\
& S_1(t+\Delta) = S_1(t) - E_1^{S1S2}(t+\Delta) - E_2^{S1S2}(t+\Delta) \\
& E_1^{S1S2}(t+\Delta) = E_1^{S1S2}(t) + E_1^{*S1S2}(t+\Delta) - I_{1a}^{*S1S2}(t+\Delta) - I_{1s}^{*S1S2}(t+\Delta) \\
& E_2^{S1S2}(t+\Delta) = E_2^{S1S2}(t) + E_2^{*S1S2}(t+\Delta) - I_{2a}^{*S1S2}(t+\Delta) - I_{2s}^{*S1S2}(t+\Delta) \\
& I_{1a}^{S1S2}(t+\Delta) = I_{1a}^{S1S2}(t) + I_{1a}^{*S1S2}(t+\Delta) - R_{1a}^{*S1S2}(t+\Delta) \\
& I_{1s}^{S1S2}(t+\Delta) = I_{1s}^{S1S2}(t) + I_{1s}^{*S1S2}(t+\Delta) - R_{1s}^{*S1S2}(t+\Delta) - D_1^{*S1S2}(t+\Delta) \\
& I_{2s}^{S1S2}(t+\Delta) = I_{2s}^{S1S2}(t) + I_{2s}^{*S1S2}(t+\Delta) - R_{2s}^{*S1S2}(t+\Delta) - D_2^{*S1S2}(t+\Delta) \\
& I_{2a}^{S1S2}(t+\Delta) = I_{2a}^{S1S2}(t) + I_{2a}^{*S1S2}(t+\Delta) - R_{2a}^{*S1S2}(t+\Delta) \\
& R_1^{S1S2}(t+\Delta) = R_1^{S1S2}(t) + R_{1a}^{*S1S2}(t+\Delta) + R_{1s}^{*S1S2}(t+\Delta) - E_2^{*R1S2}(t+\Delta) \\
& R_2^{S1S2}(t+\Delta) = R_2^{S1S2}(t) + R_{2a}^{*S1S2}(t+\Delta) + R_{2s}^{*S1S2}(t+\Delta) - E_1^{*S1R2}(t+\Delta) \\
& E_2^{R1S2}(t+\Delta) = E_2^{R1S2}(t) + E_2^{*R1S2}(t+\Delta) - I_{2a}^{*R1S2}(t+\Delta) - I_{2s}^{*R1S2}(t+\Delta) \\
& E_1^{S1R2}(t+\Delta) = E_1^{S1R2}(t) + E_1^{*S1R2}(t+\Delta) - I_{1a}^{*S1R2}(t+\Delta) - I_{1s}^{*S1R2}(t+\Delta) \\
& I_{2a}^{R1S2}(t+\Delta) = I_{2a}^{R1S2}(t) + I_{2a}^{*R1S2}(t+\Delta) - R_{12a}^{*S1S2}(t+\Delta) \\
& I_{2s}^{R1S2}(t+\Delta) = I_{2s}^{R1S2}(t) + I_{2s}^{*R1S2}(t+\Delta) - R_{12s}^{*S1S2}(t+\Delta) - D_2^{*R1S2}(t+\Delta) \\
& I_{1s}^{S1R2}(t+\Delta) = I_{1s}^{S1R2}(t) + I_{1s}^{*S1R2}(t+\Delta) - R_{1s2}^{*S1S2}(t+\Delta) - D_1^{*S1R2}(t+\Delta) \\
& I_{1a}^{S1R2}(t+\Delta) = I_{1a}^{S1R2}(t) + I_{1a}^{*S1R2}(t+\Delta) - R_{1a2}^{*S1S2}(t+\Delta)
\end{aligned}$$

$$\begin{aligned}
R_{12}^{S1S2}(t+\Delta) &= R_{12}^{S1S2}(t) + R_{1a2}^{*S1S2}(t+\Delta) + R_{1s2}^{*S1S2}(t+\Delta) + R_{12a}^{*S1S2}(t+\Delta) + R_{12s}^{*S1S2}(t+\Delta) \\
D_1^{S1S2}(t+\Delta) &= D_1^{S1S2}(t) + D_1^{*S1S2}(t+\Delta) + D_1^{*S1R2}(t+\Delta) \\
D_2^{S1S2}(t+\Delta) &= D_2^{S1S2}(t) + D_2^{*S1S2}(t+\Delta) + D_2^{*R1S2}(t+\Delta)
\end{aligned}$$

Table A2: Model 1: stochastic model specification

The next model shows the flow of individuals vaccinated against COVID-19 but not influenza.

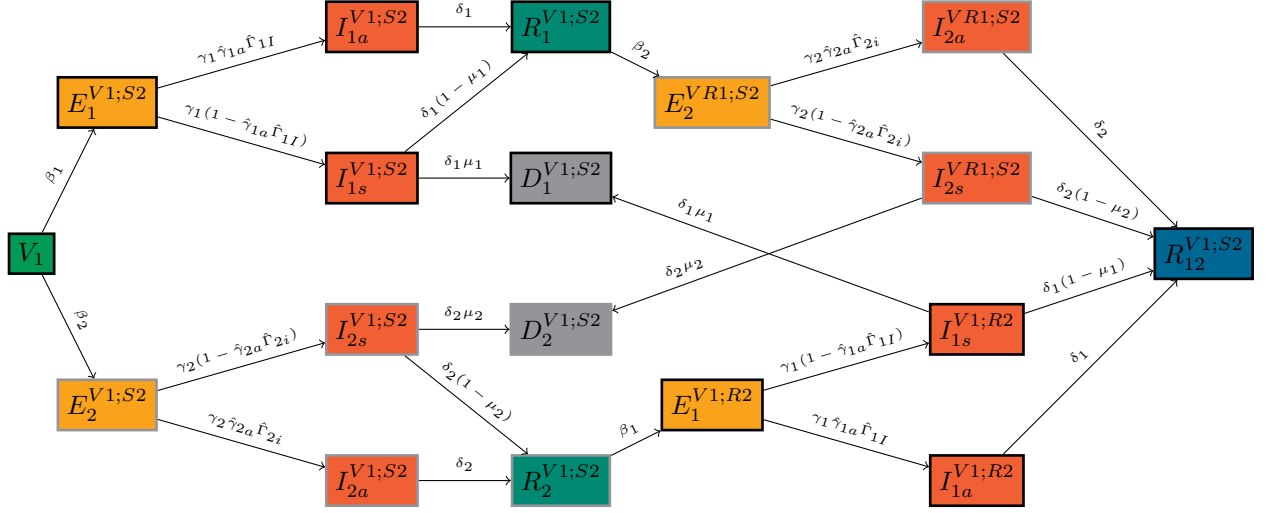


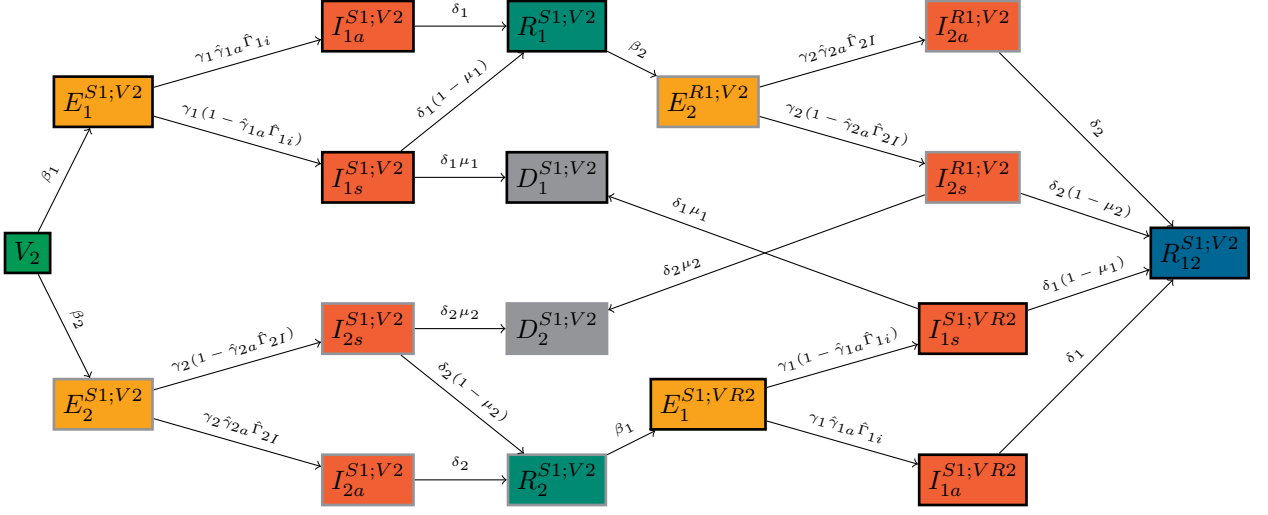
Figure A2: Model 2: disease course for individuals vaccinated against COVID-19 but not influenza

$$\begin{aligned}
V_1^*(t+\Delta) &\sim \text{Bin}(S(t), 1 - \exp[-\Delta \cdot \omega_1]) \\
E_1^{*V1S2}(t+\Delta) &\sim \text{Bin}(V_1(t), 1 - \exp\left[\frac{-\Delta}{N} \cdot \hat{\Lambda}_{1I} \cdot p_1\right]) \\
E_1^{*V1R2}(t+\Delta) &\sim \text{Bin}(R_2^{V1S2}(t), 1 - \exp\left[\frac{-\Delta}{N} \cdot \hat{\Lambda}_{1I} \cdot p_1\right]) \\
p_1 &= \beta_{1a} \cdot \left[I_{1a}^{S1S2}(t) + \hat{\lambda}_{1i} \cdot (I_{1a}^{S1R2}(t) + I_{1a}^{S1V2}(t) + I_{1a}^{S1VR2}(t)) + \hat{\lambda}_{1I} \cdot (I_{1a}^{V1S2}(t) + I_{1a}^{V1R2}(t) + I_{1a}^{V1V2}(t) + I_{1a}^{V1VR2}(t)) \right] \\
&\quad + \beta_{1s} \cdot \left[I_{1s}^{S1S2}(t) + \hat{\lambda}_{1i} \cdot (I_{1s}^{S1R2}(t) + I_{1s}^{S1V2}(t) + I_{1s}^{S1VR2}(t)) + \hat{\lambda}_{1I} \cdot (I_{1s}^{V1S2}(t) + I_{1s}^{V1R2}(t) + I_{1s}^{V1V2}(t) + I_{1s}^{V1VR2}(t)) \right] \\
I_{1a}^{*V1S2}(t+\Delta) &\sim \text{Bin}(E_1^{V1S2}(t), 1 - \exp\left[-\Delta \cdot \gamma_1 \cdot \hat{\gamma}_{1a} \cdot \hat{\Gamma}_{1I}\right]) \\
I_{1s}^{*V1S2}(t+\Delta) &\sim \text{Bin}(E_1^{V1S2}(t), 1 - \exp\left[-\Delta \cdot \gamma_1 \cdot (1 - \hat{\gamma}_{1a}) \cdot \hat{\Gamma}_{1I}\right]) \\
I_{1a}^{*V1R2}(t+\Delta) &\sim \text{Bin}(E_1^{V1R2}(t), 1 - \exp\left[-\Delta \cdot \gamma_1 \cdot \hat{\gamma}_{1a} \cdot \hat{\Gamma}_{1I}\right]) \\
I_{1s}^{*V1R2}(t+\Delta) &\sim \text{Bin}(E_1^{V1R2}(t), 1 - \exp\left[-\Delta \cdot \gamma_1 \cdot (1 - \hat{\gamma}_{1a}) \cdot \hat{\Gamma}_{1I}\right]) \\
R_{1a}^{*V1S2}(t+\Delta) &\sim \text{Bin}(I_{1a}^{V1S2}(t), 1 - \exp[-\Delta \cdot \delta_1]) \\
R_{1s}^{*V1S2}(t+\Delta) &\sim \text{Bin}(I_{1s}^{V1S2}(t), 1 - \exp[-\Delta \cdot \delta_1 \cdot (1 - \mu_1)]) \\
D_{1s}^{V1S2}(t+\Delta) &\sim \text{Bin}(I_{1s}^{V1S2}(t), 1 - \exp[-\Delta \cdot \delta_1 \cdot \mu_1]) \\
D_{1s}^{V1R2}(t+\Delta) &\sim \text{Bin}(I_{1s}^{V1R2}(t), 1 - \exp[-\Delta \cdot \delta_1 \cdot \mu_1]) \\
E_2^{*V1S2}(t+\Delta) &\sim \text{Bin}(V_1(t), 1 - \exp\left[\frac{-\Delta}{N} \cdot \hat{\Lambda}_{2i} \cdot p_2\right]) \\
E_2^{*VR1S2}(t+\Delta) &\sim \text{Bin}(R_1^{V1S2}(t), 1 - \exp\left[\frac{-\Delta}{N} \cdot \hat{\Lambda}_{2i} \cdot p_2\right]) \\
p_2 &= \beta_{2a} \cdot \left[I_{2a}^{S1S2}(t) + \hat{\lambda}_{2i} \cdot (I_{2a}^{R1S2}(t) + I_{2a}^{V1S2}(t) + I_{2a}^{VR1S2}(t)) + \hat{\lambda}_{1I} \cdot (I_{2a}^{S1V2}(t) + I_{2a}^{R1V2}(t) + I_{2a}^{V1V2}(t) + I_{2a}^{VR1V2}(t)) \right] \\
&\quad + \beta_{2s} \cdot \left[I_{2s}^{S1S2}(t) + \hat{\lambda}_{2i} \cdot (I_{2s}^{R1S2}(t) + I_{2s}^{V1S2}(t) + I_{2s}^{VR1S2}(t)) + \hat{\lambda}_{2I} \cdot (I_{2s}^{S1V2}(t) + I_{2s}^{R1V2}(t) + I_{2s}^{V1V2}(t) + I_{2s}^{VR1V2}(t)) \right] \\
I_{2a}^{*V1S2}(t+\Delta) &\sim \text{Bin}(E_2^{V1S2}(t), 1 - \exp\left[-\Delta \cdot \gamma_2 \cdot \hat{\gamma}_{2a} \cdot \hat{\Gamma}_{2i}\right])
\end{aligned}$$

$I_{2s}^*V1S2(t+\Delta) \sim Bin(E_2^{V1S2}(t), 1 - \exp[-\Delta \cdot \gamma_2 \cdot (1 - \hat{\gamma}_{2a} \cdot \hat{\Gamma}_{2i})])$
$I_{2a}^*VR1S2(t+\Delta) \sim Bin(E_2^{VR1S2}(t), 1 - \exp[-\Delta \cdot \gamma_2 \cdot \hat{\gamma}_{2a} \cdot \hat{\Gamma}_{2i}])$
$I_{2s}^*VR1S2(t+\Delta) \sim Bin(E_2^{VR1S2}(t), 1 - \exp[-\Delta \cdot \gamma_2 \cdot (1 - \hat{\gamma}_{2a} \cdot \hat{\Gamma}_{2i})])$
$R_{2a}^*V1S2(t+\Delta) \sim Bin(I_{2a}^{V1S2}(t), 1 - \exp[-\Delta \cdot \delta_2])$
$R_{2s}^*V1S2(t+\Delta) \sim Bin(I_{2s}^{V1S2}(t), 1 - \exp[-\Delta \cdot \delta_2 \cdot (1 - \mu_2)])$
$D_{2s}^{V1S2}(t+\Delta) \sim Bin(I_{2s}^{V1S2}, 1 - \exp[-\Delta \cdot \delta_2 \cdot \mu_2])$
$D_{2s}^{VR1S2}(t+\Delta) \sim Bin(I_{2s}^{VR1S2}, 1 - \exp[-\Delta \cdot \delta_2 \cdot \mu_2])$
$R_{1s2}^{S1S2}(t+\Delta) \sim Bin(I_{1s}^{S1R2}, 1 - \exp[-\Delta \cdot \delta_1 \cdot (1 - \mu_1)])$
$R_{VR1s2}^{V1S2}(t+\Delta) \sim Bin(I_{1s}^{V1R2}, 1 - \exp[-\Delta \cdot \delta_1 \cdot (1 - \mu_1)])$
$R_{1s2}^{S1V2}(t+\Delta) \sim Bin(I_{1s}^{S1VR2}, 1 - \exp[-\Delta \cdot \delta_1 \cdot (1 - \mu_1)])$
$R_{1s2}^{V1V2}(t+\Delta) \sim Bin(I_{1s}^{V1VR2}, 1 - \exp[-\Delta \cdot \delta_1 \cdot (1 - \mu_1)])$
$V_1(t+\Delta) = V_1(t) + V_1^*(t+\Delta) - E_1^{V1S2}(t+\Delta) - E_2^{V1S2}(t+\Delta)$
$E_1^{V1S2}(t+\Delta) = E_1^{V1S2}(t) + E_1^*V1S2(t+\Delta) - I_{1a}^*V1S2(t+\Delta) - I_{1s}^*V1S2(t+\Delta)$
$E_2^{V1S2}(t+\Delta) = E_2^{V1S2}(t) + E_2^*V1S2(t+\Delta) - I_{2a}^*V1S2(t+\Delta) - I_{2s}^*V1S2(t+\Delta)$
$I_{1a}^{V1S2}(t+\Delta) = I_{1a}^{V1S2}(t) + I_{1a}^*V1S2(t+\Delta) - R_{1a}^*V1S2(t+\Delta)$
$I_{1s}^{V1S2}(t+\Delta) = I_{1s}^{V1S2}(t) + I_{1s}^*V1S2(t+\Delta) - R_{1s}^*V1S2(t+\Delta) - D_1^*V1S2(t+\Delta)$
$I_{2s}^{V1S2}(t+\Delta) = I_{2s}^{V1S2}(t) + I_{2s}^*V1S2(t+\Delta) - R_{2s}^*V1S2(t+\Delta) - D_2^*V1S2(t+\Delta)$
$I_{2a}^{V1S2}(t+\Delta) = I_{2a}^{V1S2}(t) + I_{2a}^*V1S2(t+\Delta) - R_{2a}^*V1S2(t+\Delta)$
$R_{1s}^{V1S2}(t+\Delta) = R_{1s}^{V1S2}(t) + R_{1a}^*V1S2(t+\Delta) + R_{1s}^*V1S2(t+\Delta) - E_2^*VR1S2(t+\Delta)$
$R_{2s}^{V1S2}(t+\Delta) = R_{2s}^{V1S2}(t) + R_{2a}^*V1S2(t+\Delta) + R_{2s}^*V1S2(t+\Delta) - E_1^*V1R2(t+\Delta)$
$E_2^{VR1S2}(t+\Delta) = E_2^{VR1S2}(t) + E_2^*VR1S2(t+\Delta) - I_{2a}^*VR1S2(t+\Delta) - I_{2s}^*VR1S2(t+\Delta)$
$I_{2a}^{VR1S2}(t+\Delta) = I_{2a}^{VR1S2}(t) + I_{2a}^*VR1S2(t+\Delta) - R_{12a}^*V1S2(t+\Delta)$
$E_1^{V1R2}(t+\Delta) = E_1^{V1R2}(t) + E_1^*V1R2(t+\Delta) - I_{1a}^*V1R2(t+\Delta) - I_{1s}^*V1R2(t+\Delta)$
$I_{2s}^{VR1S2}(t+\Delta) = I_{2s}^{VR1S2}(t) + I_{2s}^*VR1S2(t+\Delta) - R_{12s}^*V1S2(t+\Delta) - D_2^*VR1S2(t+\Delta)$
$I_{1s}^{V1R2}(t+\Delta) = I_{1s}^{V1R2}(t) + I_{1s}^*V1R2(t+\Delta) - R_{1s2}^*V1S2(t+\Delta) - D_1^*V1R2(t+\Delta)$
$I_{1a}^{V1R2}(t+\Delta) = I_{1a}^{V1R2}(t) + I_{1a}^*V1R2(t+\Delta) - R_{1a2}^*V1S2(t+\Delta)$
$R_{12}^{V1S2}(t+\Delta) = R_{12}^{V1S2}(t) + R_{1a2}^*V1S2(t+\Delta) + R_{1s2}^*V1S2(t+\Delta) + R_{12a}^*V1S2(t+\Delta) + R_{12s}^*V1S2(t+\Delta)$
$D_1^{V1S2}(t+\Delta) = D_1^{V1S2}(t) + D_1^*V1S2(t+\Delta) + D_1^*V1R2(t+\Delta)$
$D_2^{V1S2}(t+\Delta) = D_2^{V1S2}(t) + D_2^*V1S2(t+\Delta) + D_2^*VR1S2(t+\Delta)$

Table A3: Model 2: stochastic model specification

The next model shows the flow of individuals vaccinated against influenza but not COVID-19.



Model 3: disease course for individuals vaccinated against influenza but not COVID-19.

$V_2^*(t+\Delta) \sim \text{Bin}(S(t), 1 - \exp[-\Delta \cdot \omega_2])$
$E_1^{*S1V2}(t+\Delta) \sim \text{Bin}(V_2(t), 1 - \exp\left[\frac{-\Delta}{N} \cdot \hat{\Lambda}_{1i} \cdot p_1\right])$
$E_1^{*S1VR2}(t+\Delta) \sim \text{Bin}(R_2^{S1V2}(t), 1 - \exp\left[\frac{-\Delta}{N} \cdot \hat{\Lambda}_{1i} \cdot p_1\right])$
$p_1 = \beta_{1a} \cdot \left[I_{1a}^{S1S2}(t) + \hat{\lambda}_{1i} \cdot (I_{1a}^{S1R2}(t) + I_{1a}^{S1V2}(t) + I_{1a}^{S1VR2}(t)) + \hat{\lambda}_{1I} \cdot (I_{1a}^{V1S2}(t) + I_{1a}^{V1R2}(t) + I_{1a}^{V1V2}(t) + I_{1a}^{V1VR2}(t)) \right] + \beta_{1s} \cdot \left[I_{1s}^{S1S2}(t) + \hat{\lambda}_{1i} \cdot (I_{1s}^{S1R2}(t) + I_{1s}^{S1V2}(t) + I_{1s}^{S1VR2}(t)) + \hat{\lambda}_{1I} \cdot (I_{1s}^{V1S2}(t) + I_{1s}^{V1R2}(t) + I_{1s}^{V1V2}(t) + I_{1s}^{V1VR2}(t)) \right]$
$I_{1a}^{*S1V2}(t+\Delta) \sim \text{Bin}(E_1^{S1V2}(t), 1 - \exp[-\Delta \cdot \gamma_1 \cdot \hat{\gamma}_{1a} \cdot \hat{\Gamma}_{1i}])$
$I_{1s}^{*S1V2}(t+\Delta) \sim \text{Bin}(E_1^{S1V2}(t), 1 - \exp[-\Delta \cdot \gamma_1 \cdot (1 - \hat{\gamma}_{1a} \cdot \hat{\Gamma}_{1i})])$
$I_{1a}^{*S1VR2}(t+\Delta) \sim \text{Bin}(E_1^{S1VR2}(t), 1 - \exp[-\Delta \cdot \gamma_1 \cdot \hat{\gamma}_{1a} \cdot \hat{\Gamma}_{1i}])$
$I_{1s}^{*S1VR2}(t+\Delta) \sim \text{Bin}(E_1^{S1VR2}(t), 1 - \exp[-\Delta \cdot \gamma_1 \cdot (1 - \hat{\gamma}_{1a} \cdot \hat{\Gamma}_{1i})])$
$R_{1a}^{*S1V2}(t+\Delta) \sim \text{Bin}(I_{1a}^{S1V2}(t), 1 - \exp[-\Delta \cdot \delta_1])$
$R_{1s}^{*S1V2}(t+\Delta) \sim \text{Bin}(I_{1s}^{S1V2}(t), 1 - \exp[-\Delta \cdot \delta_1 \cdot (1 - \mu_1)])$
$D_{1s}^{S1V2}(t+\Delta) \sim \text{Bin}(I_{1s}^{S1V2}, 1 - \exp[-\Delta \cdot \delta_1 \cdot \mu_1])$
$D_{1s}^{S1VR2}(t+\Delta) \sim \text{Bin}(I_{1s}^{S1VR2}, 1 - \exp[-\Delta \cdot \delta_1 \cdot \mu_1])$
$E_2^{*S1V2}(t+\Delta) \sim \text{Bin}(V_2(t), 1 - \exp\left[\frac{-\Delta}{N} \cdot \hat{\Lambda}_{2I} \cdot p_2\right])$
$E_2^{*R1V2}(t+\Delta) \sim \text{Bin}(R_1^{S1V2}(t), 1 - \exp\left[\frac{-\Delta}{N} \cdot \hat{\Lambda}_{2I} \cdot p_2\right])$
$p_2 = \beta_{2a} \cdot \left[I_{2a}^{S1S2}(t) + \hat{\lambda}_{2i} \cdot (I_{2a}^{R1S2}(t) + I_{2a}^{V1S2}(t) + I_{2a}^{V R1S2}(t)) + \hat{\lambda}_{2I} \cdot (I_{2a}^{S1V2}(t) + I_{2a}^{R1V2}(t) + I_{2a}^{V1V2}(t) + I_{2a}^{V R1V2}(t)) \right] + \beta_{2s} \cdot \left[I_{2s}^{S1S2}(t) + \hat{\lambda}_{2i} \cdot (I_{2s}^{R1S2}(t) + I_{2s}^{V1S2}(t) + I_{2s}^{V R1S2}(t)) + \hat{\lambda}_{2I} \cdot (I_{2s}^{S1V2}(t) + I_{2s}^{R1V2}(t) + I_{2s}^{V1V2}(t) + I_{2s}^{V R1V2}(t)) \right]$
$I_{2a}^{*S1V2}(t+\Delta) \sim \text{Bin}(E_2^{S1V2}(t), 1 - \exp[-\Delta \cdot \gamma_2 \cdot \hat{\gamma}_{2a} \cdot \hat{\Gamma}_{2I}])$
$I_{2s}^{*S1V2}(t+\Delta) \sim \text{Bin}(E_2^{S1V2}(t), 1 - \exp[-\Delta \cdot \gamma_2 \cdot (1 - \hat{\gamma}_{2a} \cdot \hat{\Gamma}_{2I})])$
$I_{2a}^{*R1V2}(t+\Delta) \sim \text{Bin}(E_2^{R1V2}(t), 1 - \exp[-\Delta \cdot \gamma_2 \cdot \hat{\gamma}_{2a} \cdot \hat{\Gamma}_{2I}])$
$I_{2s}^{*R1V2}(t+\Delta) \sim \text{Bin}(E_2^{R1V2}(t), 1 - \exp[-\Delta \cdot \gamma_2 \cdot (1 - \hat{\gamma}_{2a} \cdot \hat{\Gamma}_{2I})])$
$R_{2a}^{*S1V2}(t+\Delta) \sim \text{Bin}(I_{2a}^{S1V2}(t), 1 - \exp[-\Delta \cdot \delta_2])$
$R_{2s}^{*S1V2}(t+\Delta) \sim \text{Bin}(I_{2s}^{S1V2}(t), 1 - \exp[-\Delta \cdot \delta_2 \cdot (1 - \mu_2)])$
$D_{2s}^{S1V2}(t+\Delta) \sim \text{Bin}(I_{2s}^{S1V2}, 1 - \exp[-\Delta \cdot \delta_2 \cdot \mu_2])$
$D_{2s}^{R1V2}(t+\Delta) \sim \text{Bin}(I_{2s}^{R1V2}, 1 - \exp[-\Delta \cdot \delta_2 \cdot \mu_2])$
$R_{12a}^{S1S2}(t+\Delta) \sim \text{Bin}(I_{2a}^{R1S2}, 1 - \exp[-\Delta \cdot \delta_2])$

$R_{12a}^{V1S2}(t+\Delta) \sim Bin(I_{2a}^{VR1S2}, 1 - \exp[-\Delta \cdot \delta_2])$
$R_{12a}^{S1V2}(t+\Delta) \sim Bin(I_{2a}^{R1V2}, 1 - \exp[-\Delta \cdot \delta_2])$
$R_{12a}^{V1V2}(t+\Delta) \sim Bin(I_{2a}^{VR1V2}, 1 - \exp[-\Delta \cdot \delta_2])$
$V_2(t+\Delta) = V_2(t) + V_2^*(t+\Delta) - E_1^{S1V2}(t+\Delta) - E_2^{S1V2}(t+\Delta)$
$E_1^{S1V2}(t+\Delta) = E_1^{S1V2}(t) + E_1^{*S1V2}(t+\Delta) - I_{1a}^{*S1V2}(t+\Delta) - I_{1s}^{*S1V2}(t+\Delta)$
$E_2^{S1V2}(t+\Delta) = E_2^{S1V2}(t) + E_2^{*S1V2}(t+\Delta) - I_{2a}^{*S1V2}(t+\Delta) - I_{2s}^{*S1V2}(t+\Delta)$
$I_{1a}^{S1V2}(t+\Delta) = I_{1a}^{S1V2}(t) + I_{1a}^{*S1V2}(t+\Delta) - R_{1a}^{*S1V2}(t+\Delta)$
$I_{1s}^{S1V2}(t+\Delta) = I_{1s}^{S1V2}(t) + I_{1s}^{*S1V2}(t+\Delta) - R_{1s}^{*S1V2}(t+\Delta) - D_1^{*S1V2}(t+\Delta)$
$I_{2s}^{S1V2}(t+\Delta) = I_{2s}^{S1V2}(t) + I_{2s}^{*S1V2}(t+\Delta) - R_{2s}^{*S1V2}(t+\Delta) - D_2^{*S1V2}(t+\Delta)$
$I_{2a}^{S1V2}(t+\Delta) = I_{2a}^{S1V2}(t) + I_{2a}^{*S1V2}(t+\Delta) - R_{2a}^{*S1V2}(t+\Delta)$
$R_{1a}^{S1V2}(t+\Delta) = R_{1a}^{S1V2}(t) + R_{1a}^{*S1V2}(t+\Delta) + R_{1s}^{*S1V2}(t+\Delta) - E_2^{*R1V2}(t+\Delta)$
$R_{2a}^{S1V2}(t+\Delta) = R_{2a}^{S1V2}(t) + R_{2a}^{*S1V2}(t+\Delta) + R_{2s}^{*S1V2}(t+\Delta) - E_1^{*S1VR2}(t+\Delta)$
$E_2^{R1V2}(t+\Delta) = E_2^{R1V2}(t) + E_2^{*R1V2}(t+\Delta) - I_{2a}^{*R1V2}(t+\Delta) - I_{2s}^{*R1V2}(t+\Delta)$
$E_1^{S1VR2}(t+\Delta) = E_1^{S1VR2}(t) + E_1^{*S1VR2}(t+\Delta) - I_{1a}^{*S1VR2}(t+\Delta) - I_{1s}^{*S1VR2}(t+\Delta)$
$I_{2a}^{R1V2}(t+\Delta) = I_{2a}^{R1V2}(t) + I_{2a}^{*R1V2}(t+\Delta) - R_{2a}^{*S1V2}(t+\Delta)$
$I_{2s}^{R1V2}(t+\Delta) = I_{2s}^{R1V2}(t) + I_{2s}^{*R1V2}(t+\Delta) - R_{12s}^{*S1V2}(t+\Delta) - D_2^{*R1V2}(t+\Delta)$
$I_{1s}^{S1VR2}(t+\Delta) = I_{1s}^{S1VR2}(t) + I_{1s}^{*S1VR2}(t+\Delta) - R_{1s2}^{*S1V2}(t+\Delta) - D_1^{*S1VR2}(t+\Delta)$
$I_{1a}^{S1VR2}(t+\Delta) = I_{1a}^{S1VR2}(t) + I_{1a}^{*S1VR2}(t+\Delta) - R_{1a2}^{*S1V2}(t+\Delta)$
$R_{12}^{S1V2}(t+\Delta) = R_{12}^{S1V2}(t) + R_{1a}^{*S1V2}(t+\Delta) + R_{1s}^{*S1V2}(t+\Delta) + R_{12a}^{*S1V2}(t+\Delta) + R_{12s}^{*S1V2}(t+\Delta)$
$D_1^{S1V2}(t+\Delta) = D_1^{S1V2}(t) + D_1^{*S1V2}(t+\Delta) + D_1^{*S1VR2}(t+\Delta)$
$D_2^{S1V2}(t+\Delta) = D_2^{S1V2}(t) + D_2^{*S1V2}(t+\Delta) + D_2^{*R1V2}(t+\Delta)$

Table A4: Model 3: stochastic model specification

The next model shows the flow of individuals vaccinated against both, COVID-19 and influenza.

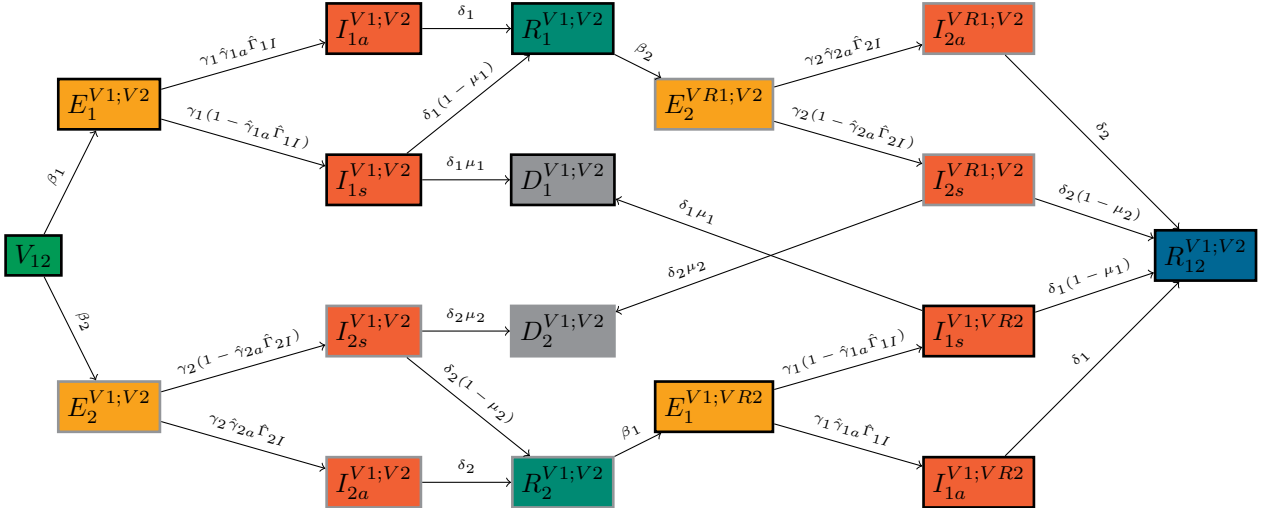


Figure A3: Model 4: disease course for individuals vaccinated against both, COVID-19 and influenza

$V_{12}^{*2}(t+\Delta) \sim Bin(V_1(t), 1 - \exp[-\Delta \cdot \omega_2])$
$V_{12}^{*1}(t+\Delta) \sim Bin(V_2(t), 1 - \exp[-\Delta \cdot \omega_1])$
$E_1^{*V1V2}(t+\Delta) \sim Bin(V_{12}(t), 1 - \exp[-\frac{\Delta}{N} \cdot \hat{\Lambda}_{1I} \cdot p_1])$

$E_1^{*V1VR2}(t+\Delta) \sim \text{Bin}\left(R_2^{V1V2}(t), 1-\exp\left[-\frac{\Delta}{N} \cdot \hat{\Lambda}_{1I} \cdot p_1\right]\right)$
$p_1 = \beta_{1a} \cdot \left[I_{1a}^{S1S2}(t) + \hat{\lambda}_{1i} \cdot (I_{1a}^{S1R2}(t) + I_{1a}^{S1V2}(t) + I_{1a}^{S1VR2}(t)) + \hat{\lambda}_{1I} \cdot (I_{1a}^{V1S2}(t) + I_{1a}^{V1R2}(t) + I_{1a}^{V1V2}(t) + I_{1a}^{V1VR2}(t)) \right] + \beta_{1s} \cdot \left[I_{1s}^{S1S2}(t) + \hat{\lambda}_{1i} \cdot (I_{1s}^{S1R2}(t) + I_{1s}^{S1V2}(t) + I_{1s}^{S1VR2}(t)) + \hat{\lambda}_{1I} \cdot (I_{1s}^{V1S2}(t) + I_{1s}^{V1R2}(t) + I_{1s}^{V1V2}(t) + I_{1s}^{V1VR2}(t)) \right]$
$I_{1a}^{*V1V2}(t+\Delta) \sim \text{Bin}\left(E_1^{V1V2}, 1-\exp\left[-\Delta \cdot \gamma_1 \cdot \hat{\gamma}_{1a} \cdot \hat{\Gamma}_{1I}\right]\right)$
$I_{1s}^{*V1V2}(t+\Delta) \sim \text{Bin}\left(E_1^{V1V2}, 1-\exp\left[-\Delta \cdot \gamma_1 \cdot (1-\hat{\gamma}_{1a}) \cdot \hat{\Gamma}_{1I}\right]\right)$
$I_{1a}^{*V1VR2}(t+\Delta) \sim \text{Bin}\left(E_1^{V1VR2}, 1-\exp\left[-\Delta \cdot \gamma_1 \cdot \hat{\gamma}_{1a} \cdot \hat{\Gamma}_{1I}\right]\right)$
$I_{1s}^{*V1VR2}(t+\Delta) \sim \text{Bin}\left(E_1^{V1VR2}, 1-\exp\left[-\Delta \cdot \gamma_1 \cdot (1-\hat{\gamma}_{1a}) \cdot \hat{\Gamma}_{1I}\right]\right)$
$R_{1a}^{*V1V2}(t+\Delta) \sim \text{Bin}\left(I_{1a}^{V1V2}(t), 1-\exp\left[-\Delta \cdot \delta_1\right]\right)$
$R_{1s}^{*V1V2}(t+\Delta) \sim \text{Bin}\left(I_{1s}^{V1V2}(t), 1-\exp\left[-\Delta \cdot \delta_1 \cdot (1-\mu_1)\right]\right)$
$D_{1s}^{V1V2}(t+\Delta) \sim \text{Bin}\left(I_{1s}^{V1V2}, 1-\exp\left[-\Delta \cdot \delta_1 \cdot \mu_1\right]\right)$
$D_{1s}^{V1VR2}(t+\Delta) \sim \text{Bin}\left(I_{1s}^{V1VR2}, 1-\exp\left[-\Delta \cdot \delta_1 \cdot \mu_1\right]\right)$
$E_2^{*V1V2}(t+\Delta) \sim \text{Bin}\left(V_{12}(t), 1-\exp\left[-\frac{\Delta}{N} \cdot \hat{\Lambda}_{2I} \cdot p_2\right]\right)$
$E_2^{*VR1V2}(t+\Delta) \sim \text{Bin}\left(R_1^{V1V2}(t), 1-\exp\left[-\frac{\Delta}{N} \cdot \hat{\Lambda}_{2I} \cdot p_2\right]\right)$
$p_2 = \beta_{2a} \cdot \left[I_{2a}^{S1S2}(t) + \hat{\lambda}_{2i} \cdot (I_{2a}^{R1S2}(t) + I_{2a}^{V1S2}(t) + I_{2a}^{VR1S2}(t)) + \hat{\lambda}_{1I} \cdot (I_{2a}^{S1V2}(t) + I_{2a}^{R1V2}(t) + I_{2a}^{V1V2}(t) + I_{2a}^{VR1V2}(t)) \right] + \beta_{2s} \cdot \left[I_{2s}^{S1S2}(t) + \hat{\lambda}_{2i} \cdot (I_{2s}^{R1S2}(t) + I_{2s}^{V1S2}(t) + I_{2s}^{VR1S2}(t)) + \hat{\lambda}_{2I} \cdot (I_{2s}^{S1V2}(t) + I_{2s}^{R1V2}(t) + I_{2s}^{V1V2}(t) + I_{2s}^{VR1V2}(t)) \right]$
$I_{2a}^{*V1V2}(t+\Delta) \sim \text{Bin}\left(E_2^{V1V2}, 1-\exp\left[-\Delta \cdot \gamma_2 \cdot \hat{\gamma}_{2a} \cdot \hat{\Gamma}_{2I}\right]\right)$
$I_{2s}^{*V1V2}(t+\Delta) \sim \text{Bin}\left(E_2^{V1V2}, 1-\exp\left[-\Delta \cdot \gamma_2 \cdot (1-\hat{\gamma}_{2a}) \cdot \hat{\Gamma}_{2I}\right]\right)$
$I_{2a}^{*VR1V2}(t+\Delta) \sim \text{Bin}\left(E_2^{VR1V2}, 1-\exp\left[-\Delta \cdot \gamma_2 \cdot \hat{\gamma}_{2a} \cdot \hat{\Gamma}_{2I}\right]\right)$
$I_{2s}^{*VR1V2}(t+\Delta) \sim \text{Bin}\left(E_2^{VR1V2}, 1-\exp\left[-\Delta \cdot \gamma_2 \cdot (1-\hat{\gamma}_{2a}) \cdot \hat{\Gamma}_{2I}\right]\right)$
$R_{2a}^{*V1V2}(t+\Delta) \sim \text{Bin}\left(I_{2a}^{V1V2}(t), 1-\exp\left[-\Delta \cdot \delta_2\right]\right)$
$R_{2s}^{*V1V2}(t+\Delta) \sim \text{Bin}\left(I_{2s}^{V1V2}(t), 1-\exp\left[-\Delta \cdot \delta_2 \cdot (1-\mu_2)\right]\right)$
$D_{2s}^{V1V2}(t+\Delta) \sim \text{Bin}\left(I_{2s}^{V1V2}, 1-\exp\left[-\Delta \cdot \delta_2 \cdot \mu_2\right]\right)$
$D_{2s}^{VR1V2}(t+\Delta) \sim \text{Bin}\left(I_{2s}^{VR1V2}, 1-\exp\left[-\Delta \cdot \delta_2 \cdot \mu_2\right]\right)$
$R_{12s}^{S1S2}(t+\Delta) \sim \text{Bin}\left(I_{2s}^{R1S2}, 1-\exp\left[-\Delta \cdot \delta_2 \cdot (1-\mu_2)\right]\right)$
$R_{12s}^{V1S2}(t+\Delta) \sim \text{Bin}\left(I_{2s}^{V1S2}, 1-\exp\left[-\Delta \cdot \delta_2 \cdot (1-\mu_2)\right]\right)$
$R_{12s}^{S1V2}(t+\Delta) \sim \text{Bin}\left(I_{2s}^{R1V2}, 1-\exp\left[-\Delta \cdot \delta_2 \cdot (1-\mu_2)\right]\right)$
$R_{12s}^{V1V2}(t+\Delta) \sim \text{Bin}\left(I_{2s}^{VR1V2}, 1-\exp\left[-\Delta \cdot \delta_2 \cdot (1-\mu_2)\right]\right)$
$V_{12}(t+\Delta) = V_{12}(t) + V_{12}^{*1}(t+\Delta) + V_{12}^{*2}(t+\Delta) - E_1^{V1V2}(t+\Delta) - E_2^{V1V2}(t+\Delta)$
$E_1^{V1V2}(t+\Delta) = E_1^{V1V2}(t) + E_1^{*V1V2}(t+\Delta) - I_{1a}^{V1V2}(t+\Delta) - I_{1s}^{V1V2}(t+\Delta)$
$E_2^{V1V2}(t+\Delta) = E_2^{V1V2}(t) + E_2^{*V1V2}(t+\Delta) - I_{2a}^{*V1V2}(t+\Delta) - I_{2s}^{*V1V2}(t+\Delta)$
$I_{1a}^{V1V2}(t+\Delta) = I_{1a}^{V1V2}(t) + I_{1a}^{*V1V2}(t+\Delta) - R_{1a}^{*V1V2}(t+\Delta)$
$I_{1s}^{V1V2}(t+\Delta) = I_{1s}^{V1V2}(t) + I_{1s}^{*V1V2}(t+\Delta) - R_{1s}^{*V1V2}(t+\Delta) - D_1^{*V1V2}(t+\Delta)$
$I_{2s}^{V1V2}(t+\Delta) = I_{2s}^{V1V2}(t) + I_{2s}^{*V1V2}(t+\Delta) - R_{2s}^{*V1V2}(t+\Delta) - D_2^{*V1V2}(t+\Delta)$
$I_{2a}^{V1V2}(t+\Delta) = I_{2a}^{V1V2}(t) + I_{2a}^{*V1V2}(t+\Delta) - R_{2a}^{*V1V2}(t+\Delta)$
$R_1^{V1V2}(t+\Delta) = R_1^{V1V2}(t) + R_{1a}^{*V1V2}(t+\Delta) + R_{1s}^{*V1V2}(t+\Delta) - E_2^{*VR1V2}(t+\Delta)$
$R_2^{V1V2}(t+\Delta) = R_2^{V1V2}(t) + R_{2a}^{*V1V2}(t+\Delta) + R_{2s}^{*V1V2}(t+\Delta) - E_1^{*}(t+\Delta)$
$E_2^{VR1V2}(t+\Delta) = E_2^{VR1V2}(t) + E_2^{*VR1V2}(t+\Delta) - I_{2a}^{*VR1V2}(t+\Delta) - I_{2s}^{*VR1V2}(t+\Delta)$
$E_1^{V1VR2}(t+\Delta) = E_1^{V1VR2}(t) + E_1^{*V1VR2}(t+\Delta) - I_{1a}^{*V1VR2}(t+\Delta) - I_{1s}^{*V1VR2}(t+\Delta)$
$I_{2a}^{VR1V2}(t+\Delta) = I_{2a}^{VR1V2}(t) + I_{2a}^{*VR1V2}(t+\Delta) - R_{2a}^{*V1V2}(t+\Delta)$
$I_{2s}^{VR1V2}(t+\Delta) = I_{2s}^{VR1V2}(t) + I_{2s}^{*VR1V2}(t+\Delta) - R_{12s}^{*V1V2}(t+\Delta) - D_2^{*VR1V2}(t+\Delta)$
$I_{1s}^{V1VR2}(t+\Delta) = I_{1s}^{V1VR2}(t) + I_{1s}^{*V1VR2}(t+\Delta) - R_{1s2}^{*V1V2}(t+\Delta) - D_1^{*V1VR2}(t+\Delta)$

$I_{1a}^{V1VR2}(t+\Delta) = I_{1a}^{V1VR2}(t) + I_{1a}^{*V1VR2}(t+\Delta) - R_{1a2}^{*V1V2}(t+\Delta)$
$R_{12}^{V1V2}(t+\Delta) = R_{12}^{V1V2}(t) + R_{1a2}^{*V1V2}(t+\Delta) + R_{1s2}^{*V1V2}(t+\Delta) + R_{12a}^{*V1V2}(t+\Delta) + R_{12s}^{*V1V2}(t+\Delta)$
$D_1^{V1V2}(t+\Delta) = D_1^{V1V2}(t) + D_1^{*V1V2}(t+\Delta) + D_1^{*V1VR2}(t+\Delta)$
$D_2^{V1V2}(t+\Delta) = D_2^{V1V2}(t) + D_2^{*V1V2}(t+\Delta) + D_2^{*V1V2}(t+\Delta)$

Table A5: Model 4: stochastic model specification

Appendix B - Model Parameters

Parameter Settings

Parameter	Description	Value	Reference
β_{1a}	transmission rate between susceptible individuals and infected asymptomatic individuals for COVID-19	$0.55 \times \beta_{1s}$	[18]
β_{1s}	transmission rate between susceptible individuals and infected symptomatic individuals for COVID-19	0.375	see Section ??
β_{2a}	transmission rate between susceptible individuals and infected asymptomatic individuals for influenza	$0.51 \times \beta_{2s}$	[32]
β_{2s}	transmission rate between susceptible individuals and infected symptomatic individuals for influenza	0.300	see Section ??
γ_1^{-1}	latent period for COVID-19	2	[1]
γ_2^{-1}	latent period for influenza	1.6	[7]
$\hat{\gamma}_{1a}$	probability of asymptomatic infection for COVID-19	0.308	[24]
$\hat{\gamma}_{2a}$	probability of asymptomatic infection for influenza	0.331	[6]
δ_1^{-1}	length of infectious period for COVID-19	10.2	[1]
δ_2^{-1}	length of infectious period for influenza	4.8	[6]
μ_1	mortality probability (due to symptomatic infection) for COVID-19	0.015	[12]
μ_2	mortality probability (due to symptomatic infection) for influenza	0.004	[30]
ω_1	rate of vaccination for COVID-19 (based on the vaccination coverage in Belgium)	0.05	[3]
ω_2	rate of vaccination for influenza (based on the vaccination coverage in the Netherlands)	0.01	[15]
Immunity effects			
$\hat{\lambda}_{1i}$	Effect of heterologous immunity on the infectiousness with COVID-19	1	fixed
$\hat{\lambda}_{1I}$	Effect of homologous immunity on the infectiousness with COVID-19	1	fixed
$\hat{\lambda}_{2i}$	Effect of heterologous immunity on the infectiousness with influenza	1	fixed
$\hat{\lambda}_{2I}$	Effect of homologous immunity on the infectiousness with influenza	1	fixed
$\hat{\Lambda}_{1i}$	Effect of heterologous immunity on the susceptibility to COVID-19		
$\hat{\Lambda}_{1I}$	Effect of homologous immunity on the susceptibility to COVID-19	(1-0.863)	[14]
$\hat{\Lambda}_{2i}$	Effect of heterologous immunity on the susceptibility to influenza		
$\hat{\Lambda}_{2I}$	Effect of homologous immunity on the susceptibility to influenza	(1-0.349)	[26]
$\hat{\Gamma}_{1i}$	effect of heterologous immunity on the probability of developing symptoms for COVID-19	1	assumed

$\hat{\Gamma}_{1I}$	effect of homologous immunity (vaccine) on the probability of developing symptoms for COVID-19	1	assumed
$\hat{\Gamma}_{2i}$	effect of heterologous immunity on the probability of developing symptoms for influenza	1	assumed
$\hat{\Gamma}_{2I}$	effect of homologous immunity (vaccine) on the probability of developing symptoms for influenza	1	assumed

Table B1: A list of all model parameters along with their respective values, descriptions, and sources. If a parameter value is derived from scientific literature, it indicates that the value is chosen based on previous research. Transmission rates are estimated in this thesis, and the reference directs the reader to the corresponding section. "Fixed" indicates that parameter values are determined in the experiments, depending on the scenario, and "Assumed" means the value is chosen by the author of this thesis.

Fitting Procedure

$E^*(t + \Delta) \sim \{S(t), 1 - \exp[-\Delta/N(\beta_a I_a(t) + \beta_s I_s(t))]\}$	$S(t + \Delta) = S(t) - E^*(t + \Delta)$
$I_a^*(t + \Delta) \sim \{E(t), 1 - \exp(-\Delta\gamma\hat{\gamma}_a)\}$	$E(t + \Delta) = E(t) + E^*(t + \Delta) - I_a^*(t + \Delta) - I_s^*(t + \Delta)$
$I_s^*(t + \Delta) \sim \{E(t), 1 - \exp(-\Delta\gamma(1 - \hat{\gamma}_a))\}$	$I_a(t + \Delta) = I_a(t) + I_a^*(t + \Delta) - R_a^*(t + \Delta)$
$R_a^*(t + \Delta) \sim \{I_a(t), 1 - \exp(-\Delta\delta)\}$	$I_s(t + \Delta) = I_s(t) + I_s^*(t + \Delta) - R_s^*(t + \Delta) - D^*(t + \Delta)$
$R_s^*(t + \Delta) \sim \{I_s(t), 1 - \exp(-\Delta\delta(1 - \mu))\}$	$R(t + \Delta) = R(t) + R_a^*(t + \Delta) + R_s^*(t + \Delta)$
$D^*(t + \Delta) \sim \{I_s(t), 1 - \exp(-\Delta\delta\mu)\}$	$D(t + \Delta) = D(t) + D^*(t + \Delta)$

Table B2: Set of equations describing the stochastic version of the SEIR Model from figure 2

Derivation of R_0 with the Next Generation Approach

Table B3 shows the set of ODE's corresponding to the SEIR-model in Figure 2.

$$\begin{aligned}
 \frac{d}{dt}S(t) &= \frac{-S}{N}(I_a(t)\beta_a + I_s(t)\beta_s) \\
 \frac{d}{dt}E(t) &= \frac{S}{N}(I_a(t)\beta_a + I_s(t)\beta_s) - \gamma E(t) \\
 \frac{d}{dt}I_a(t) &= \gamma\gamma_a E(t) - \delta I_a(t) \\
 \frac{d}{dt}I_s(t) &= \gamma(1 - \gamma_a)E(t) - \delta I_s(t) \\
 \frac{d}{dt}R(t) &= \delta I_a(t) + \delta(1 - \mu)I_s(t) \\
 \frac{d}{dt}D(t) &= \mu I_s(t)
 \end{aligned}$$

Table B3: ODE's corresponding to the SEIR model in Figure 2

This system has three disease-classes (E , I_a and I_s) and three non-disease classes (S , R and D).

The vector \mathbf{f} contains the different ways that new infections can occur and vector \mathbf{v} contains the different ways that infections can be transferred from one class to another.

$$\mathbf{f} = \begin{pmatrix} \frac{S}{N}(I_a\beta_a + I_s\beta_s) \\ 0 \\ 0 \end{pmatrix} \text{ and } \mathbf{v} = \begin{pmatrix} -\gamma E \\ \gamma\gamma_a E - \delta I_a \\ \gamma(1 - \gamma_a)E - \delta I_s \end{pmatrix}$$

The next generation matrix \mathbf{G} is the product of two components: $\mathbf{F} = \frac{\partial f_i(x_0)}{\partial x_j}$ and \mathbf{V}^{-1} with $\mathbf{V} = \frac{\partial v_i(x_0)}{\partial x_j}$ and x_0 corresponding to the disease-free equilibrium state (at which $E = I_a = I_s = R = D = 0$, hence $S = N$ and $S/N = 1$).

The two components of \mathbf{G} are:

$$\mathbf{F} = \begin{pmatrix} \frac{\partial(I_a\beta_a+I_s\beta_s)}{\partial E} & \frac{\partial(I_a\beta_a+I_s\beta_s)}{\partial I_a} & \frac{\partial(I_a\beta_a+I_s\beta_s)}{\partial I_s} \\ \frac{\partial 0}{\partial E} & \frac{\partial 0}{\partial I_a} & \frac{\partial 0}{\partial I_s} \\ \frac{\partial 0}{\partial E} & \frac{\partial 0}{\partial I_a} & \frac{\partial 0}{\partial I_s} \end{pmatrix} = \begin{pmatrix} 0 & \beta_a & \beta_s \\ 0 & 0 & 0 \\ 0 & 0 & 0 \end{pmatrix}$$

and

$$\mathbf{V} = \begin{pmatrix} \frac{\partial(-\gamma E)}{\partial E} & \frac{\partial(-\gamma E)}{\partial I_a} & \frac{\partial(-\gamma E)}{\partial I_s} \\ \frac{\partial(\gamma\gamma_a E - \delta I_a)}{\partial E} & \frac{\partial(\gamma\gamma_a E - \delta I_a)}{\partial I_a} & \frac{\partial(\gamma\gamma_a E - \delta I_a)}{\partial I_s} \\ \frac{\partial(\gamma(1-\gamma_a)E - \delta I_s)}{\partial E} & \frac{\partial(\gamma(1-\gamma_a)E - \delta I_s)}{\partial I_a} & \frac{\partial(\gamma(1-\gamma_a)E - \delta I_s)}{\partial I_s} \end{pmatrix} = \begin{pmatrix} -\gamma & 0 & 0 \\ \gamma\gamma_a & -\delta & 0 \\ \gamma(1-\gamma_a) & 0 & -\delta \end{pmatrix}$$

To find \mathbf{V}^{-1} , the adjugate matrix $\text{adj}(\mathbf{V})$ is needed. It corresponds to the transpose of the cofactor matrix \mathbf{C} of \mathbf{F} :

$$\begin{aligned} \text{adj}(\mathbf{V}) = \mathbf{C}^T &= \begin{pmatrix} \begin{vmatrix} -\delta & 0 \\ 0 & -\delta \end{vmatrix} & -\begin{vmatrix} \gamma\gamma_a & 0 \\ \gamma(1-\gamma_a) & -\delta \end{vmatrix} & \begin{vmatrix} \gamma\gamma_a & -\delta \\ \gamma(1-\gamma_a) & 0 \end{vmatrix} \\ -\begin{vmatrix} 0 & 0 \\ 0 & -\delta \end{vmatrix} & \begin{vmatrix} -\gamma & 0 \\ \gamma(1-\gamma_a) & -\delta \end{vmatrix} & -\begin{vmatrix} -\gamma & 0 \\ \gamma(1-\gamma_a) & 0 \end{vmatrix} \\ \begin{vmatrix} 0 & 0 \\ -\delta & 0 \end{vmatrix} & -\begin{vmatrix} -\gamma & 0 \\ \gamma\gamma_a & 0 \end{vmatrix} & \begin{vmatrix} -\gamma & 0 \\ \gamma\gamma_a & -\delta \end{vmatrix} \end{pmatrix}^T \\ &= \begin{pmatrix} \delta^2 & \gamma\gamma_a\delta & \gamma(1-\gamma_a)\delta \\ 0 & \gamma\delta & 0 \\ 0 & 0 & \gamma\delta \end{pmatrix}^T = \begin{pmatrix} \delta^2 & 0 & 0 \\ \gamma\gamma_a\delta & \gamma\delta & 0 \\ \gamma(1-\gamma_a)\delta & 0 & \gamma\delta \end{pmatrix} \end{aligned}$$

$\mathbf{V}^{-1} = \frac{\text{adj}(\mathbf{V})}{|\mathbf{V}|}$ with $|\mathbf{V}| = -\gamma\delta^2$:

$$\mathbf{V}^{-1} = \begin{pmatrix} \frac{-1}{\gamma} & 0 & 0 \\ -\frac{\gamma_a}{\delta} & \frac{-1}{\delta} & 0 \\ \frac{-(1-\gamma_a)}{\delta} & 0 & \frac{-1}{\delta} \end{pmatrix}$$

The next generation matrix is:

$$\mathbf{G} = \mathbf{F}\mathbf{V}^{-1} = \begin{pmatrix} 0 & \beta_a & \beta_s \\ 0 & 0 & 0 \\ 0 & 0 & 0 \end{pmatrix} \begin{pmatrix} \frac{-1}{\gamma} & 0 & 0 \\ -\frac{\gamma_a}{\delta} & \frac{-1}{\delta} & 0 \\ \frac{-(1-\gamma_a)}{\delta} & 0 & \frac{-1}{\delta} \end{pmatrix} = \begin{pmatrix} \frac{\beta_a\gamma_a}{\delta} + \frac{\beta_s\gamma_s}{\delta} & \frac{-\beta_a}{\delta} & \frac{-\beta_s}{\delta} \\ 0 & 0 & 0 \\ 0 & 0 & 0 \end{pmatrix}$$

R_0 is the leading Eigenvalue of \mathbf{G} . To find this Eigenvalue, solve the following equality:

$$\begin{aligned} |\mathbf{G} - \lambda\mathbf{I}| &= 0 \\ \Leftrightarrow \begin{vmatrix} \frac{\beta_a\gamma_a}{\delta} + \frac{\beta_s(1-\gamma_a)}{\delta} - \lambda & \frac{-\beta_a}{\delta} & \frac{-\beta_s}{\delta} \\ 0 & -\lambda & 0 \\ 0 & 0 & -\lambda \end{vmatrix} &= 0 \\ \Leftrightarrow \left(\frac{\beta_a\gamma_a}{\delta} + \frac{\beta_s(1-\gamma_a)}{\delta} - \lambda \right) \cdot \lambda^2 &= 0 \\ \Leftrightarrow \lambda = R_0 = \frac{\beta_a\gamma_a + \beta_s(1-\gamma_a)}{\delta} \end{aligned}$$

Appendix C - Additional Results

Scenario 1 - Co-circulation versus Independence

Attack Rate - All Simulations						
	COVID-19			Influenza		
	mean	median	95% QR	mean	median	95% QR
Independence	0.7543	0.9635	[0.0001;0.9688]	0.1664	0.0004	[0.0001;0.4861]
Co-circulation	0.7570	0.9631	[0.0001;0.9685]	0.1440	0.0004	[0.0001;0.4720]

Attack Rate - Outbreaks Only						
	COVID-19			Influenza		
	mean	median	95% QR	mean	median	95% QR
Independence	0.9642	0.9644	[0.9590;0.9690]	0.4544	0.4548	[0.4042;0.4934]
Co-circulation	0.9641	0.9641	[0.9589;0.9690]	0.4311	0.4323	[0.3671;0.4843]

Table C1: (Scenario 1) Mean, median and 95% quantile range (QR) of attack rates including all simulations (upper panel) and including only major outbreaks (lower panel) for the scenarios of independence and co-circulation

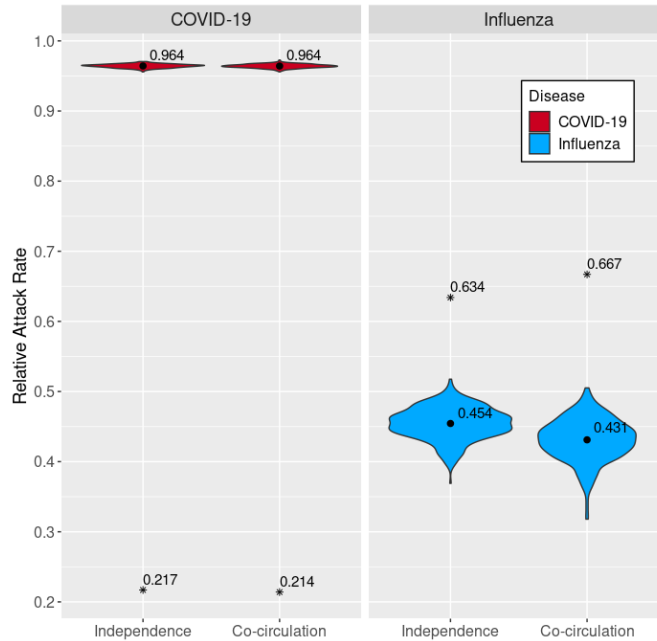


Figure C1: (Scenario 1) Distribution of attack rates for major outbreaks only

Cases at Peak - All Simulations									
	COVID-19			Influenza			Both		
	mean	median	95% QR	mean	median	95% QR	mean	median	95% QR
Independence	0.2222	0.2813	[0.0001;0.2954]	0.0100	0.0002	[0.0001;0.0333]	-	-	-
Co-circulation	0.2226	0.2807	[0.0001;0.2947]	0.0077	0.0002	[0.0001;0.0295]	0.225	0.2819	[0.0001;0.2950]

Cases at Peak - Major Outbreaks Only									
	COVID-19			Influenza			Both		
	mean	median	95% QR	mean	median	95% QR	mean	median	95% QR
Independence	0.2838	0.2835	[0.2707;0.2966]	0.0269	0.0269	[0.0190;0.0359]	-	-	-
Co-circulation	0.2831	0.2831	[0.2708;0.2950]	0.0227	0.0227	[0.0143;0.0315]	0.2582	0.2830	[0.0238;0.2952]

Day of the Peak - All Simulations									
	COVID-19			Influenza			Both		
	mean	median	95% QR	mean	median	95% QR	mean	median	95% QR

	COVID-19			Influenza			Both		
	mean	median	95% QR	mean	median	95% QR	mean	median	95% QR
Independence	59.8	72.0	[1.0;90.0]	63.2	9.0	[1.0;212.1]	-	-	-
Co-circulation	60.1	72.0	[1.5;90.0]	72.2	9	[1;259]	73.6	74.0	[2.5;167.0]

Day of the Peak - Outbreaks Only									
	COVID-19			Influenza			Both		
	mean	median	95% QR	mean	median	95% QR	mean	median	95% QR
Independence	75.2	75.0	[64.0;91.0]	160.5	155.5	[109.0;234.9]	-	-	-
Co-circulation	75.2	74.0	[64.6;91]	198.5	198.0	[121;284]	83.3	75	[65;171.2]

Table C2: (Scenario 1) Mean, median and 95% quantile range (QR) of the prevalence at peak and the day of the peak including all simulations (upper panels) and including only major outbreaks (lower panels) for the scenarios of independence and co-circulation

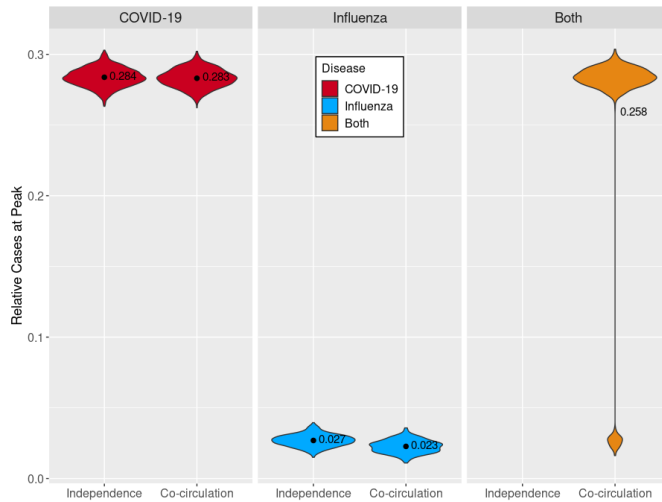


Figure C2: (Scenario 1) Distribution of cases at peak for major outbreaks only

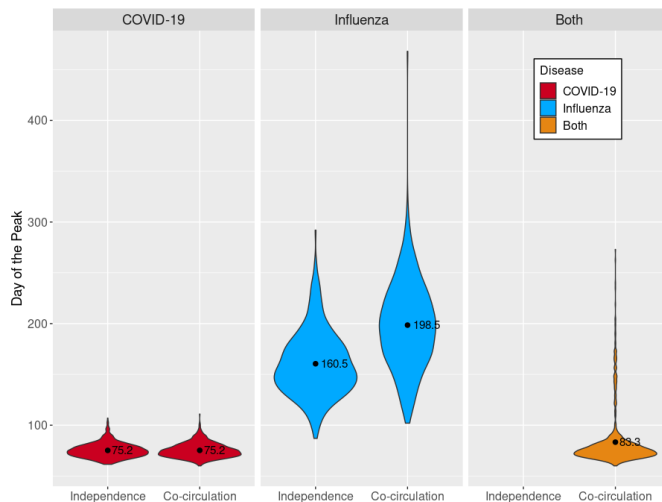


Figure C3: (Scenario 1) Distribution of the day of the peak for major outbreaks only

Scenario 2 - Effect of Vaccination

Attack Rate - All Simulations	
COVID-19	Influenza

	mean	median	95% QR	mean	median	95% QR
No Vaccination	0.7570	0.9631	[0.0001;0.9685]	0.1440	0.0004	[0.0001;0.4720]
Vaccination	0.0041	0.0027	[0.0001;0.0147]	0.237	0.0001	[0.0001;0.1411]

(Scenario 2) Mean, median and 95% quantile range (QR) of attack rates including all simulations for the scenarios with and without vaccination

Cases at Peak - All Simulations									
	COVID-19			Influenza			Both		
	mean	median	95% QR	mean	median	95% QR	mean	median	95% QR
No Vaccination	0.2226	0.2807	[0.0001;0.2947]	0.0077	0.0002	[0.0001;0.0295]	0.2255	0.2819	[0.0001;0.2950]
Vaccination	0.0010	0.0007	[0.0001;0.0033]	0.0014	0.0002	[0.0001;0.0075]	0.0021	0.0014	[0.0001;0.0077]

Day of the Peak - All Simulations									
	COVID-19			Influenza			Both		
	mean	median	95% QR	mean	median	95% QR	mean	median	95% QR
No Vaccination	60.1	72.0	[1.5;90.0]	72.2	9.0	[1.0;259.0]	73.6	74.0	[2.5;167.0]
Vaccination	30.2	31.5	[1.5;72.0]	40.5	7.0	[1.0;179.0]	52.3	40.0	[2.0;168.0]

Table C4: (Scenario 2) Mean, median and 95% quantile range (QR) of the prevalence at peak and the day of the peak including all simulations for the scenarios with and without vaccination.

Scenario 3: Less Aggressive COVID-19

Attack Rate - All Simulations						
	COVID-19			Influenza		
	mean	median	95% QR	mean	median	95% QR
Original	0.7570	0.9631	[0.0001;0.9685]	0.1440	0.0004	[0.0001;0.4720]
Less Aggressive	0.1266	0.0004	[0.0001;0.4285]	0.1581	0.0003	[0.0001;0.4848]

Attack Rate - Outbreaks Only						
	COVID-19			Influenza		
	mean	median	95% QR	mean	median	95% QR
Original	0.9641	0.9641	[0.9589;0.9690]	0.4311	0.4323	[0.3671;0.4843]
Less Aggressive	0.3853	0.3829	[0.3205;0.4426]	0.4502	0.4528	[0.3920;0.4926]

Table C5: (Scenario 1) Mean, median and 95% quantile range (QR) of attack rates including all simulations (upper panel) and including only major outbreaks (lower panel) for the scenarios with the original and a less aggressive COVID-19 strain.

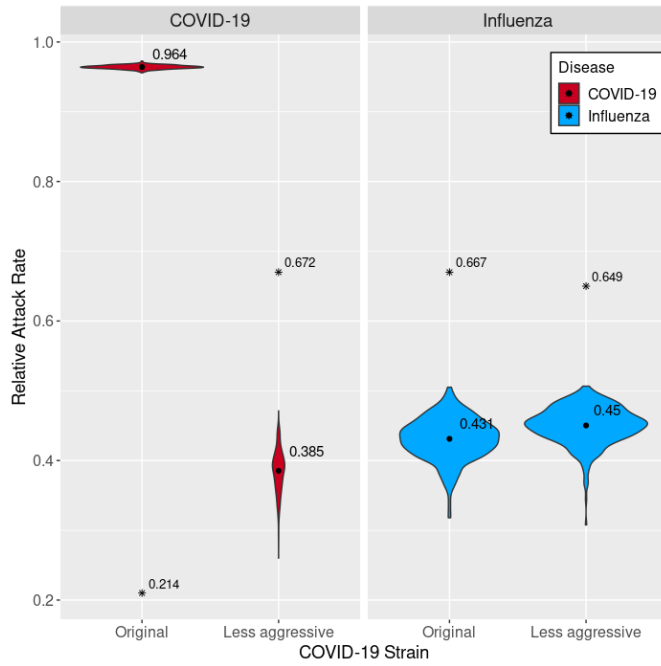


Figure C4: (Scenario 3) Distribution of attack rates for major outbreaks only for the scenarios with the original and a less aggressive COVID-19 strain.

Cases at Peak - All Simulations										
	COVID-19			Influenza			Both			
	mean	median	95% QR	mean	median	95% QR	mean	median	95% QR	
Original	0.2226	0.2807	[0.0001;0.2947]	0.0077	0.0002	[0.0001;0.0295]	0.225	0.2819	[0.0001;0.2950]	
Less Aggressive	0.0072	0.0002	[0.0001;0.0276]	0.0094	0.0002	[0.0001;0.0324]	0.0150	0.0192	[0.0001;0.0362]	
Cases at Peak - Major Outbreaks Only										
	COVID-19			Influenza			Both			
	mean	median	95% QR	mean	median	95% QR	mean	median	95% QR	
Original	0.2831	0.2831	[0.2708;0.2950]	0.0227	0.0227	[0.0143;0.0315]	0.2582	0.2830	[0.0238;0.2952]	
Less Aggressive	0.0214	0.0214	[0.0123;0.0307]	0.0266	0.0268	[0.0173;0.0348]	0.0153	0.0196	[0.0001;0.0361]	
Day of the Peak - All Simulations										
	COVID-19			Influenza			Both			
	mean	median	95% QR	mean	median	95% QR	mean	median	95% QR	
Original	60.1	72.0	[1.5;90.0]	72.2	9	[1;259]	73.6	74.0	[2.5;167.0]	
Less Aggressive	111.1	13	[1.5;425]	59.5	8	[1;216]		132.9	132	[1.5;407]
Day of the Peak - Outbreaks Only										
	COVID-19			Influenza			Both			
	mean	median	95% QR	mean	median	95% QR	mean	median	95% QR	
Original	75.2	74.0	[64.6;91]	198.5	198.0	[121;284]	83.3	75	[65;171.2]	
Less Aggressive	313.1	294.8	[205.2;530.5]	157.8	149	[108.8;242.5]	136.5	135	[1.5;408.1]	

Table C6: (Scenario 3) Mean, median and 95% quantile range (QR) of the prevalence at peak and the day of the peak including all simulations (upper panels) and including only major outbreaks (lower panels) for the scenarios with the original and a less aggressive COVID-19 strain.

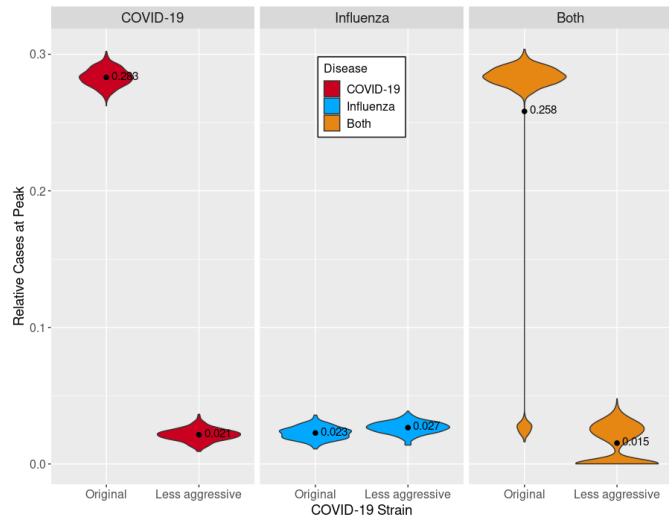


Figure C5: (Scenario 3) Distribution of cases at peak for major outbreaks only for the scenarios with the original and a less aggressive COVID-19 strain.

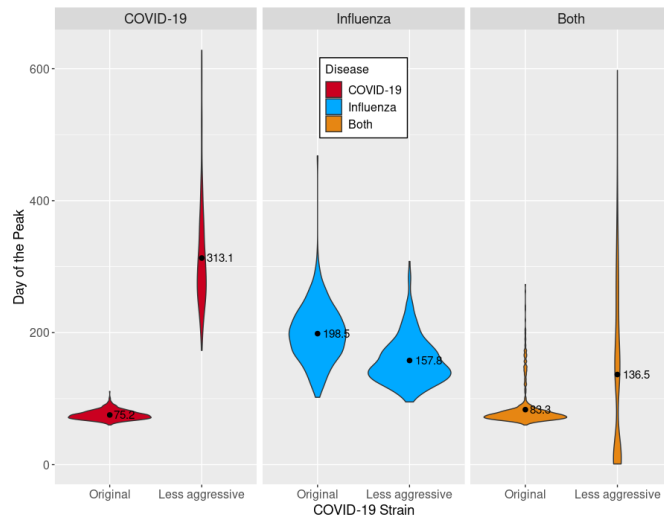


Figure C6: (Scenario 3) Distribution of the day of the peak for major outbreaks only for the scenarios with the original and a less aggressive COVID-19 strain.

Scenario 4: Co-Circulation Accounting for Heterologous Immunity

Attack Rate - All Simulations						
λ	COVID-19			Influenza		
	mean	median	95% QR	mean	median	95% QR
1	0.7570	0.9631	[0.0001;0.9685]	0.1440	0.0004	[0.0001;0.4720]
0.9	0.7432	0.9626	[0.0001;0.9684]	0.1155	0.0005	[0.0001;0.4693]
0.8	0.7848	0.9631	[0.0001;0.9689]	0.0550	0.0004	[0.0001;0.4655]
0.7	0.7383	0.9627	[0.0001;0.9687]	0.0517	0.0004	[0.0001;0.4674]
Attack Rate - Outbreaks Only						
λ	COVID-19			Influenza		
	mean	median	95% QR	mean	median	95% QR
1	0.9641	0.9641	[0.9590;0.9689]	0.4311	0.4323	[0.3671;0.4843]
0.9	0.9637	0.9638	[0.9578;0.9687]	0.3307	0.3080	[0.1972;0.4851]
0.8	0.9638	0.9639	[0.9578;0.9692]	0.2786	0.1941	[0.1067;0.4857]
0.7	0.9636	0.9639	[0.9567;0.9691]	0.4179	0.4477	[0.1106;0.4923]

Table C7: (Scenario 4) Mean, median and 95% quantile range (QR) of attack rates including all simulations (upper panel) and including only major outbreaks (lower panel) for the scenarios with no (0%), low (10%), moderate (20%) and high (30%) heterologous effect on the susceptibility to infection.

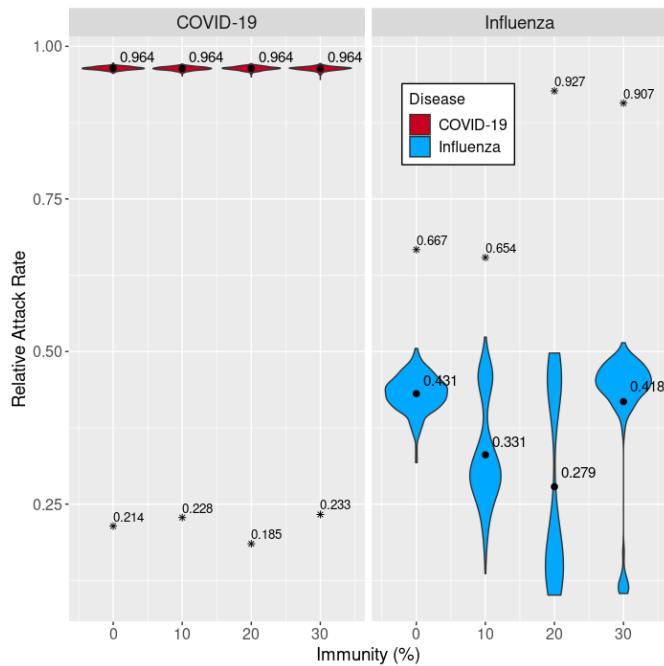


Figure C7: (Scenario 4) Distribution of attack rates for major outbreaks only for the scenarios with no (0%), low (10%), moderate (20%) and high (30%) heterologous effect on the susceptibility to infection.

Cases at Peak - All Simulations									
λ	COVID-19			Influenza			Both		
	mean	median	95% QR	mean	median	95% QR	mean	median	95% QR
1	0.2226	0.2807	[0.0001;0.2947]	0.0077	0.0002	[0.0001;0.0295]	0.2255	0.2819	[0.0001;0.2950]
0.9	0.2182	0.2805	[0.0001;0.2940]	0.0054	0.0002	[0.0001;0.0299]	0.2213	0.2813	[0.0001;0.2944]
0.8	0.2304	0.2808	[0.0001;0.2947]	0.0031	0.0002	[0.0001;0.0274]	0.2329	0.2814	[0.0002;0.2953]
0.7	0.2169	0.2803	[0.0001;0.2945]	0.0034	0.0002	[0.0001;0.0289]	0.2198	0.2809	[0.0001;0.2952]
Cases at Peak - Outbreaks Only									
λ	COVID-19			Influenza			Both		
	mean	median	95% QR	mean	median	95% QR	mean	median	95% QR
1	0.2831	0.2831	[0.2708;0.2950]	0.0227	0.0227	[0.0143;0.0315]	0.2582	0.2830	[0.0238;0.2952]
0.9	0.2827	0.2825	[0.2709;0.2946]	0.0151	0.0125	[0.0057;0.0327]	0.2576	0.2827	[0.0239;0.2948]
0.8	0.2827	0.2825	[0.2700;0.1954]	0.0263	0.0263	[0.0181;0.0330]	0.2625	0.2824	[0.0251;0.2956]
0.7	0.2828	0.2828	[0.2694;0.2956]	0.0261	0.0264	[0.0164;0.0330]	0.2556	0.2825	[0.0228;0.2956]
Day of the Peak - All Simulations									
λ	COVID-19			Influenza			Both		
	mean	median	95% QR	mean	median	95% QR	mean	median	95% QR
1	60.1	72.0	[1.5;90.0]	72.2	9.0	[1.0;259.2]	73.6	74.0	[2.5;167.0]
0.9	59.4	72.0	[1.5;91.0]	84.3	12.0	[1.0;335.2]	72.8	74.0	[2.0;165.0]
0.8	62.4	73.0	[1.0;92.0]	53.4	9.7	[1.0;308.1]	73.9	74.0	[2.0;165.0]
0.7	58.9	72.0	[1.5;91.0]	41.0	10.0	[1.0;190.0]	73.7	74.0	[2.5;174.1]
Day of the Peak - Outbreaks Only									
λ	COVID-19			Influenza			Both		
	mean	median	95% QR	mean	median	95% QR	mean	median	95% QR
1	75.2	74.0	[64.6;91.0]	198.5	198.0	[121.0;284.0]	83.3	75.0	[65.0;171.2]
0.9	75.6	75.0	[65.0;91.7]	219.9	216.5	[69.9;378.6]	83.6	76.0	[65.0;170.6]
0.8	75.6	74.0	[64.0;93.0]	160.2	155.0	[114.6;224.6]	82.3	75.0	[65.0;172.6]
0.7	75.6	74.0	[64.0;92.9]	159.3	158.0	[108.1;224.7]	84.6	75.0	[64.0;180.0]

Table C8: (Scenario 4) Mean, median and 95% quantile range (QR) of the prevalence at peak and the day of the peak including all simulations (upper panels) and including only major outbreaks (lower panels) for the scenarios with no (0%), low (10%), moderate (20%) and high (30%) heterologous effect on the susceptibility to infection.

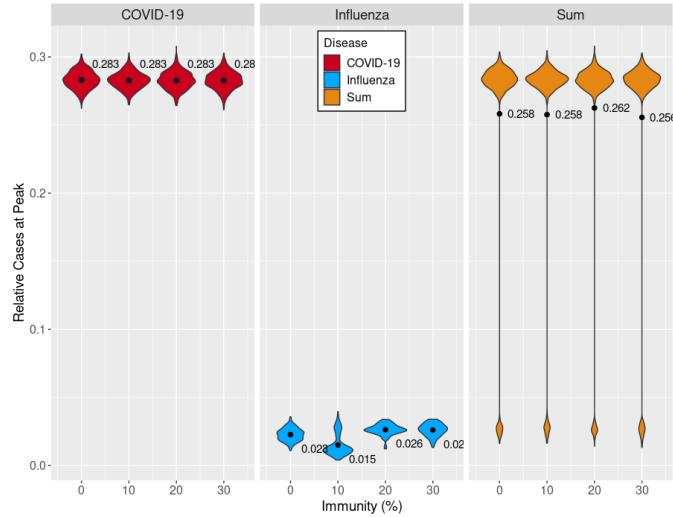


Figure C8: (Scenario 4) Distribution of cases at peak for major outbreaks only for the scenarios with no (0%), low (10%), moderate (20%) and high (30%) heterologous effect on the susceptibility to infection.

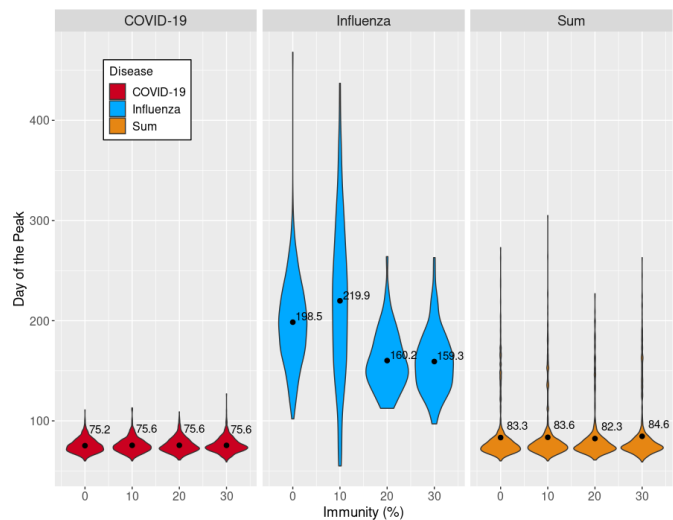


Figure C9: (Scenario 4) Distribution of the day of the peak for major outbreaks only for the scenarios with no (0%), low (10%), moderate (20%) and high (30%) heterologous effect on the susceptibility to infection.

Scenario 5: Co-Circulation Accounting for Heterologous Immunity with a less Aggressive Variant of COVID-19

Attack Rate - All Simulations						
λ	COVID-19			Influenza		
	mean	median	95% QR	mean	median	95% QR
1	0.1266	0.0004	[0.0001;0.4285]	0.1581	0.0003	[0.0001;0.4848]
0.9	0.1172	0.0003	[0.0001;0.4223]	0.1639	0.0004	[0.0001;0.4858]
0.8	0.0987	0.0002	[0.0001;0.4200]	0.1588	0.0002	[0.0001;0.4928]

0.7	0.0979	0.0003	[0.0001;0.4213]	0.1700	0.0004	[0.0001;0.4885]
Attack Rate - Outbreaks Only						
λ	COVID-19			Influenza		
	mean	median	95% QR	mean	median	95% QR
1	0.3853	0.3892	[0.3205;0.4426]	0.4502	0.4528	[0.3920;0.4926]
0.9	0.3635	0.3694	[0.2549;0.4378]	0.4499	0.4519	[0.3883;0.5001]
0.8	0.3430	0.3643	[0.1962;0.4329]	0.4510	0.3917	[0.5016;0.4512]
0.7	0.3167	0.3632	[0.1044;0.4304]	0.4485	0.4524	[0.3805;0.5032]

Table C9: (Scenario 5) Mean, median and 95% quantile range (QR) of attack rates including all simulations (upper panel) and including only major outbreaks (lower panel) for the scenarios with no (0%), low (10%), moderate (20%) and high (30%) heterologous effect on the susceptibility to infection considering a less aggressive COVID-19 strain.

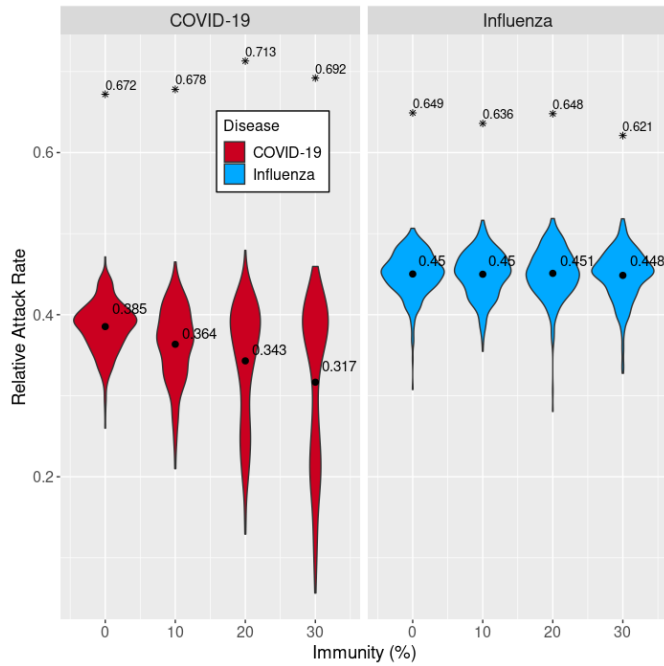


Figure C10: (Scenario 5) Distribution of attack rates for major outbreaks only for the scenarios with no (0%), low (10%), moderate (20%) and high (30%) heterologous effect on the susceptibility to infection considering a less aggressive COVID-19 strain.

Cases at Peak - All Simulations									
λ	COVID-19			Influenza			Both		
	mean	median	95% QR	mean	median	95% QR	mean	median	95% QR
1	0.0072	0.0002	[0.0001;0.0276]	0.0094	0.0002	[0.0001;0.0324]	0.0150	0.0192	[0.0001;0.0362]
0.9	0.0065	0.0002	[0.0001;0.0276]	0.0098	0.0002	[0.0001;0.0327]	0.0151	0.0191	[0.0001;0.0371]
0.8	0.0055	0.0002	[0.0001;0.0275]	0.0095	0.0002	[0.0001;0.0326]	0.0144	0.0184	[0.0001;0.0352]
0.7	0.0055	0.0002	[0.0001;0.0270]	0.0101	0.0002	[0.0001;0.0329]	0.0150	0.0200	[0.0001;0.0351]
Cases at Peak - Outbreaks Only									
λ	COVID-19			Influenza			Both		
	mean	median	95% QR	mean	median	95% QR	mean	median	95% QR
1	0.0214	0.0214	[0.0123;0.0307]	0.0266	0.0268	[0.0173;0.0348]	0.0258	0.0258	[0.0141;0.0381]
0.9	0.0199	0.0197	[0.0098;0.0301]	0.0266	0.0265	[0.0182;0.0353]	0.0262	0.0261	[0.0150;0.0402]
0.8	0.0188	0.0194	[0.0066;0.0314]	0.0267	0.0267	[0.0183;0.0347]	0.0261	0.0261	[0.0158;0.0376]
0.7	0.0173	0.0188	[0.0047;0.0297]	0.0264	0.0263	[0.0175;0.0360]	0.0260	0.0262	[0.0158;0.0361]
Day of the Peak - All Simulations									
λ	COVID-19			Influenza			Both		
	mean	median	95% QR	mean	median	95% QR	mean	median	95% QR
1	111.1	13	[1.5;425]	59.5	8	[1;216.1]	132.9	132	[1.5;407]
0.9	109.4	12.2	[1;435.1]	61.9	10	[1;205]	127.6	132	[2;395.1]

0.8	99.7	11	[1;468.5]	59.3	9	[1;205]	121.9	126.5	[1.5;405.1]
0.7	103.7	12.5	[1;462]	63.6	9	[1;208]	125.6	131.2	[2;383.1]
Day of the Peak - Outbreaks Only									
λ	COVID-19			Influenza			Both		
	mean	median	95% QR	mean	median	95% QR	mean	median	95% QR
1	313.1	294.8	[205.2;530.5]	157.8	149	[108.8;242.5]	220.9	189	[111;448]
0.9	312.9	292	[190;203.8]	157.5	153	[112;226.9]	213.2	181	[116;421.3]
0.8	317	302.5	[178.2;566]	156.3	150	[109.4;228]	213.1	177	[113;461.4]
0.7	306.2	290	[173.4;553.3]	157.9	153	[108;223.1]	210.7	178	[110;430]

Table C10: (Scenario 5) Mean, median and 95% quantile range (QR) of the prevalence at peak and the day of the peak including all simulations (upper panels) and including only major outbreaks (lower panels) for the scenarios with no (0%), low (10%), moderate (20%) and high (30%) heterologous effect on the susceptibility to infection considering a less aggressive COVID-19 strain.

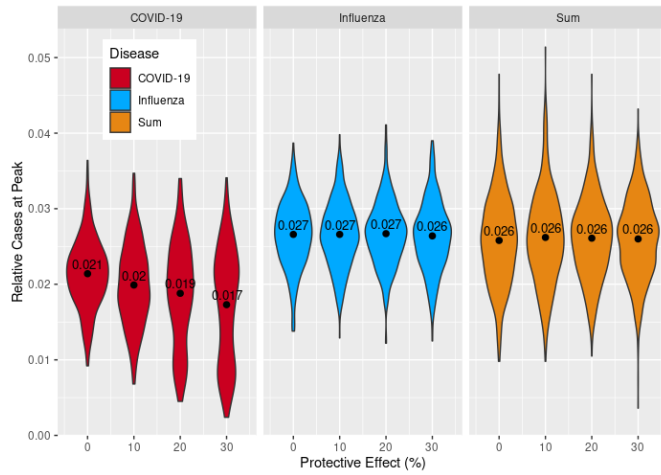


Figure C11: (Scenario 5) Distribution of cases at peak for major outbreaks only for the scenarios with no (0%), low (10%), moderate (20%) and high (30%) heterologous effect on the susceptibility to infection considering a less aggressive COVID-19 strain.

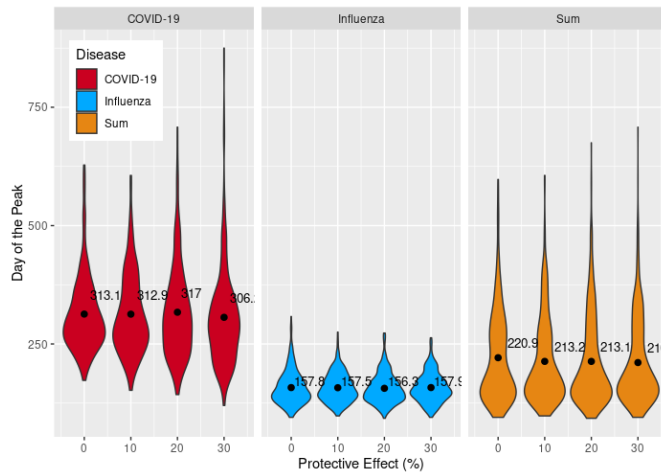


Figure C12: (Scenario 4) Distribution of the day of the peak for major outbreaks only for the scenarios with no (0%), low (10%), moderate (20%) and high (30%) heterologous effect on the susceptibility to infection.

5.1 Scenario 6: Heterologous Immunity Effect with Vaccination

Attack Rate - All Simulations						
λ	COVID-19			Influenza		
	mean	median	95% QR	mean	median	95% QR
1	0.0041	0.0027	[0.0001;0.0147]	0.0237	0.0003	[0.0001;0.1411]
0.9	0.0035	0.0022	[0.0001;0.0139]	0.0160	0.0004	[0.0001;0.0892]
0.8	0.0035	0.0023	[0.0001;0.0126]	0.0086	0.0003	[0.0001;0.0606]
0.7	0.0033	0.0020	[0.0001;0.0126]	0.0046	0.0003	[0.0001;0.0388]

Table C11: (Scenario 5) Mean, median and 95% quantile range (QR) of attack rates including all simulations (upper panel) and including only major outbreaks (lower panel) for the scenarios with no (0%), low (10%), moderate (20%) and high (30%) heterologous effect on the susceptibility to infection with vaccination.

Cases at Peak - All Simulations									
λ	COVID-19			Influenza			Both		
	mean	median	95% QR	mean	median	95% QR	mean	median	95% QR
1	0.0010	0.0007	[0.0001;0.0033]	0.0014	0.0002	[0.0001;0.0075]	0.0021	0.0014	[0.0001;0.0029]
0.9	0.0009	0.0007	[0.0001;0.0029]	0.0011	0.0002	[0.0001;0.0051]	0.0017	0.0013	[0.0001;0.0052]
0.8	0.0009	0.0007	[0.0001;0.0028]	0.0007	0.0002	[0.0001;0.0035]	0.0014	0.0011	[0.0001;0.0042]
0.7	0.0008	0.0006	[0.0001;0.0027]	0.0005	0.0002	[0.0001;0.0027]	0.0012	0.0010	[0.0001;0.0033]

Day of the Peak - All Simulations									
λ	COVID-19			Influenza			Both		
	mean	median	95% QR	mean	median	95% QR	mean	median	95% QR
1	30.2	31.5	[1.5;72]	40.5	7	[1;179]	52.3	40	[2;168]
0.9	28	28.5	[1.5;66]	38.6	10	[1;170]	48.8	39	[2;166]
0.8	29	29.5	[1.5;69.5]	31.2	8.5	[1;170]	42.4	36	[2;149]
0.7	28	28	[1.5;68.5]	23	7	[1;121]	36.6	33	[2;113]

Table C12: (Scenario 5) Mean, median and 95% quantile range (QR) of the prevalence at peak and the day of the peak including all simulations (upper panels) and including only major outbreaks (lower panels) for the scenarios with no (0%), low (10%), moderate (20%) and high (30%) heterologous effect on the susceptibility to infection with vaccination.

Appendix D - Software Code

The code is available at GitHub: [nadine-barth/Co-circulation-Model-COVID-19-and-Influenza](https://github.com/nadine-barth/Co-circulation-Model-COVID-19-and-Influenza)